Sliding Seal Materials for Low Heat Rejection Engines

Kevin Beaty, James Lankford, and Shannon Vinyard
Southwest Research Institute

July 1989

IN–37
237509

Sliding Seal Materials for Low Heat Rejection Engines

Kevin Beaty, James Lankford, and Shannon Vinyard
Southwest Research Institute
San Antonio, Texas 78284

July 1989

TABLE OF CONTENTS

iii

TABLE OF CONTENTS

SUMMARY

An essential task in the development of the heavy-duty, low heat rejection (LHR) diesel engine is the identification and improvement of reliable, low-friction piston seal materials. This report describes a three-phase effort to accomplish this objective. During Phase I, the sliding friction coefficients and wear rates of promising carbide, oxide, and nitride materials were measured under temperature, environmental, velocity, and loading conditions representative of the LHR engine environment. Phase II involved investigating silicon nitride and partially stabilized zirconia disks ion-implanted with TiNi, Ni, Co, and Cr, and subsequently run against carbide pins, with the objective of reducing friction via solid lubrication at elevated temperature. Finally, during Phase III, the most promising material combinations identified in Phase II were tested in a reciprocating friction test rig and single-cylinder diesel engine.

Unmodified ceramic sliding couples were characterized at all temperatures by friction coefficients of 0.24 and above. On the other hand, the friction coefficient at 800°C in an oxidizing environment was reduced to below 0.1, for certain material combinations, by the ion-implantation of TiNi or Co. This beneficial effect was found to derive from lubricious Ti, Ni, and Co oxides.

Friction results for the reciprocating friction test rig indicated similar friction levels for cast iron rings and liners under hydrodynamic lubrication compared with certain ceramic rings and liner with no lubrication. These results were observed at much lower temperatures (approximately 65 to 100°C) than the 800°C considered during Phase II. Reciprocating friction rig and single-cylinder engine tests demonstrated the structural integrity and feasibility of certain ceramic materials for application as piston rings and cylinder liners.

1

I. INTRODUCTION

A. Background

Since ten to thirty percent of the work output of an internal combustion engine is expended on the cooling system[1], there is great interest in developing an uncooled diesel engine. Low heat rejection (LHR) operation and recovery of exhaust heat in a turbocompounding system could increase the thermal efficiency of such an engine to 48 percent[2]. Additional benefits could be multi-fuel capability, reduced noise, reduced white smoke emissions, lower compression ratio, and reduced maintenance[2]. The engine would be lighter and easier to produce because of the elimination of the need for a cooling jacket. A study by Teledyne Continental Motors for NASA-Lewis Research Center projected important benefits of the use of light-weight LHR diesel engines in general aviation aircraft[3,4]. The study indicated that use of cylinder liners and piston caps of ceramic could save 18 percent in fuel consumption over current technology.

Over the past decade there have been several small-scale demonstrations that ceramic components could perform successfully in small laboratory diesel engines[1,2,5]. In the last few years more ambitious programs have been undertaken to demonstrate the commercial feasibility of LHR diesel engines utilizing ceramic parts. In the U.S.A., the largest effort has been the Cummins Engine Company program supported by the U.S. Army Tank Automotive Command (TACOM), which is developing a six-cylinder diesel of about 500 hp for use in armored vehicles. The design incorporates an insulating ceramic piston cap, cylinder head firedeck, deck spacer, exhaust ports, manifold, valves, and injectors of insulating ceramic. One experimental engine utilized hot-pressed silicon nitride, one used zirconia, and another used lithium-aluminum-silicate glass ceramics[2]. An interesting approach explored by this program was the use of plasma-sprayed zirconia as a piston crown coating for thermal insulation. Although spalling due to thermal expansion mismatch sets an upper limit on coating thickness, coated pistons have been successfully demonstrated in a laboratory engine.

Other countries are also competing to develop LHR engines. In particular, the Ministry of International Trade and Industry of Japan recently launched a ten-year project to improve high-technology ceramics, largely for heat engine applications. NGK Spark Plug has reported successful operation of an "all-ceramic" (silicon nitride) diesel engine, which achieved a 30 percent fuel consumption reduction because the cooling system was eliminated. Kyoto Ceramics, in cooperation with Isuzu Motors[6], has demonstrated a radiatorless, ceramic diesel engine in an automobile, wherein the silicon nitride piston reportedly experienced temperatures of up to 1200°C without failure.

In comparison to the overall effort on ceramic diesel engine development, little work has been done in the important area of developing a ceramic seal system capable of performing adequately under these harsh conditions. This report

3

describes the results of a three-phase research program which has provided material development information on candidate ceramic materials, and enabled the design and fabrication of actual piston rings and cylinder liners for the LHR diesel engine. Phases I and II studied the friction and wear mechanisms of several candidate ceramic materials, with and without surface modification by ion-implantation. Phase III included the design and fabrication of ceramic piston rings and cylinder liners for testing in a friction rig and single-cylinder diesel research engine.

B. Required Properties of Seal Materials

As outlined above, there has been considerable progress in development of ceramic pistons (or piston caps) and cylinder liners for LHR diesel engines. Designs which involve a ceramic piston cap in a partially cooled, crosshead configuration (Figure 1') can use conventional chromium-plated cast iron rings and low-temperature lubrication, which offers a very low friction coefficient (about 0.05) and low wear rates. However, in an uncooled engine configuration, the temperature of the metal is likely to become unacceptably high. Further, this type of design is bulky, involving extra piston weight and high inertial forces on the connecting rod and the joint between the piston and ceramic piston cap. A simpler design in which the entire cylinder is ceramic-lined (Figure 2) requires that the piston ring slide against the ceramic liner, which will be quite hot. For this purpose, there is an urgent need to find materials from which sliding seal rings can be made which will exhibit low friction and low ring and liner wear while sliding against a ceramic cylinder liner at high velocity and high temperature.

The piston crown temperature must be raised to at least 882°C in order to achieve significant energy savings in the LHR diesel engine. Kyoto Ceramics has operated an engine with peak crown temperatures of 1200°C, and there is interest in pushing the temperature to 1500°C with zirconia engine parts. Thus the prime requirements of the cylinder liner/seal ring system are resistance to thermal shock and retention of strength to temperatures much higher than that which the top ring in a conventional diesel may experience. The liner/ring combination must exhibit acceptable wear rates not only at high temperature, but also at high velocities of as much as 5-10 m/s, under conditions of exposure to combustion products and excess oxygen. Low friction is essential. The liner materials of interest have been silicon carbide, silicon nitride, and partially-stabilized zirconia. The silicon carbide, although it has been used for solid lifters and precombustion chambers in the heavy-duty diesel program, has a high thermal conductivity, which reduces its usefulness for piston crown and cylinder liner applications. Silicon nitride has been the material of choice in most of the recent work, because of its low thermal conductivity, relatively high strength at temperatures to about 1100°C, resistance to thermal shock, and relative ease of manufacture in complex shapes. However, in the press for still higher temperatures the limits for silicon nitride are already being approached. Zirconia, which is strong even at 1500°C, offers better insulating properties than silicon nitride.

'All Figures can be found in Appendix A

4

C. Wear Behavior of Ceramics

Ceramic systems exhibit a number of wear mechanisms. Adhesion, which is a common cause of wear in metal systems, can also occur between nonmetallic materials, even at low temperature, if clean surfaces of suitably oriented crystals come into contact. However, due to adsorption and lubrication effects, adhesive wear is not a common problem in ceramic/ceramic sliding couples[7], although it can be a problem with metal/ceramic couples. When metal rubs against ceramic the metal frequently adheres to the ceramic surface (especially if the metal is chemically active, or has a large percentage of d-electron shell character in its bonding[8,9]). The friction and wear phenomena may then become more a matter of the metal sliding against itself than of metal/ceramic sliding, and the friction often becomes quite high. Ductile plowing is another mode of wear which is common in metals, but which occurs only rarely in ceramic/ceramic systems. A more common wear mode in ceramics seems to be cracking (abrasive wear), which can take many forms[10]: cleavage of individual grains, intergranular cracking, lateral cracking or chipping, etc.

Recently, progress has been made in modeling certain types of abrasive wear. It has been established, for example, that for indentation by a sharp indenter, the critical load (P_c) (Newtons) for subsurface lateral (parallel to the surface) microfracture is given by[11]

$$P_c = A_1 \left(\frac{K_c}{H} \right)^3 K_c$$

where A_1 is a dimensionless geometric constant, K_c is the fracture toughness (MPa $\sqrt{m}$), and H is the hardness (MPa). But, if the indenter were to slide over the surface, and if the normal loading P were to exceed P_c, one would anticipate that, within the plastic wake of the indenter, a family of lateral cracks would be produced. The removal of these flakes of material following the initial or subsequent passes would then constitute the principal wear mechanism.

Analysis[12] indicates that during the sliding of a sharp indenter, the size of lateral cracks in the wake will be on the order of

$$C = A_2 \left[\frac{(E/E)^{3/5}}{K_c^{1/2} H^{1/8}} \right] f(P, \mu)$$

where A_2 is a dimensionless constant, E is the elastic modulus (MPa), and μ is the friction coefficient. The associated volume removed is then

$$V = A_3 \left[\frac{(E/H)^{4/5}}{K_c^{1/2} H^{5/8}} \right] f(P,\mu) L$$

5

where A_3 is a constant, and L is the distance (m) slid by the indenter.

It has been observed that when a sharp diamond indenter slides across aluminum oxide[13], wear proceeds by lateral cracking, as predicted in the above analysis. Similarly, sliding of a hemispherical diamond over silicon carbide produces circular ring cracks whose interaction and intersection to produce wear particles has been observed[10] and predicted[14]. However, sliding and wear of macroscopic surfaces, neither of which is as hard as diamond, presents a more complicated situation than the idealized cases cited above. That is, the particular relationship between V and E, H, K_c, H and μ outlined above may not hold. Nevertheless, it seems reasonable to believe, based on these analyses, that K_c and H in particular should be significant controlling factors in abrasive ceramic/ceramic wear under many circumstances.

The chemical environment also plays a critical role in the wear performance of ceramic materials[10]. Adsorbed water promotes near-surface plasticity leading to a soft surface layer some 1-10 micrometers thick. This soft surface layer seems to prevent adhesion and to lubricate ceramics as they slide over each other, so that the friction coefficient (μ) is often only about $0.2^{(7)}$. In alumina, for instance, the coefficient of friction rose from 0.25 to 0.8 as the temperature of the experiment was raised from room temperature to 400°C, driving off the adsorbed water[15]. Introduction of moist air then produced an immediate reduction of μ. Adsorbed organic substances also tend to lubricate and soften the surface of ceramics. Myristic acid, for instance, enhances surface plasticity and suppresses cracking during sliding of steel on lithium fluoride[7]. Chemisorbed oxygen appears to reduce the friction coefficient of titanium carbide by one-half[16].

Particularly pertinent to this program is a 1977 study reported by Shimura and Tsuya[17], who investigated atmospheric and temperature effects on the friction and wear of some ceramics (tungsten carbide, titanium carbide, chromium carbide, aluminum oxide) and their cermets. It was found that wear rates and coefficients of friction are higher in vacuum than in air. Based on characterization of the wear surfaces, the results were explained in terms of a postulated thin, soft lubricating surface layer which is formed by interaction of the ceramic/cermet with adsorbed moisture.

D. Potential Seal Materials

Although there is little experimental data on friction and wear of ceramics under conditions that would be experienced by the sliding piston seal in an advanced diesel engine (aside from the preceding work by Shimura and Tsuya[17]), the information that is available is fairly consistent in that the carbides are identified as outstanding sliding seal materials. Finkin, Calabrese, and Peterson[18] performed oscillatory pin-on-plate sliding experiments with various ceramic/cermet couples in air at 316-982°C. A Ni-Mo bonded titanium carbide cermet, sliding on dense magnesia-stabilized zirconia was identified as the most promising material couple. A poor

6

second was the Ni-Mo bonded TiC sliding on itself. Zirconia sliding on itself suffered catastrophic wear.

Another study[19] used pad-on-disc sliding experiments at 30-60 m/s, 5-79 psi, and temperatures up to 982°C, in an oxidizing combustion product atmosphere. Thermal shock was a major mechanism of wear. Promising materials were Cr-Mo bonded alumina, silicon carbide, and Ni-Mo bonded titanium carbide.

A recent research program sponsored by the U.S. Department of Energy has been testing ceramic materials for sliding seals in large diesel engines used in stationary applications[20]. The goal of the program is to identify coatings or monolithic ceramics which could resist corrosion and abrasion in engines using substandard fuel and which could permit operation at higher mean effective pressure. This study used pin-on-disc experiments at temperatures up to 427°C in air to assess the wear resistance of various ceramics. In these screening tests the pin and disc were of the same material. For unlubricated service, the best material was aluminum oxide (UHA-99/NTK and A473/Kyocera); SiC, TiC, and B_4C were also judged to be outstanding. By far the lowest coefficient of dry sliding friction was 0.25, for hot-pressed TiC and also for hot-pressed NbC-TaC. A blue oxide which formed on both hot-pressed TiC and a TiC cermet was felt to have a beneficial lubricating effect.

II. EXPERIMENTAL APPROACH

A. Background

The research program outlined here was designed to refine the information base regarding carbide seal ring/ceramic cylinder liner combinations for use in the high-performance, LHR diesel engine. The emphasis was focussed on obtaining quantitative and qualitative information about the wear behavior of candidate carbides run against potential cylinder liner materials (silicon nitride and partially-stabilized zirconia), under conditions representative of the service environment of seal rings in the LHR diesel. These conditions include temperatures of 23°C to 800°C, in order to evaluate the severity of wear during and following the startup period. Sliding velocities of up to 10 m/s are pertinent to published concept studies of a lightweight diesel engine for aircraft[3] and for heavy-duty trucks[2]; the information now available from work related to large stationary diesels is from tests at 0.3 m/s[20]. The wear experiments exposed the sliding materials to atmospheres that resemble the combustion atmosphere in a diesel cylinder.

In addition to measuring the performance of the best candidate materials under realistic conditions, these experiments also explored the potential benefits of a novel approach to seal wear control. This concept is based on the control of electrical processes in the wear mechanism(s). It has been demonstrated that electrical phenomena can be important in the wear of carbide metal-cutting tools[21], and that imposed electric fields can produce significant increases (up to 60 percent) in the hardness of semiconducting materials such as transition metal carbides. This investigation considers the effect of applied potential fields on the wear behavior, hardness, and fracture toughness of ceramics which might be used for sliding piston seals and cylinder liners.

Hot hardness tests under relevant atmospheric conditions were carried out to aid in interpreting the wear test results. As discussed in the previous section on wear behavior of ceramics, $H(T)$ and $K_c(T)$ (T = temperature) obtained for a realistic service environment should be key parameters in controlling friction and wear under equivalent conditions.

In addition, silicon nitride and partially stabilized zirconia disks were ion-implanted with TiNi, Ni, Co, and Cr, and subsequently run against carbide pins, with the objective of producing reduced friction via solid lubrication at elevated temperatures. Based on these test results, the two most promising ceramic/ceramic couples were chosen for further testing in a reciprocating friction test rig and single-cylinder diesel engine. The couples selected were TiNi implanted PSZ liner and Ni-Moly-TiC rings, and TiNi implanted Si_3N_4 liner with hot-pressed TiC rings.

Actual piston rings and cylinder liners were designed utilizing the two most promising ceramic/ceramic material couples which were identified during the pin-on-disk work. These piston rings and cylinder liners were tested in a reciprocating

friction test rig for correlation with the pin-on-disk friction results. The rings and liners were also installed in a single-cylinder diesel research engine for demonstration of the components' structural integrity and verification of their high temperature capabilities.

B. Materials

Candidate cylinder liner materials for the LHR diesel are silicon nitride, silicon carbide, and zirconia, with silicon nitride having received most of the emphasis to date. Silicon nitride has good thermal shock resistance, moderate thermal conductivity, reasonably low thermal expansion, and a well-developed technology for production of large parts. However, the strength of the material declines at high temperatures, so that its use is limited to no more than 1100°C. Silicon carbide retains its strength to higher temperatures, but it has a thermal conductivity two to four times higher than silicon nitride which reduces its attractiveness as an insulating cylinder liner. Zirconia, with a thermal conductivity of only 1.9 W/m·K in contrast to silicon nitride at 29.7 W/m·K, is a prime candidate for cylinder liners. It also retains its strength to much higher temperatures (>1500°C) than silicon nitride, and partially-stabilized grades can be heat treated for transformation toughening. Zirconia has a high coefficient of friction (0.7) in sliding against itself, but the wear rate can be quite low[22]. Based on these considerations, the liner materials used for discs in the pin-on-disc experiments performed in this study were silicon nitride and partially-stabilized zirconia (PSZ).

The pin candidate ring materials used were composed of SiC (discussed above), hot-pressed titanium carbide (TiC), and nickel-molybdenum bonded TiC cermets. Rationales for the TiC systems were based on the limited friction and wear work[18-20] discussed earlier.

Properties of the materials selected are given in Table 1.

C. Unmodified Ceramics

1. Wear Testing

A special wear testing machine was constructed to permit testing under conditions that are pertinent to the service environment of sliding seal materials in the LHR diesel engine. As sketched in Figure 3, the basic configuration of the machine was that of a rotating disc against which three flat-ended pins of identical material slide under controlled normal force. The pin and disc assembly were housed within a heated environmental chamber. Since the pins suffered continuous sliding, while any point on the disc surface experienced only periodic passage of a pin, the pin materials operated under conditions similar to those imposed on a sliding seal ring, and the disc material experienced conditions analogous to those of cylinder liner materials.

10

Table 1. Material Properties

Material	E (GPa)	H (GPa)	K_{IC} (MNm$^{-3/2}$)	Grain Size (μm)	Tensile Strength (MPa)
SiC[1]	380	32	4.4	3-5	345
HP TiC[2]	450	32	5.0	30	~260
Ni-Mo-TiC (K162B)[3]	407	12	~15	3	1587
Si$_3$N$_4$ (NC 132)[4]	310	19	4.8	0.5-3	810
PSZ[5]	210	10	8-15	60	600

[1]Carborundum sintered alpha SiC.
[2]Ceradyne, Inc.
[3]Kennametal Corporation.
[4]Norton Company.
[5]Nilsen (Nilcra) TS grade PSZ.

Conditions under which the wear tests were run (Table 2) were chosen to represent the LHR adiabatic engine. The simulated diesel exhaust (DE) environment consisted of 7.8 percent CO_2, 8.9 percent O_2, and balance N_2; both DE and pure Ar environments were maintained at 40 psi pressure. Disks and pins were run-in for five minutes at temperature at the start of each test, following evacuation and purging in of the system with either DE or Ar and a minimum 20 minute pre-test soak at test temperature. After the initial run-in, the test continued with voltage being varied between -6V and +6V in one volt increments spaced one to two minutes apart.

During the test, the normal load was controlled at 5 pounds, with the disk rotational speed at the point of pin/disk contact being 1 m/sec. Separate tests were conducted at 23°C, 400°C, and 800°C, for the wear couples shown in Table 2.

11

Table 2. Friction and Wear Test Parameters

Type of Test:	Three-Pin on Disk
Load:	5 pounds
Internal Pressure:	40 psi
T:	23, 400, 800 (°C)
Environment:	Simulated Diesel Exhaust, Dry Argon
Voltage:	-6 to +6 (volts)
Material Couples (disk/pin):	PSZ/SiC
	PSZ/TiC
	PSZ/Ni-Mo-TiC (K 162B)
	Si_3N_4 (NC 132)/SiC
	Si_3N_4 (NC 132)/TiC
	Si_3N_4 (NC 132)/Ni-Mo-TiC (K 162B)

2. Microhardness Tests

Microhardness tests were performed using a standard Tukon tester totally enclosed in a special environmental chamber. A test load of 800 gm was applied to a high temperature diamond indenter. A heating unit was used to bring the ceramic specimens to the test temperature, monitored by means of a thermocouple affixed near the indentation site. The indenter was electrically insulated from the test specimen.

Prior to testing, the chamber was purged for several hours with either DE or Ar environments. Indentation tests were performed at 23, 200, 400, 600, 800°C in each atmosphere; at each temperature the indenter/specimen electric potential was varied between -6V and +6V. Certain electric potential tests were repeated in 100 percent relative humidity air as a means to enhance the effect of potential. Indents and their associated radial corner cracks were used to evaluate hardness and fracture toughness, respectively. The latter was evaluated according to the analysis of Evans and Charles[23].

12

3. Wear Characterization

Prior to testing, both pins and disks were carefully polished to a 0.5 μm diamond finish. To overcome a slight error in parallelism between pins and disk surfaces at installation, a small stable wear flat was produced on each pin by run-in prior to test measurements. For subsequent wear characterization, the polished surfaces provided reference "no-damage" regions, while the boundaries of the pin flats constituted regions in which damage development could be observed from its inception to equilibrium wear. Similarly, the width of the annular wear track on each disk slowly expanded with the pin flats, so that again, by tracking across the boundary one passed quickly from no damage through the various stages of damage development leading to equilibrium wear.

Scanning electron microscopy was the principal technique used to characterize wear mechanisms. In some cases, energy dispersive spectroscopy (EDS) was employed to characterize wear particles and transfer layers.

Additionally, wear rates were characterized by weighing pins before and after testing in a precision balance (these tests were frequently compromised by chipping and/or oxidation weight gain). A more reliable measure of weight loss was provided by profilometry of the disk wear tracks. These latter measurements provided the main body of reliable wear rate data.

D. Surface Modified Ceramics

1. Ion Implantation

The implantation process used[2] was actually a variant known as ion mixing. In this technique, a thin coating of metal is vapor deposited onto the ceramic substrate, and argon ions are accelerated through a potential field, driving the deposited metal atoms into the substrate. In the case of the TiNi implant, Ni was first deposited, followed by the Ti; both layers were then simultaneously ion mixed.

The argon ions were accelerated using a beam voltage of 140 keV, with a fluency of 1×10^{17} ions/cm^2, and a flux of $\sim 10^{12}$ ions/cm^2-s. Implant layer thickness was estimated to be on the order of 400 nm, based on subsequent Auger analysis.

2. Friction and Wear Testing

The same wear testing machine constructed for the unmodified ceramics was used to permit friction and wear testing of the ion-implanted materials. Testing was performed from 23°C to 800°C, in both argon and simulated diesel exhaust (DE) environments, although most of the ion-implant tests were carried out at 800°C in the DE environment consisting of 7.8 percent CO_2, 8.9 percent O_2, and the balance

---

[2] Westinghouse R&D Center, Pittsburgh, PA.

N_2. The conditions and procedure for these tests was identical to that described for the unmodified ceramics. Run time ranged from 40 minutes to one hour.

3. Wear Characterization

Scanning electron microscopy was used to characterize wear mechanisms, while scanning Auger electron spectroscopy (AES), and energy dispersive spectroscopy (EDS) were employed to characterize wear particles and transfer layers. Surface profilometry was used as a measure of relative material loss. Because of problems associated with chipping and oxidation, wear rate determination by the measurement of specimen weight change was frequently compromised. The procedure used for wear characterization of the ion-implanted materials duplicated that used for the simple ceramics.

E. Piston Ring and Cylinder Liner Tests

1. Friction Rig Testing

The ceramic couples showing the best friction and wear behavior in the bench tests were used to produce piston rings and cylinder liners for testing in a single-cylinder test rig and a single-cylinder research engine. These materials included cast iron rings and liners, Ni-Moly-bonded TiC rings on a PSZ liner (material combination no. 1), and hot-pressed TiC rings on a Si_3N_4 liner (material combination no. 2) as shown in Figure 4. The PSZ ceramic liners were ion-implanted with a double layer of Ti and Ni. The cast iron components served as a baseline condition.

Four sets of rings were produced for material combination no. 1, and two sets were produced for material combination no. 2. These sets are identified in Figure 5, where each set consists of two identical rings. The low tensile strength of the hot-pressed TiC dictated that only low tension (~ 1 lb$_f$) rings be fabricated from this material. However, both low and high tension (5 lb$_f$) rings were fabricated from the Ni-Mo-TiC material. This was done to allow direct comparison between the low tension ceramic rings and to correlate those results with the cast iron baseline through the use of the high tension Ni-Mo-TiC rings.

The single-cylinder test rig is represented schematically in Figure 6. The purpose of this test rig was to simulate reciprocating engine motion; obtain actual friction data in a piston-cylinder configuration, not easily done in an actual engine; and to screen materials to prevent premature breakage in the actual single-cylinder research engine. The test rig consisted of a stationary piston and reciprocating liner. The rig was mounted on the research engine, replacing the block and cylinder head, and was driven by the engine's crankshaft and connecting rod. A general view of the friction test rig is shown in Figure 7. A load cell installed in the piston rod was used to measure the frictional force between the rings and the liner. Air pressure was supplied to load the rings as in gas loading during combustion and the expansion strokes. The rig was capable of operation at speeds up to 2000 rpm with variable

14

N_2. The conditions and procedure for these tests was identical to that described for the unmodified ceramics. Run time ranged from 40 minutes to one hour.

3. Wear Characterization

Scanning electron microscopy was used to characterize wear mechanisms, while scanning Auger electron spectroscopy (AES), and energy dispersive spectroscopy (EDS) were employed to characterize wear particles and transfer layers. Surface profilometry was used as a measure of relative material loss. Because of problems associated with chipping and oxidation, wear rate determination by the measurement of specimen weight change was frequently compromised. The procedure used for wear characterization of the ion-implanted materials duplicated that used for the simple ceramics.

E. Piston Ring and Cylinder Liner Tests

1. Friction Rig Testing

The ceramic couples showing the best friction and wear behavior in the bench tests were used to produce piston rings and cylinder liners for testing in a single-cylinder test rig and a single-cylinder research engine. These materials included cast iron rings and liners, Ni-Moly-bonded TiC rings on a PSZ liner (material combination no. 1), and hot-pressed TiC rings on a Si_3N_4 liner (material combination no. 2) as shown in Figure 4. The PSZ ceramic liners were ion-implanted with a double layer of Ti and Ni. The cast iron components served as a baseline condition.

Four sets of rings were produced for material combination no. 1, and two sets were produced for material combination no. 2. These sets are identified in Figure 5, where each set consists of two identical rings. The low tensile strength of the hot-pressed TiC dictated that only low tension (~ 1 lb_f) rings be fabricated from this material. However, both low and high tension (5 lb_f) rings were fabricated from the low tension ceramic rings and to correlate those results with the cast iron baseline through the use of the high tension Ni-Mo-TiC rings.

The single-cylinder test rig is represented schematically in Figure 6. The purpose of this test rig was to simulate reciprocating engine motion; obtain actual friction data in a piston-cylinder configuration, not easily done in an actual engine; and to screen materials to prevent premature breakage in the actual single-cylinder research engine. The test rig consisted of a stationary piston and reciprocating liner. The rig was mounted on the research engine, replacing the block and cylinder head, and was driven by the engine's crankshaft and connecting rod. A general view of the friction test rig is shown in Figure 7. A load cell installed in the piston rod was used to measure the frictional force between the rings and the liner. Air pressure was supplied to load the rings as in gas loading during combustion and the expansion strokes. The rig was capable of operation at speeds up to 2000 rpm with variable

14

air pressure loads to the rings. Oil seal rings were provided to prevent engine lubrication from entering the test region.

Most of the parts of the test rig are standard engine parts. The reciprocating cylinder liner was designed around the engine's standard cylinder liner as well as the engine's standard connecting rod and wrist pin. This liner served as a carrier for the cast-iron and monolithic ceramic cylinder inserts. Photographs of the liner with a PSZ insert installed using a shrink fit, before and after TiNi ion-implantation, are given in Figures 8 and 9, respectively. The piston consisted of three parts, allowing separation at the ring grooves to eliminate ring damage during installation and removal. A photograph of the piston is shown in Figure 10.

The basic test procedure for the test rig included operating the rig at speeds of 800 and 1200 rpm. Ring gas loads of 0, 100, and 200 psi were applied at each of these speeds. For each speed and load, ring/liner friction force characteristics and temperatures were recorded after all component temperatures had stabilized. Nominal ring groove temperatures measured during friction rig tests were approximately 150°F.

2. Engine Testing

Actual engine testing was conducted in a Labeco Cooperative Lubricant Research (CLR) single-cylinder engine. This engine is a direct-injection diesel engine with a bore of 97 mm, stroke of 95 mm, and rated speed of 2500 rpm. The block of this engine was modified to be heated by a liner heater, permitting selective heating of the top ring reversal area without endangering other engine components. The piston was modified to allow installation and removal of the ceramic piston rings without expanding them. This was accomplished by screwing removable alloy ring lands on and off the piston. The modified piston and a standard D-I diesel piston are shown in Figure 11. The stock cylinder head and block were removable to allow mounting of the reciprocating liner test rig directly to the engine's crankcase.

The planned engine test procedure involved running the engine up to 100 hours at each of three temperature conditions, i.e., 180°F water jacket temperature, 230°F water jacket temperature, and 700°F top ring reversal temperature. Provisions were made to measure hp, BSFC, motoring friction, and blowby at 5 hour intervals during each 100 hour test. These data were required at speeds of 1000, 1500, and 2000 rpm. At the end of each 100 hour test, ring and liner wear examination was scheduled.

However, the actual engine test procedure was limited to running the ceramic engine for 30 hours at 180°F coolant temperature as explained in Section III. C.2. Data for hp, BSFC, motoring friction, and blowby were taken every five hours during the test. Motoring data were recorded at speeds of 500, 1000, and 1500 rpm. Performance data were recorded at 1000 rpm under varied load conditions. At the end of the 30 hour test, the rings and liner were examined for wear.

3. Wear Analysis and Comparison

For both the test rig and engine tests, ring and liner wear was determined by weight loss measurements and optical examination. Where useful, the specimens were also examined for wear chemistry and wear morphology using auger and secondary electron spectroscopy, respectively.

Comparisons of friction and wear between the pin-on-disk and friction rig tests were planned. These comparisons were intended to correlate the friction rig results with the pin-on-disk results for the two ceramic couples tested. Since only one (Ni-Mo-TiC rings/PSZ liner) couple was tested in the friction rig, as explained in Section III.C.1, comparison analyses were not conducted.

16

III. EXPERIMENTAL RESULTS

A. Unmodified Ceramics

The term "unmodified ceramics" refers to monolithic ceramics and cermets whose sliding surfaces have not been modified by the addition of any type of lubricious-oxide forming metallic ions. These materials were investigated during the first phase of this program. The experimental results obtained for the unmodified ceramics are described in this section.

1. Indentation Tests

Hardness - The effects of temperature (T) and diesel exhaust (DE) and Argon (Ar) environments upon hardness (H) is shown for each individual ceramic in Figures 12 through 16. In all cases, H decreases with increasing T. The effect of environment, though evident in particular for TiC (Figure 16), is not great. On the other hand, it is very instructive to compare the H(T) curves for the various materials versus a selected environment, as shown in Figure 17 for DE. From the latter, it is clear that there exist large differences in hardness over the entire temperature range. At 800°C, the SiC and NC 132 (Si_3N_4) disk materials are roughly twice as hard as the three pin materials.

Essentially no effect of electric potential upon hardness was observed. An example is shown in Figure 18 for SiC tested in air at 23°C; the open and closed circles represent two different test series run under identical conditions.

Fracture Toughness - As shown in Figures 19 through 21, environment plays a significant role in the fracture toughness (K_c) of ceramics. Further, the effect is qualitatively different from one ceramic system to another. For NC 132 (Si_3N_4), Figure 19 shows K_c is **higher** in Ar than in DE at each T, with a maximum at T = 400°C in either environment. In the case of SiC, Figure 19 shows K_c is **lower** in Ar than in DE over most of the temperature range of interest, with a maximum in both curves at T = 500°C.

The case for TiC (Figure 21) appears to be rather more complex. As T increases, K_c in DE rises, while that in Ar falls, the greatest differential occurring at T = 200°C. Above this temperature, K_c falls precipitously in DE, while in Ar staying constant at a low level before rising sharply at T = 500°C. Data could not be obtained at higher temperatures for the TiC, due to degradation of the surface.

The smoothed curve $K_c(T)$ values for these three materials in the DE environment are shown in Figure 22. Wide quantitative and qualitative differences are apparent.

Indents in PSZ and NiMo-TiC did not produce cracking at the imposed load of 800 gm, hence K_c could not be measured. Subsequent hardness tests at higher indentation loads will be required for these materials in order to produce microfracture (K_c) data.

The only instance in which electric potential seemed to alter K_c involved SiC tested in humid air at 23°C, as shown in Figure 23. Here, in two separate test series (open and closed symbols) K_c apparently increased approximately 30 percent at a potential of -4.5 to -5 volts. It is interesting to note that within this narrow voltage band, scatter in the measured K_c values is nearly triple that for other potentials.

2. Wear Tests

Friction Coefficients - Friction coefficients (μ) for the six individual pin/disk couples in DE and Ar are shown as functions of temperature in Figures 24 through 29. It can be seen that μ ranges from a high value of more than 1.0 (SiC pins/Nc 132 disk in DE at 800°C), to a minimum of 0.24 (K162B pins/NC 132 disk, again in DE at 800°C). However, a more effective mode of presentation for subsequent discussion is to combine the curves for all three pin materials sliding on one disk in a given environment as in Figures 30 through 33.

As shown in Figure 30, μ lies between 0.6 and 0.8 for all three pin materials run against PSZ in Ar. For NC 132 disks in the same environment (Figure 31), μ for all pins decreases slightly, from ~0.8 to ~0.6, as T increases. Behavior running in a DE environment was significantly different as shown in Figure 32. For PSZ disks in DE, μ rises rapidly with T for SiC and TiC, peaks at ~400°C, and then decreases rapidly with further increase in T. For K162B, on the other hand, μ decreases steadily from its initial room temperature value of ~0.9, to a low of ~0.45 at 800°C. For NC 132 disks in DE (Figure 33), the K162B material behaves much as it does for PSZ disks in the same environment, dropping from ~0.75 at 23°C to 0.24 at 800°C. However, μ for SiC and TiC increases steadily up to 800°C without mid-range reversal and is relatively high for both.

In none of these tests was there any measurable effect related to varying the pin/disk electrical potential.

Wear Rates - Because of the oxidation and chipping problems associated with wear measurements on the pins, pin wear analysis is limited to qualitative characterization in the following section.

As shown in Figure 34, wear rate (W) for PSZ disks run in Ar increases with T for all three pin materials. It is interesting that at room temperature in Ar, SiC pins produced essentially no disk wear. For the same disk material in DE (Figure 35), wear against SiC pins is again low at 23°C, but is catastrophic at 800°C. On the other hand, K162B and TiC pins produced remarkably low disk wear at 800°C.

For NC 132 disks (Figure 36), wear rate data is less complete, due to disk damage during some of the Ar tests. Nevertheless, some interesting trends emerged. In particular, the DE environment tests resulted in rapid disk wear by SiC pins with increasing temperature, while the disk wear rate was very low against TiC, and essentially unmeasurable against K162B, over the entire temperature range of interest. It should be noted that NC 132 disks run against K162B pins in Ar also exhibited low wear rates at 800°C.

3. Wear Characterization

Somewhat surprisingly, wear via cone and/or radial crack formation was not the most commonly observed mode of damage. In fact. it was observed clearly in only one instance, i.e., for SiC pins sliding on an NC 132 disk at 23°C in DE environment. As shown in Figure 37 (b and c), the cracks penetrate at a fairly steep angle, and interact to form irregularly-shaped chips (wear particles). The NC 132 disk on the other hand, manifests the much more commonly observed wear mechanism of delamination, the early stages of which, associated with the edges of plastic wear tracks, are shown in Figure 37a. Examples of such wear, during later stages, are shown in Figure 38 for NC 132 and PSZ disks.

The development of delamination in PSZ disks using SiC pins can be seen in Figure 39, which shows several aspects of the process. In Figure 39a, delaminates (arrows) have formed after no more than a few passes. Close study of equilibrium wear regions (Figure 39b) shows that they are composed of thin sheets in the process of being removed (Figure 39c) surrounded by delaminated zones (Figure 39d) which once held material, and now consist of depressed regions containing fine wear particles. Delaminated sheets of PSZ can be found lying here and there on the disk (Figure 40), on the SiC pins (Figure 41a), and within pores in the SiC (Figure 41b). Energy dispersive X-ray spectroscopy was used to identify the latter.

It is interesting to observe the inverse influence of PSZ disks upon SiC pins. Figures 42a and 42b shows views of unworn and worn sectors of a pin. Figures 42c and 42d shows similar views at higher magnification. Generally, where the materials studied were known insulators, the SEM specimens were coated with palladium to prevent charge build-up. In this case, the specimen was not coated, since it was considered to be a semi-conductor. The characteristic glow of charge build-up was observed at some spots indicating presence of PSZ particles or sheets transferred to the pins. In contrast, the SiC specimen in Figure 41 was coated. Further, extensive plastic deformation of the SiC is evident in Figure 42d. This is somewhat surprising, since the hardness of PSZ under these conditions (23°C, DE) is about 10.5 GPa, while that of SiC is approximately 31.0 GPa, almost three times higher.

This plastic deformation has a profound effect on the wear of the SiC, as seen in Figure 43. In the first stage of wear (Figure 43a), plastic flow outlines certain carbides. As wear proceeds, adjoining particles are placed in higher relief (Figure 43b) by the plastic flow process, and eventually pits (Figure 43c) are eroded around

19

the carbides. Finally, the particles are fully exposed (Figure 43d). Their subsequent removal is a major component of pin weight loss.

At times it was observed that apparently similar features had distinctly dissimilar origins. Figure 44, for example, shows pin and disk wear surfaces for K162 pins run on NC 132 disks at 23°C in DE. The equilibrium pin wear surface (Figure 44a) wore via delamination, and was covered with particulate debris. No evidence of plastic scoring was observed. The corresponding disk surface (Figure 44b) exhibited very low wear, and had a transfer coating composed of Ni, Mo (identified by energy dispersive spectroscopy), and possibly oxygen [3]. As shown in Figure 44c, this coating itself experienced delamination.

Figure 45 shows results of a similar test in an Ar environment. In this case, the pin still delaminates, but the laminae exhibit plastic scoring (Figure 45a), and are relatively smooth. No debris particles are present. The disk wear track, showing essentially no wear, is composed of a NiMo coating (Figure 45b) with little or no oxygen, since the environment was inert. Again, this coating was apparently delaminated in sheets (Figure 45c). The ductility of the Ar-environment coating is evident in its flexure adjacent to the delaminated region.

K162B was not the only pin material which produced disk transfer layers. In particular, TiC pins run against NC 132 and PSZ disks produced layers tentatively identified as TiO_2 via EDS. The lubricating qualities of these deposits, formed at all temperatures, tended to minimize disk wear (Figure 46). The TiO_2 deposit appeared much more brittle and fragile than the NiMo-based K162B coatings discussed previously.

It appears that Ni and Mo can transfer from K162B whether or not oxygen is present. Figure 47 shows a K162B pin following wear against an NC 132 disk at 800°C in Ar. As shown in Figure 47a, the transition wear region is quite complex. The earliest stages of damage are seen in region A, and equilibrium wear in region B. Figures 47b and 47c shows higher magnification views of these respective regions. Region A seems to consist of laminate sheets in the early stages of formation, while Region B is a plastically scored, delaminated area. The effect of this surface degradation upon a mating NC 132 disk is shown in Figure 48 in the form of a rather coarse textured coating of NiMo.

The preceding situation contrasts remarkably with that which prevails upon changing the environment from Ar to DE. In this case, the transition region (Figure 49a) is even more complex than for Ar. The early (A) and equilibrium (B) sectors border a band in which the lath-like TiC particles have been completely exposed by selective removal of the surrounding NiMo matrix. During the initial stages of wear (Figure 49b), the TiC particles are gradually exposed, lying in between matrix regions which have an etched appearance. The equilibrium wear surface (Figure

---

[3] Pending Auger spectroscopic analysis.

20

49c) displays worn or broken TiC particles lying on a rough etched background with no evidence of delamination. The mating disk surface (Figure 49d) shows no wear, but is covered with small, smooth, apparently loosely adherent, particles. There is no continuous surface film, as in numerous other instances involving K162B pins. It should be recalled that this last case exhibited absolutely no measurable wear, and the lowest measured friction coefficient, i.e., 0.24.

Similar results were observed for K162B pins run against PSZ, although characterization of the transfer products is presently incomplete. It also was observed that at elevated temperature and high wear conditions, especially with SiC pins, there was a tendency for the color of the wear track to change from cream to light yellow. The potential significance of this will be discussed in the following section.

For non-ion-implanted ceramic-ceramic couples, by far the most commonly observed wear mechanism was delamination parallel to the sliding direction. Radial cracking/chipping, in fact, was observed in only one instance, i.e., for SiC pins sliding on an Si_3N_4 disk at 23°C in diesel exhaust environment. The cracks penetrated at a fairly steep angle, and interacted to form irregularly-shaped chips (Figure 37). The Si_3N_4 disk on the other hand, manifested the much more commonly observed wear mechanism of delamination, the early stages of which are associated with the edges of plastic wear tracks.

The development of delamination in Si_3N_4 and zirconia disks were shown in Figure 38. In Figure 38a, the delaminations formed after no more than a few passes. Close study of equilibrium wear regions (Figure 38b) show that they were composed of thin sheets in the process of being removed (Figure 38c). Delaminated sheets of zirconia were observed lying at random on the disks and on the pins.

Delamination-type disk wear prevailed in all tests involving SiC pins, and those involving zirconia in argon. In all of the other tests, where the lower friction coefficients were measured, erosion occurred primarily by pin delamination combined with the transfer of pin material, either titanium oxide in the case of TiC pins, or titanium and/or nickel oxide[4], in the case of Ni-Mo bonded TiC (Molybdenum transfer was not observed, since Mo rapidly volatilizes as MoO_3 at 800°C). An example of such a film transfer process was shown in Figure 46, in which TiO_2 transferred from TiC pins to Si_3N_4 disks at 23°C and 800°C in the diesel exhaust environment.

B. Surface Modified Ceramics

The results obtained during the first phase of this program with the unmodified ceramics indicated problems of high friction coefficients and wear rates. However,

---

[4] We shall use TiO_2 and NiO to indicate these oxides, although the exact stoichiometry was not determined.

the use of ion-implantation to introduce metal ions into the ceramic's substrate was identified as a potential solution. It was thought that the combination of certain metallic ions and sliding materials would react and form lubricious oxides at elevated temperatures. This theory was tested during the second phase of the program. These results are reported in the following section.

1. Friction Coefficients

As presented in the previous section, friction coefficients μ for a typical unmodified ceramic-ceramic pin/disk couple in diesel exhaust (DE) and argon (Ar) are shown as a function of temperature over the range 0 to 800°C.

Since most of the ion-implanted disks were run at a single, elevated temperature (800°C), it is most convenient to consider the corresponding friction coefficients as shown in Figure 50. Clearly, ion-implantation with Cr is no more beneficial to friction behavior than is the use of unmodified ceramic couples. However, Ni-Mo-TiC pins run against zirconia disks implanted with TiNi and with Co have coefficients of friction of 0.09 and 0.06, respectively. Similarly, TiC pins with Si_3N_4 implanted with TiNi exhibit a coefficient of 0.09. These are extremely low friction coefficients, lying in the upper end of the range of values normally achieved through conventional liquid lubrication at low (<300°C) temperatures.

It is interesting to note that TiC pins running against Ni implanted silicon nitride demonstrated a coefficient of friction, $\mu_f \geq 0.14$, significantly higher than the value of 0.09 obtained running against TiNi implanted silicon nitride. Further, it is obvious that reduction in friction coefficient level is very sensitive to the material/surface modification combination involved. For example, titanium carbide is less desirable than Ni-Mo-TiC running against TiNi implanted zirconia, whereas the Ni-Mo-TiC is less desirable than TiC running against TiNi implanted Si_3N_4. (Figure 50).

2. Wear Characterization

Before discussing the wear behavior of the ion-implanted material, it is instructive to consider the nature of the implanted "coatings". As shown in Figure 51a, the Ti and Ni are mixed together reasonably well, but contain relatively little of the underlying Si_3N_4 (indicated by the Si profile). Some oxygen is present near the surface, predominantly within the Ti-rich portion of the "alloy". However, after a 30 minute soak at 800°C in the diesel environment (Figure 51b), both the Ti and, especially, the Ni, have diffused together, oxidized, and mixed with the Si_3N_4. The thickness of the implanted coating is estimated, on the basis of previous sputtering rate work, to be around 0.40 μm. Further discussion of this point is given in the following section, Characterization of Ion-Implanted Ceramic Wear Surfaces Using Auger Electron Spectroscopy.

During wear tests, the pins oxidize, and then develop small wear zones where they have been in contact with the ion-implanted disks. An example of such a zone is shown in Figure 52 for a Ni-Mo bonded TiC pin run against TiNi ion-implanted

zirconia. Based on the sizes of such zones, the contact stress was typically on the order of 3.5-7 MPa.

Inspection of the "wear zones" shows that they actually do not represent pin wear; instead, they are thin lubricating films transferred from the ion-implanted disks. Auger spectroscopy, which is discussed in detail in the following section, indicates that the films are composed of TiO_2 and NiO. Similar results were found for the Co-implanted zirconia disks tested against Ni-Mo bonded TiC pins, i.e, CoO was transferred from disk to pin.

3. Characterization of Ion-Implanted Ceramic Wear Surfaces Using Auger Electron Spectroscopy

It is clear that the conditions present at the contact interface between the pins and the disks, and the chemical and mechanical processes occurring there determine the overall friction and wear behavior of the various ceramic pin-disk combinations. In order to determine the role of interfacial properties on the friction and wear behavior of the more promising ion-implanted ceramics, surface analysis techniques were used to examine the properties of the wear surfaces on the pins and on the disks. Scanning Auger electron microscopy was used to determine the chemical makeup of the wear surfaces, while scanning electron microscopy was used to investigate the physical properties of the wear surfaces.

Experimental Procedure

The pins and disks analyzed in this portion of the study are listed in Table 3. Pin-disk combinations 1 and 4 with the titanium-nickel implant showed the best friction characteristics of those investigated during the friction and wear testing. Pin-disk combinations 2 and 3 showed less favorable frictional characteristics and a possible role of pin material in the wear process. The cobalt implanted and nickel implanted disks also showed promising results, although not as favorable as those of titanium-nickel implanted disks. These pin-disk combinations were therefore chosen for extensive analysis using Auger electron spectroscopy (AES). The results of AES or energy dispersive spectroscopy (EDS) analyses of the surfaces of other pin-disk combinations showing poorer wear characteristics will be discussed as necessary.

The investigations of the wear surfaces of both pins and disks listed in Table 3 were performed with a PHI 595 scanning Auger electron microscope. While Auger electron spectroscopy is now used routinely to investigate surface properties of metals, there are still unresolved problems when it comes to dealing with bulk semiconducting, or in this case, non-conducting materials. These include charging of the materials due to the accumulation of positive or negative charge at the analyzed region[24,25], and alteration of the analyzed surface by the electron beam, or by the ion beam during sputtering[25,26].

23

Table 3. Pin-Disk Combinations Tested in Diesel (O, N, CO_2, H_2O) Environment at 800°C Chosen for Surface Analysis*

Disk**	Pin**	μ
1. Silicon nitride Si_3N_4 (Ti, Ni)	TiC	0.09
2. Silicon nitride Si_3N_4 (Ti, Ni)	TiC-5Ni-5Mo	0.22
3. Partially stabilized zirconia PSZ (Ti, Ni)	TiC	0.25
4. Partially stabilized zirconia PSZ (Ti, Ni)	TiC-5Ni-5Mo	0.09
5. Partially stabilized zirconia PSZ (Co)	TiC-5Ni-5Mo	0.06
6. Partially stabilized zirconia PSZ (Co)	TiC	0.25
7. Silicon nitride Si_3N_4 (Ni)	TiC	0.14
8. Silicon nitride Si_3N_4 (Ni) (tested at room temperature)	TiC	0.28

*   The elements given in parenthesis are those ion-implanted into the surfaces of the disks.

** Specimen dimensions:

Disk diam. = 7.62 cm   thickness = 0.95 cm
Pin diam. = 0.64 cm   length = 1.27 cm

The problem of charging can manifest itself in two ways in scanning Auger microscopy: electrostatic charging which disturbs the secondary electron image as commonly found in secondary electron microscopy[27], and charge induced shifts in Auger peak positions[24,25,28]. The charging of insulating samples is due to their inability to remove excess charge by conduction. In the case of electron microscopy, excess charge is created through the production of secondary electrons by the

24

incident beam. The dependence of the secondary electron yield, δ, on the primary electron energy is shown schematically in Figure 53. The energy range of interest for AES is that between the two crossover points, E_1 and E_2, where $\delta > 1$[25,28]. In this range, however, a net positive charge will build up at the surface of an insulating specimen because more electrons leave the specimen than are incident on it. This positive charge will retard the emitted Auger electrons and therefore cause a shift of the Auger peak heights to lower energies[28]. This will cause little problem with normal elemental identification since surface charging should effect all Auger peak positions by the same amount. Some caution should be exercised, however, in analyzing Auger spectra for chemical information related to peak energy shifts. By considering the changes in the differences between Auger peak position, rather than the absolute value of the peak positions, as well as the peak shapes, chemical binding information can still be obtained. However, alteration of surface chemistry by ionic drift as well as by electron beam heating must still be accounted for[25,26].

Several methods can be used to reduce the problem of charging of insulating specimens, although these require some sacrifice in resolution and sensitivity. The energy range E_1 to E_2 generally falls below 2kV for such materials, and therefore indicates that primary beam energies lower than those normally used for conducting specimens should be used[28]. Reducing the irradiation dosage (C/cm^2) by reducing either the primary beam current or the analysis time can delay the onset of the maximum charging effect, as well as the onset of electron beam-induced damage[29]. Reducing the angle of incidence results in a reduction of the secondary emission yield at a given beam condition, thus reducing charging[25,29]. Non-beam related methods include coating the specimen in a conductor such as gold or silver while masking off a small area for analysis[27,30]. The neutralizing beam concept is also used for the reduction of charging during ion sputtering[28].

Alteration of specimen surfaces, either conducting or nonconducting, by the electron beam or ion beam sputtering can occur by electron beam reduction of the surface[29], migration of ionic species by charge buildup[26], beam heating[26,29], and preferential sputtering[31]. These problems will have an important effect on the interpretation of quantitative and chemical Auger data. The results of this preliminary study are not greatly influenced by the surface alteration problems, but further work on the fundamental mechanisms of these wear processes will require careful consideration of these issues.

The major consideration for this study was the problem of surface charging. Use of primary beam energies above 2 kV, and beam currents above about 10^{-8} A resulted in secondary image distortion, and distortion of the low energy end of the Auger spectra, as well as random spiking throughout the spectra. It was found that a combination of the previously mentioned remedies could reduce the charging problem to a maximum shift of ~ -5 eV in the Auger spectra.

In the case of the disks, a thin film of silver was first vapor deposited onto the specimens. It was found that sputtering away an analysis area with concurrent

25

elemental analysis was better than masking, since even a small uncoated area seemed to charge up quickly. The specimens were then tightly wrapped in aluminum foil with a small area left uncovered for analysis, strapped to a specimen holder with copper wire, and mounted in the chamber. The disks were analyzed at the 60° angle of incidence set by the specimen holder in the 595 system at a primary beam energy of 1.5 kV, a beam current of $\leq$ 5x10^{-9} A, and a beam size of < 450 nm. To avoid further charging, the beam was blanked while preliminary data handling and analysis was being performed. Depth profiling was performed using argon ion sputtering with a beam energy of 2 kV, current density of ~ 70 μA/cm^2, and a 2 mm x 2 mm raster size. The sputtering rate for the combination of materials used in this study was not known, and the depth scale is therefore given as sputtering time. Use of these sputtering conditions on a Ta$_2$O$_5$ film, however, gave a sputter rate of about 11.0 nm/min.

Because of the small size of the worn area of the pins and the fine scale of the features found there, the pins were not silver coated. They were, however, wrapped in aluminum foil, leaving the worn end uncovered. Examination at glancing incidence of the electron beam was required to avoid charging problems.

Results of Analysis on Titanium-Nickel Implanted Disks

Pins

All of the pins run against the titanium-nickel implanted disks exhibited an apparent burnish mark where the pin was in contact with the disk. The burnish marks of the pins with higher values of coefficient of friction, μ_f, were larger than those with lower values. A typical burnish mark from a TiC pin run against a Si$_3$N$_4$ (Ti,Ni) disk (low μ_f couple) is shown in Figure 54a. It appears that the burnish mark is actually a layer of material which was transferred from the disk to the pin, and was then broken up later in the wear run. This is more clearly seen at higher magnification in Figures 54b and 54c. Arrows indicate areas (usually darker) where the pin "base" material appears beneath the burnish layer. This mark will thus be referred to from this point on as a "transfer layer".

Typical Auger spectra from the unworn surface of the pin and the transfer layer are shown in Figures 55a and 55d. The main difference between the two areas, as seen by comparing Figures 55ab with 55cd, is the presence of nickel on the transfer layer. Since these spectra came from the TiC pin, the nickel could only have transferred from the TiNi implanted disk to the pin. It is not clear whether or not the nickel is present in the oxidized state, because the peak energy and shape changes associated with the oxidation of nickel are too small to be resolved under the present specimen and beam conditions[36]. Titanium, however, clearly is present in the oxidized state, as evidenced by the absence of the elemental Ti (27 eV) peak and the presence of the oxidized Ti (40 eV) peak[32], and the fact that the Ti (387 eV) peak is larger than the Ti (418 eV) peak[32-35].

26

Carbon is also present in significant amounts, with a greater amount of carbon being found on the transfer layer (Figure 55a) than on the unworn surface (Figure 55c); this is indicated by the larger peak height ratio $C(272 eV)/0(510 eV)$ for the transfer layer. Sputtering of the pin surface resulted in a reduction of the carbon signal with depth, while the titanium oxide peaks remain strong. However, the presence of a small amount of carbon even after 30 minutes of sputtering indicates that this carbon layer consists of more than just carbon adsorbed during specimen handling. While the TiC pin is probably oxidized to a significant depth, this relatively thick carbon layer is probably the result of the interaction of the diesel environment with the pin surface, although some transfer of carbon originally implanted in the disks is also a possibility (see next section). The apparently higher surface concentration of carbon on the transfer layer would be due to the higher temperatures existing at the contact point, and/or the direct contact with the carbon-containing implanted layer on the disk.

The results for the other pins run against the TiNi implanted disks shown in Table 3 were similar to those for the TiC pin just described. The Ni-Mo-TiC pin run against Si_3N_4 (couple 2), however, had a much higher nickel signal on the transfer layer, as well as having nickel on the unworn area. The transfer layer was much larger than even the other high μ_f pin (couple 3), and could account for some smearing of nickel onto the unworn areas. Since μ_f for this pin is the same as that for the TiC pin of couple 3, it is suspected that this difference could be related to slight variations in the orientation between the pin surfaces and the disks.

While little difference was found between the pin surfaces except as mentioned above, it appears that the pin composition could have played a role in the wear characteristics, although in a contradictory manner. The addition of nickel and molybdenum appeared to improve the wear characteristics of the partially stabilized zirconia - TiC couple, but not those of the Si_3N_4-TiC couple. Molybdenum was not detected on the surfaces of the Ni-Mo-TiC pins, however, probably due to its high volatility at the temperatures expected at the pin-disk interface. Since nickel transferred from the disk to the pins as shown for the case of the TiC pins, it also is not clear what role the addition of nickel to the pins played in the wear behavior.

Disks

The results of the analysis of the TiNi implanted disks are shown in Figures 56 through 63. Secondary electron micrographs and corresponding Auger elemental peak maps are given in Figures 56 through 59, while typical Auger spectra and elemental depth profiles taken on, as well as distant from, the wear tracks are shown in Figure 51. The results displayed in Figure 50 were taken at approximately the same sputter depth to facilitate comparison (sputter time was 10-15 minutes, including ~ 5-6 minutes to remove the silver coating). It was found during depth profiling that the implanted layers varied in thickness over the disk surfaces. Therefore, the profiles shown indicate the relative trends of elemental composition with depth, but no quantitative information is implied.

27

Elemental depth profiles of the disks as received after ion-implantation are shown in Figure 60. The layer is clearly not homogeneously mixed, with the components lying more or less as they were put down--substrate, nickel, titanium. The titanium layer was probably slightly oxidized during implantation, and some carbon, probably from specimen handling, has also been implanted in the outer layer. As previously mentioned, this may account for some of the carbon found in the transfer layers on the pins.

The morphology of the wear tracks is shown in the secondary electron micrographs of Figures 56 through 59. A comparison of Figures 56 and 57a for Si_3N_4, and Figures 58a and 59 for the zirconia, indicate that the wear tracks of the low μ_f disks have a finer structure than those of the corresponding high μ_f disks. The mechanism of wear appears to be that of delamination as first suggested by Suh[37], where material is removed in thin sheets by a shear-type deformation. The delamination generally occurs at the implanted layer-substrate interface, with the high μ_f disks showing a much larger degree of such delamination than the low μ_f disks. For the Si_3N_4 case, this can be seen in Figures 57b through 57d, where the flat regions, examples of which are indicated by the arrows, correspond to regions of silicon and lack of the implant layer as seen in the Auger peak maps. The low μ_f Si_3N_4 disk also shows a delamination type of wear, seen by streaks of silver left where laminates have shadowed the neighboring region from the ion beam, Figure 56, but little sign of the substrate was observed. Implant-substrate delamination is more obvious on the low μ_f zirconia disk, Figure 58a through 58c, where arrows again indicate examples of where the substrate appears (Zr (147 eV) signal). The high μ_f zirconia disk, however, clearly shows the greater degree of delamination, Figure 59, where the dark laminates consist of titanium and nickel, and the light areas are zirconium oxide.

While quantitative depth analysis of these specimens is made difficult due to surface roughness and composition induced preferential sputtering, elemental depth profiling has provided useful qualitative information about the chemistry of the observed wear tracks. Elemental depth profiles taken at various points on and away from the wear tracks indicate that, under the temperature and/or pin pressure conditions of the tests, the composition profile of the implant layer had changed considerably during the tests from that of the as-received disks, Figure 60.

Typical depth profiles taken away from the wear track are shown in Figure 61. In the case of the Si_3N_4 disks, Figure 61a, it appears that the titanium layer has retained its profile while the nickel has diffused to the surface of the disk. While not obvious from the profiles themselves, examination of the individual spectra used to make up the silicon profiles indicate that silicon becomes detectable approximately halfway through the profile. The titanium profile has also been retained on the zirconia disk, Figure 61b, but the layer is not as thick as that on the Si_3N_4 disk, nor is nickel present on the surface. Zirconium was not detectable until near the end of the implanted layer. The implanted layer on both types of disks were clearly oxidized under the test conditions. The shape of the oxygen profile follows that of the titanium layer and changes in the titanium Auger spectra were similar to those observed for the pins, as shown in Figure 62. This definitely does not, however,

28

preclude the fact that the nickel layer may also be oxidized, since the nickel profile was flat.

Nickel tends to vaporize fairly easily at high temperature. A loss of nickel at the surface of the disks would thus not be unexpected. However, the presence of nickel on the surface of the Si_3N_4 disk, along with evidence of mixing of the substrate, indicates that the implanted layer may be better bound to Si_3N_4 than to zirconia. This could also be concluded from the SEM observations, where both the low and high μ_f zirconia disks exhibit more exposed substrate than the corresponding Si_3N_4 disks.

A typical elemental depth profile from the implanted layer left on the wear track is shown in Figure 63. This example from a Si_3N_4 disk shows a small amount of nickel at the surface, followed by the titanium layer mixed with nickel. This is in contrast to the unworn areas which showed a thicker surface nickel layer as measured by sputter time. Slight variations in the thickness of the surface nickel layer on the wear tracks were noted depending on how high or low a particular lamination was situated relative to its surroundings. The laminates left on the zirconia disk wear tracks showed virtually no surface nickel. The pins run against them did, however, show a large amount of nickel. Analogous to the case of the unworn areas, it is possible that nickel diffused to the surface of the disks and then transferred to the pins. The fact that some nickel remained on the surface of the Si_3N_4 disks and not the zirconia disks again indicates that the implant layer may be better bonded to Si_3N_4.

The thickness of the laminates could not be determined because of surface roughness effects on sputtering. Low regions, especially any exposed substrate, tended to be preferentially sputtered, making the laminates appear very thick. Assuming that nickel was removed from the surface (and possibly deposited on the pins), it would be logical to assume that the laminates would be thinner than the original implant layer. It is also possible, however, that material could have piled up locally on the wear track. The pin would then be riding on this raised lamination layer. This does not seem as likely, since a pileup would be indicated by a significant compositional change in the depth profiles, rather than just the removal of surface nickel.

Further evidence for the better mixing of the implant layer on Si_3N_4 rather than zirconia was obtained from analysis of the delaminated regions of the wear track. A thin layer of nickel generally covered these regions, although the substrate signal appeared fairly strong. Upon sputtering however, the nickel signal disappeared fairly rapidly from the zirconia disks, while it remained for some time on the Si_3N_4 disks.

Results of Analyses on Cobalt-Implanted and Nickel-Implanted Disks

The results of the tests on cobalt implanted disks showed behavior in some ways similar to the titanium-nickel implanted disks. The cobalt implanted zirconia disks

29

showed a low coefficient of friction when run against the Ni-Mo-TiC pin and a much higher value when run against the TiC pin. However, unlike the titanium-nickel case, the Si$_3$N$_4$ disks showed no improvement when ion-implanted with cobalt.

Auger analysis of the cobalt implanted zirconia disks and the corresponding pins indicates that cobalt transfers from the disk surface to the pins. Elemental depth profiles indicate that both the pin and the disk cobalt layers are oxidized, implying the presence of a lubricating cobalt oxide film analogous to the titanium-nickel case. Disturbing, however, are the physical characteristics of the wear tracks, especially for the low coefficient of friction disk. Both wear tracks showed delamination of the cobalt layer, leaving exposed substrate. The wear track of the low coefficient of friction disk varied in width and amount of wear, ranging from the width of the pin and wear as heavy as that visible on the other three disks, to areas where the wear track is practically non existent. It is thus possible that the zirconia/Ni-Mo-TiC results were influenced by the alignment of the pins and disk. In any case, the cobalt results indicate the transfer and possible lubricating effect of a cobalt oxide layer.

The surface of the Ni-Mo-TiC pin also showed the strong presence of nickel. This indicates that nickel segregates to the pin surface, and may play a role in the friction and wear behavior of ceramic couples. This also implies that nickel may have segregated from the pins in the case of the TiNi implant tests, but would not be observable due to the nickel component of the implanted layer.

The results of the titanium-nickel and the cobalt implanted disks indicate that nickel may play a role in the friction and wear behavior of ion-implanted ceramics, either as a part of the implanted layer, or due to its presence in the pins. Therefore, two Si$_3$N$_4$ disks were ion-implanted with a layer of nickel, and tested in diesel environment at 800°C and at room temperature.

The results of the friction and wear tests indicated that nickel improved the coefficient of friction of Si$_3$N$_4$, but not to the degree as that of the titanium-nickel implants, or the cobalt in zirconia implant. Analysis of the wear surfaces of the disks and the pins showed that the nickel layer was completely worn off the disk, and that no nickel transferred to the pins. The wear track showed cracking, especially near the edge of the crack, typical of the wear tracks of unmodified ceramics. The pin surfaces showed clear signs of wear, as opposed to the adherence of a transfer layer seen in the case of titanium-nickel and cobalt. Examination of the unworn areas after testing showed, however, that the nickel layer was much better mixed into the substrate than in the two previous cases.

C. Piston Ring and Cylinder Liner Tests

1. Friction Rig Tests

Following the pin-on-disk screening tests, piston rings and liners produced using the selected material combination (reference Figures 4 and 5) were subjected to friction

30

rig tests. Axial thrust load, related to ring/cylinder friction force, was measured versus crankangle as a basis for comparison.

Figure 64 illustrates typical friction force traces obtained with the baseline cast iron rings and liner under normal hydrodynamic lubrication conditions. As the relative velocity between the rings and liner approaches zero near the ring reversals, friction force "spikes" are observed. These friction spikes are caused by the loss of the hydrodynamic oil film created by the ring's speed. As the ring reverses direction, hydrodynamic lubrication is resumed and the friction force is reduced. The remainder of the stroke indicates typical hydrodynamic behavior. The traces obtained at 1200 rpm indicate similar results although more noise was present in the signal.

Figure 65 illustrates typical friction force traces for the ceramic material combination no. 1 under boundary lubrication. Boundary lubrication is defined as the condition where the lubricating layer is only of molecular thickness, and is readily absorbed into the material surface rather than forming a lubricant film. The characteristics of these traces are similar to those of the cast iron baseline. It was hoped that the ion-implanted ceramics would result in the elimination of the friction "spikes" at the ring reversals. This idea was based on the formation of the kinds of lubricious oxides which were observed during the pin-on-disk work. Unlike hydrodynamic lubrication, a lubricious oxide has the potential of providing significant lubrication at the ring reversals since it does not depend directly on piston speed for lubrication. However, the friction rig tests were conducted at much lower temperatures than those required to form the lubricous oxide. The need to lubricate the reciprocating liner with conventional lubricant from the crankcase prevented significant heat from being applied to the test region. Typical ring groove temperatures observed for the cast iron and ceramic rings ranged from 100 to 150°F. The maximum ring groove temperature measured was 221°F for ring set 2.

The ceramic rings and liner from material combination no. 1 were tested under boundary lubrication and non-lubricated conditions. These tests indicated very little difference in friction force for the two lubrication conditions as shown in Figure 66.

A summary of the friction rig results for material combination no. 1 is shown in Figures 67 and 68. Under non-lubricated conditions at 800 rpm, ring sets 1 and 3 showed approximately a 50 percent reduction in friction compared with the cast iron rings and liner under hydrodynamic lubrication. It should be noted, however, that ring sets 1 and 3 had a lower ring tension (normal force) than the cast iron rings. The results for ring set 2 were obtained just prior to breakage of one of the rings. Subsequent investigation indicated that an inadequate ring end gap was responsible for the ring failure. As a result, the normal force for the ring set 2 was unpredictably high and most likely caused the friction to be higher than normal.

At 1200 rpm, the friction force for ring sets 1 and 3 approached that of the cast iron baseline. It is interesting to note that the friction "spikes" at the ring reversals were eliminated for ring set 3. One explanation for this result is that, at the higher

speed, enough micro-localized heat was generated by shearing of the surface asperities of the two materials to cause the local formation of lubricious Ti and Ni oxides. This could have provided lubrication needed at the ring reversals to reduce friction at those points.

Friction results are not shown for ring set 4 since one of the rings broke during installation of the stationary piston into the reciprocating liner. The fracture surface of this ring was analyzed. Figure 69 shows a cross-sectional view of the failed surface of the ring and an SEM photomicrograph of the surface at 500X. The latter shows the presence of a cavity along the outer ring surface where the ring stress was the greatest; higher magnification study (Figure 70) indicates that ring failure was caused by this 15 μm diameter cavity introduced during fabrication.

Friction rig tests were not conducted for material combination No. 2 (hot-pressed TiC rings and Si_3N_4 liner). These components were unavailable for testing due to fabrication problems.

The hot-pressed TiC piston rings were broken by the supplier during final grinding operations. The inability of the supplier to fabricate these rings indicates the poor feasibility of TiC for use as piston rings.

Inspection of the Si_3N_4 liners supplied to SwRI indicated small (0.5" diameter) mottled regions within the material; a photograph of one of the liners is shown in Figure 71. The regions in question were discolored, and penetrated the full thickness of the liner wall. No differences in surface finish were noticed between these regions and the normal material. The vendor was contacted, and the liners were returned for their analysis and comments. It was determined that the discolored regions were caused by an over-abundance of sintering aid, which segregated out of the grain boundaries during sintering. However, the supplier claimed that their experience indicated that the relevant mechanical properties of the material were not effected.

2. Engine Tests

Baseline data for the single-cylinder diesel research engine was obtained using cast iron components. These were run at 180°F coolant temperature prior to initial testing of the ceramic components.

Engine testing with the ceramic components began by motoring the engine under preheated conditions of 180°F coolant temperature and 160°F oil temperature. Motoring tests began at 500 rpm with blowby and motoring friction measurements being taken. Data were also obtained at 700 and 1000 rpm. The engine apparently seized during the attempt to motor at 1500 rpm.

Following a brief cool-down and a visual and manual check for free rotation, the decision was made to attempt to run the engine again before disassembly. The

32

engine started and data was taken at 1000 rpm under light load. Under these load conditions, occasional misfire was experienced. This was considered to be due to the use of the low tension set of Ni-Mo-TiC rings and their inability to seal consistently under hydrodynamic conditions. The load was then increased to approximately 25 percent of full load and combustion became much more stable. A full set of data was taken at this point and the load was increased to 40 percent of full load. The engine seized at this condition before blowby measurements were completed.

The engine was then disassembled for inspection. There was no evidence of damage to the PSZ liner or Ni-Mo-TiC piston rings. However, the aluminum piston skirt showed signs of heavy scuffing and material removal. This is shown in Figure 72. The scuffing pattern was typical of inadequate piston-to-bore clearance. The skirt was reground to provide assured clearance, and oil cooling to the piston skirt area was increased.

Engine testing with the ceramic components continued at 180°F coolant temperature after the piston-to-bore clearance was increased from .002 inches to .015 inches. Increased oil cooling was provided to the piston skirt by drilling additional holes in the small end of the connecting rod.

Thirty hours of engine testing were accomplished with the low-tension, Ni-Moly bonded TiC piston rings and TiNi ion-implanted PSZ cylinder liner at 180°F coolant temperature. The majority of the run-time was performed at 1000 rpm, 40 percent load conditions. Exceptions to this occurred at five hour increments where performance data were obtained.

Blowby fluctuated significantly during the 30 hours of testing with the ceramic rings and liner. This is shown in Figure 73. The magnitude and variation of the blowby indicates poor ring sealing most likely caused by the combination of low ring tension and hydrodynamic lubrication.

Performance results for the thirty hours of run time using the ceramics are shown in Figure 74. This figure plots BSFC versus engine hours for the ceramic engine running at 1000 rpm, 40 percent load, and 180°F coolant temperature. The BSFC varied around .70 lb/bhp-hr for the first 20 hours and dropped to approximately .64 lb/bhp-hr for the next three to four hours. The BSFC increased to .67 lb/bhp-hr toward the end of the test. This variation in BSFC with run time cannot be correlated with variations in ring sealing, according to the blowby results in Figure 73. However, the ceramic component motoring friction decreased significantly (19 percent at 1000 rpm) from zero hours to twenty-five hours, as illustrated in Figure 75. Although the reduction in motoring friction is not completely understood, polishing of the piston skirt could have been responsible. Surface finish measurements of the TiNi implanted PSZ liner were taken before and after the thirty hour engine test, as shown in Figure 76. The PSZ liner had a 25 μ in surface finish before installation in the engine (Figure 76a), and it remained virtually unchanged (24 μ in) after thirty hours of engine operation (Figure 76b). The surface finish of the narrow, bright regions shown in Figure 81 was smoother (7μ in) than

33

the metallic regions (Figure 76c). The wear results of the PSZ cylinder liner are discussed in more detail in the Wear Results section.

Figure 77 shows a reduction in motoring friction for the ceramics compared with the baseline cast iron components after the first few hours of break-in. As illustrated in Figure 75, the motoring friction for the ceramics decreased with engine hours at all speeds tested.

Similar reductions in BSFC were observed with increasing engine hours, as shown in Figure 78, comparing BSFC versus BHP for the ceramics and the cast iron baseline operating at 1000 rpm. This figure shows a significant advantage, in terms of fuel efficiency, for the cast iron components. However, the BSFC for the ceramics demonstrated a strong trend toward the baseline BSFC during the first twenty five hours of run time. The lower fuel consumption observed for the cast iron components is attributed to their higher ring tension and improved sealing characteristics.

3. Wear Results

Wear trends were determined for the friction rig and engine tests using weight loss measurements and visible inspection. Weight loss measurements were recorded for each of the ceramic rings before and after testing on the friction rig. The results of these measurements are given in Table 4. The nominal run time for each of the ring sets was 10 to 20 hours, with the exception of ring set 1 which accumulated approximately 50 hours of run time on the friction rig.

Table 4. Friction Rig Ceramic Piston Ring Weight Loss Measurements

Ring Set	Ring No.	Weight Before (gm)	Weight After (gm)
1	1	7.9300	7.8913
1	2	7.9034	7.9027
2	1	11.4	11.4
2	2	10.7	10.7
3	1	7.6	7.6
3	2	7.6	7.6
4	1	11.3342	11.3300
4	2	11.2196	11.2145

Ring set 1 experienced an average weight loss of 19.7 mg per ring during approximately 50 hours of run time. No visible signs of scuffing or wear were observed on the rings or liner.

No measurable wear was observed for ring sets 2 and 3 using the weight loss technique. In addition, no scuffing or visible wear patterns were noted, despite the fact that the top ring of ring set No. 2 broke into nine separate pieces during the tests.

Ring set No. 4 experienced an average weight loss of 4.65 mg per ring during its brief test period. The test duration was short for ring set No. 4 due to the early breakage of its top ring; the latter was discussed in detail in a previous section. However, the resulting scuff patterns (Figure 79) on the TiNi implanted PSZ liner were not discussed.

Several observations were made based on the scuffed liner and rings from ring set No. 4. As the weight loss measurements indicate (Table 4), wear of the broken and unbroken rings was almost identical, suggesting that very little material was removed from the broken Ni-Mo-TiC ring as it scuffed the liner. A soft, powdery substance, most likely removed from the liner during scuffing, was found on the piston. The scuff material was analyzed using energy dispersive spectroscopy (EDS). This analysis is shown in Figure 80 and indicates that the scuffed material consisted of 96.73 percent zirconia, 0.74 percent titanium, 0.72 percent nickel, 0.20 percent chromium and 1.61 percent hafnium. The zirconia, Ti, and Ni are assumed to have been removed from the liner. There is no evidence of ring material present in the scuffed material sample. This is significant since it suggests that the Ni-Mo-TiC piston rings have exceptional wear resistance, even under severe scuffing conditions. In general, the absence of piston ring wear during the friction rig tests is attributed to the high hardness of the Ni-Mo-TiC material, the relatively low gas loads and temperature conditions at top ring reversal, and the short duration of the tests performed.

Piston ring wear during the engine tests also was determined using weight loss measurements, as shown in Table 5. These measurements indicated no measurable ring wear for the engine tests.

Table 5. Ceramic Engine Test Piston Ring Weight Loss Measurements

Ring Set	Ring No.	Weight Before (gm)	Weight After (gm)
1	1	7.9	7.9
3	2	7.5	7.5

A teardown of the engine after thirty hours of run time with the ceramics was performed. Photographs of the liner and piston are shown in Figures 81 and 82, respectively. The liner appeared to have visible signs of wear at the top ring reversals (TRR's) for the ceramic top compression ring and the cast iron oil control ring. Ring reversal was less noticeable for the ceramic second compression ring. This was probably caused by the lower gas loads and increased oil film present on the second compression ring compared with the top compression ring. The liner also showed visible indications of axial wear patterns which gave the impression that the ion-implanted Ti and Ni may have been transferred to the rings, as observed in the preceding pin-on-disk tests. SEM and Energy dispersive spectroscopy (EDS) were used to analyze the cylinder liner surface as shown in Figures 83 through 85.

An SEM photograph of the cylinder liner at TRR after 30 hours is shown in Figure 83. This photograph illustrates very sharp surface asperity peaks and valleys in the radial direction. These cuts are opposite to the piston's direction of travel and are most likely the result of diamond grinding before engine operation. The clear distinction of each cut suggests that very little wear of the cylinder occurred at TRR during the first thirty hours of testing. Faint regions of darker and lighter streaks in the direction of piston travel can also be distinguished on the photograph. These are probably the streaks which are seen in Figure 81 and could have been caused by removal of the asperity peaks and possible filling in of the valleys.

The chemical composition of the PSZ liner after 30 hours was determined using EDS techniques. EDS analyses were performed on the dark and light regions at TRR and on the baseline portion of the liner below bottom ring reversal (BRR). These results are shown in Figures 84 and 85.

An EDS comparison of the dark and light regions at TRR is made in Figure 84. This figure shows almost identical compositions for the two regions, although slightly higher Ti, Ni, and Fe concentrations were recorded for the light region compared with the dark. This suggests two results. First, the higher Ti and Ni count for the light region indicates that material was deposited in this region, filling in the surface asperity valleys. This conclusion agrees with the surface finish measurements made in Figure 76. Also, the presence of iron (Fe) suggests that material was removed from the oil control ring and transported to the TRR area by the lubricating oil.

Since virtually no difference in chemical composition was found between the dark and light regions at TRR, a comparison was made between the TRR location and the unworn portion of the liner below BRR. This comparison is given in Figure 85. The BRR location can be considered as a baseline material condition before running in the engine, since neither the piston skirt or rings rubbed against this surface.

Higher levels of Ti were found in the baseline area compared to the TRR region, with very little sign of Ni. This can be explained by the ion-implantation process, where a layer of Ni was deposited first, followed by a layer of Ti. Thus, the baseline region showed high levels of the surface layer component. However, some of the

Ti was evidently worn away, exposing more of the Ni at TRR which yielded a lower Ti level and much higher Ni level. The TRR region also had a noticeably higher level of iron present.

An investigation of the piston and rings (Figure 82) showed typical polishing marks on the top compression ring. However, the second compression ring was polished only near the ring ends and around the outside of the ring opposite the end gap. Evidence of blowby and poor sealing was present on either side of the polished areas at the end gap. This could have been caused by the low ring tension, reduced gas load, or ovality in the piston ring. The piston skirt also showed atypical polishing marks due to the non-conventional method used to reduce the skirt diameter to allow for thermal expansion inside the ceramic cylinder liner.

37

IV. DISCUSSION OF RESULTS

The friction and wear behavior of the unmodified ceramic couples which were tested during the first phase reflected the important roles of environment and temperature. Overall, the friction results for the unmodified ceramics were disappointing. However, the results of the modified ceramic couples showed significant improvements in friction coefficient. These results were duplicated with the friction test rig, in which the surface-modified piston rings and cylinder liner demonstrated low friction under non-lubricated conditions. Single-cylinder engine tests showed a lowering trend in motoring friction with increasing engine hours. The Ni-Mo-TiC piston rings and PSZ liner tested in the friction rig and engine showed good promise for LHR engine application.

A. Unmodified Ceramics

When disk (and heavy pin) wear was observed in laboratory tests, it usually was in the form of delamination. This is a form of adhesive wear, in which intermittent contact nucleates shallow subsurface cracks which eventually grow to the surface, creating a thin delaminated sheet of material. This is similar to delamination which has been observed in metals[38] and in ceramics[39], and modeled based on a theory[37,40] of cyclic crack growth. However, in the present case, delaminate sheets often form within only a few passes, possibly even one pass. This was observed by Yamamoto and Buckley[41] for 304 stainless steel wear sheets produced by sliding against Al$_2$O$_3$. In fact, the photomicrographs of wear layers in the steel alloy studied by the latter look almost identical to those observed (Figures 39 and 40) in the present ceramics. Prevention of this process must involve either 1) provision of sufficient lubrication to inhibit ceramic-ceramic adhesion, and/or 2) increase in the near-surface crack growth resistance of the delaminating material.

Although the friction coefficients of all of the unmodified couples exceeded 0.2, there were encouraging results regarding wear resistance. For those cases in which TiC or Ni-Mo-TiC material was transferred to disks in the form of titanium oxide films, disk wear was essentially non-existent (unmeasurable via surface profilometry), and pin wear did not appear to be high once the initial sacrificial material transfer was accomplished. Apparently these films, which can form from room temperature to 800°C, are lubricious, in terms of wear.

B. Surface Modified Ceramics

The true potential of the films, of course, seems to have been realized by first ion-implanting and then oxidizing the ceramic disks. Under these circumstances, titanium oxide, nickel oxide, and cobalt oxide transfer selectively, i.e., from certain disks to certain pins (Figures 86 and 87), and serve as liquid-like lubricants at the operational temperature. Based on the results of Breznak, et al[39], it would be reasonable to suspect that the temperature rise at the sliding interface was at least 300°C above the test temperature of 800°C, hence the lubricant temperature

probably was at least 1100°C. This should be sufficient to significantly enhance the viscosity of a ternary or quaternary alloy (oxide). In this regard, it is interesting to note that the friction coefficient of Ni-implanted Si_3N_4 run against TiC on diesel exhaust was 0.14 at 800°C, but rose to 0.4 when testing was performed at room temperature. Evidently the NiO, which was observed to transfer during sliding, was not sufficiently hot at 23°C (plus ~300°C due to sliding contact) to serve as an effective lubricant. TiNi implanted Si_3N_4 run against TiC on diesel exhaust produced the lowest friction coefficient of 0.06 at 800°C.

It should be borne in mind that work to date has emphasized relatively short term tests designed to screen, and provide specimens to evaluate the best pin-disk couples. It will be very important to evaluate the ability of the self-lubricating couples which have been identified to maintain their desirable traits over extended operating time.

The results of the Auger Electron Spectroscopy surface investigation into the wear of ion-implanted ceramic disks indicate that several factors may govern the wear properties of these materials in the high temperature environment used. These include the adhesion of the implanted layer to the ceramic, the transfer of material between the surfaces of the pins and disks, and the chemical state of the disk surface material (oxide) and the pin material.

The adhesion at the implant layer-ceramic boundary is clearly important in a delamination type of wear, since this would be the weakest interface. Both the micrographs and depth profiles indicate that for the TiNi implanted disks, the TiNi layer adhered better to the Si_3N_4 than the zirconia in the low as well as the high μ_f Si_3N_4 disk. Small amounts of relatively bare substrate were occasionally detected, thus raising the possibility that a longer term test might result in the eventual removal of the implanted layer on all of the disks. The wear resistance of the layer on Si_3N_4 would then be of only temporary benefit. The cobalt and nickel layers did not appear to be bound as well to their respective substrates. It may be noted here that chromium implantation produced no beneficial effects in either disk material. On the contrary, it was almost completely worn off, leaving virtually no trace on the wear track, thus indicating poor adhesion to the substrate.

The transfer of material, or the formation of a surface oxide has been shown to be beneficial to the wear characteristics of many systems[42,43]. In the present case, nickel appears to have been transferred from the disks to the pins, or vice versa as indicated by the results obtained from the pins run against the Co-implanted disks. Although it is highly likely that titanium transferred to the pins, it was not possible to determine definitely whether or not this was the case; a radioactive tracer technique would be useful in the case of either nickel or titanium. There is no doubt that the titanium present in both the pins and the implant layer has been oxidized. It is not clear whether one, or both, processes, nickel transfer and/or implant layer oxidation, are required to improve wear characteristics. Wear tests run at high temperatures in argon showed poorer wear characteristics than in the oxygen containing diesel environments, even though material transfer took place. However, as will be discussed shortly, TiC and Ni-Mo-TiC pins run against unmodified ceramic

disks showed better wear characteristics than other pin materials, due to the transfer and oxidation of titanium from the pins to the disks.

Related to the material transfer question is the choice of pin material. For the present pin disk combinations involving the TiNi implant, the pin material played a confusing role. Nickel was clearly transferred to all four pins, but the two pin materials had opposite effects with respect to disk material in couples 1 through 4. On the other hand, nickel segregated from the Ni-Mo-TiC pins may have played a role in the case of the Co-implanted disks. This behavior is at the moment not understood. However, the choice of pin material has played a major role in other pin-disk systems. TiC or Ni-Mo-TiC pins have produced lower coefficients of friction than silicon carbide pins when run against unmodified Si_3N_4 and zirconia, and chromium implanted Si_3N_4 and zirconia, disks. This probably is due to the fact that titanium transferred from the pins to the disks, while silicon did not (as observed using energy dispersive spectroscopy, EDS).

The results of the tests conducted on disks implanted only with nickel indicate that while nickel alone does not improve the friction and wear behavior of ceramics as well as other implant species, it may help provide better bonding of those species and/or their lubricating oxides. In the case of the titanium-nickel implants, titanium oxide appears to be responsible for the improved friction and wear behavior, but the nickel layer appears to be the bonding species which mixes into the substrate, especially in the case of Si_3N_4. In the case of the cobalt implant, segregation of nickel from the Ni-Mo-TiC pin may be responsible for the transferred cobalt adhering to the pin surface at least temporarily, thus delaying the degradation of the friction and wear properties due to the removal of the cobalt layer from the disk surface. Further work is required to determine the influence of nickel on the bonding and/or friction and wear behavior of ion-implanted ceramics. Also of interest would be to determine those species which can be coupled with nickel in an implant layer to provide those beneficial results. For example, the implantation of chromium alone apparently had no beneficial influence on the friction and wear behavior of either Si_3N_4 or zirconia, even when run against Ni-Mo-TiC pins. Chromium ion-mixed with nickel might do much better.

C. Piston Ring and Cylinder Liner Tests

Friction results obtained with the friction test rig showed little difference in friction between the baseline cast iron components and the ceramic rings and liner. This is significant because the cast iron components were tested under full-film hydrodynamic lubrication and the ceramics were tested without any lubricant. These results agree with the pin-on-disk studies, in which friction coefficients observed for the TiNi ion implanted PSZ and Ni-Mo-TiC running dry at 800°C were similar to those normally found for hydrodynamic cast iron components. However, the friction levels observed for the unlubricated ceramics in the friction test rig were measured at much lower temperatures (approximately 65 -100°C) than those required for oxide formation on the pins and disks.

41

Although no analyses were performed to determine the presence or absence of lubricious oxide on the piston rings, the difference in relative velocities between the rings and liner and the pins and disk could explain the low friction at lower temperatures. Maximum relative velocities between the piston rings and cylinder liner were 4 ^{m}/sec and 6 ^{m}/sec at 800 and 1200 rpm, respectively, in the friction rig. The relative velocity between the pins and disk was constant at 1 ^{m}/sec. It is possible that the higher surface speeds and higher resultant friction heat with the friction rig could have led to the formation of lubricious oxides at lower temperatures.

In general, the Ni-Mo-TiC material shows good promise for application to piston rings. However, some piston ring breakages were experienced. One failure was the result of inadequate ring end gap clearance and the other resulted from a material flaw in the ring surface. Once the processing control of this material has advanced to the technological level required, it should make a fine piston ring material. Likewise, no problems were encountered with the PSZ, although its high thermal insulating characteristics could prevent its widespread use in certain internal combustion engines. The high insulating properties lead to higher surface temperatures and reduced charge air density.

The single-cylinder, diesel engine tests demonstrated the overall feasibility of these materials for engine application. Thirty hours of run time were accumulated with the ceramic rings and liner with no signs of ring wear, and very little evidence of liner wear. In addition, the ceramic liner and rings were subjected to two engine seizures due to piston scuffing without breakage of the ceramic components.

Ceramic engine performance was characterized by high combustion gas blowby with random variations, a reduction in motoring friction with run time, and relatively high BSFC values compared with the cast iron baseline. The high blowby values with the ceramic rings were caused by low ring tension levels compared to the cast iron rings. The random variation in blowby indicates inconsistent ring sealing and points out the need for improved ring design with the ceramic material. The reduction in friction with run time could have resulted from piston skirt polishing with little cause or effect from the ceramic components. The high BSFC values observed for the ceramic engine were attributed to the poor ring sealing and resultant decrease in mechanical efficiency.

Material problems encountered with the piston rings and cylinder liners indicate the need for improvements in the processing of these components. Failure of the Ni-Mo-TiC piston ring was caused by a surface cavity in the material. Breakage of the TiC rings during final machining by the supplier probably was related to the material's high elastic modulus and relatively low transverse rupture strength. Finally, the silicon nitride liners displayed visible signs of inconsistent material processing, evidenced by numerous agglomerated regions involving excess sintering aid. Gas pressure sintered Si_3N_4 (GPSSN) could provide significant improvements in the material properties[44], by reducing the amount of sintering aid.

42

V. CONCLUSIONS

Friction and wear tests have been conducted on a variety of ceramic/ceramic couples in the unmodified state or surface modified by ion-implantation in both Argon and an environment typical of high temperature adiabatic diesel engines. It has been found that:

- Low friction coefficients for unmodified ceramic couples correspond to the formation of lubricious oxide films.

- Oxide film formation depends on disk/pin combination, temperature, and environment.

- Wear rates are low only when either lubricating films or (possibly) rolling element particles are formed.

- The most common and destructive mode of wear is delamination.

- For unmodified ceramic pin/disk combinations, the lowest friction coefficient obtained was 0.24, and the highest coefficient was 1.24.

- Ion-implantation of disks with TiNi or CO reduces coefficients of friction at 800°C in simulated diesel exhaust environment to 0.06 - 0.09, for certain specific pin-disk combinations.

- Ni-Mo-TiC piston rings/PSZ cylinder liner appear to be attractive candidates for the LHR diesel engine.

- TiC rings/Si_3N_4 liner appeared to be a candidate combination after pin-on-disk tests, but low tensile strength of TiC is not feasible for piston ring application.

- The combination of Ni-Mo-TiC rings running against a TiNi implanted Si_3N_4 liner could be a strong candidate for engine application.

- The Ni-Mo-TiC rings used in the tests exhibited inconsistent material properties partially attributed to the presence of crack initiating surface cavities.

- There is a strong need for improved manufacturing process controls used for fabrication of these advanced materials.

- A great deal of work remains to be done in this area, particularly in the areas of processing and quality control of the ceramic materials, and friction research of candidate materials under varying lubrication and temperature conditions.

43

VI. RECOMMENDATIONS

The following recommendations are based on the results and observations formed during this project.

- Additional friction and wear studies should be conducted with actual rings and liners of several materials under varying lubrication and temperature conditions.

- Friction and wear tests should be conducted for Ni-Mo-TiC rings running on a TiNi implanted Si_3N_4 liner.

- The differences in reciprocating friction and wear should be investigated for unmodified and surface modified ceramics using the friction rig at temperatures between 70°C and 200°C.

- Extensive research should be conducted to determine the relationships between manufacturing processes for ceramic materials and their material properties.

45

REFERENCES

1. D. J. Godfrey, Paper No. 45 in Ceramic for High Performance Applications II, J. J. Burke, E. N. Lenoe, and R. N. Katz, editors, pp. 877-892 (1978).

2. R. Kamo and W. Bryzik, SAE Paper No. 490645 (1979).

3. Anonymous, Automotive Engineering 88: 60-68 (1980).

4. Alex P. Bronwers, NASA Contractors Report No. 756, NAS3-20830 (1979).

5. D. J. Godfrey, Trans. SAE 83: 1036-1045 (1974).

6. R. Kamo, M. Woods, T. Yamada, and M. Mori, ASME Paper No. 80-DGP-14 (1980).

7. Donald H. Buckley, Ceramic Bulletin 51: 884-905 (1972).

8. Kazuhisa Miyoshi and Donald H. Buckley, Wear 77: 253-264 (1982).

9. Kazuhisa Miyoshi and Donald H. Buckley, ASLE Trans. 22: 146-153 (1979).

10. D. H. Buckley and K. Miyoshi, Wear 100: 333 (1984).

11. B. R. Lawn and A. G. Evans, J. Mat. Sci. 12: 2195 (1977).

12. A. G. Evans and D. B. Marshall, "Wear Mechanisms in Ceramics," Fundamentals of Friction and Wear of Materials, ASME, Metals Park, OH, 439 (1980).

13. M. V. Swain, Wear 35: 185 (1975).

14. B. R. Lawn, S. M. Wiederhorn, and D. E. Roberts, J. Mat. Sci. 19: 2561 (1984).

15. R. P. Steijn, Wear 7: 48-66 (1964).

16. D. J. Barnes and B. D. Powell, Wear 32: 195-202 (1975).

17. H. Shimura and Y. Tsuya, Proc. Int. Conf. Wear of Mats., St. Louis, April 1977, ASME, N.Y., 452 (1977).

46 INTENTIONALLY BLANK

18. E. F. Finkin, S. J. Calabrese, M. B. Peterson, ASLE Preprint No. 72LC-7C-2 (1972).

19. L. B. Sibley and C. M. Allen, Wear 5: 312-329 (1962).

20. Advanced Mechanical Technology, Inc., "Evaluation of Improved Materials for Stationary Diesel Engines Operating on Residual and Coal Based Fuels," U. S. Department of energy Contract No. DE-AC-03-79ET15444 (1980).

21. H. S. Shan and P. C. Pandey, Wear 32: 167-179 (1975).

22. Alan West (Advanced Mechanical Technology, Inc.), personal communication (1982).

23. A. G. Evans and E. A. Charles, J. Am. Cer. Soc. 59: 371 (1976).

24. B. Carriere, et al, Vacuum 22(10): 485-487 (1972).

25. B. Carriere and B. Lang, Surf. Sci. 64: 209-223 (1977).

26. F. Fransen, et al, Surf. and Interface Anal. 7(2): 79-87 (1985).

27. O. C. Wells, et al, in Scanning Electron Microscopy, McGraw-Hill Book Co., NY, 150-156 (1974).

28. H. L. Marcus, et al, in Fracture Mechanics of Ceramics Vol. 1 Concepts, Flaws and Fractography, R. C. Bradt et al, eds., Plenum Press, NY, 387-398 (1974).

29. C. G. Pantano and T. E. Madey, Appl. of Surf. Sci. 7: 115-141 (1981).

30. H. Viefhaus, Private Communication.

31. S. Hoffmann in Practical Surface Analysis by Auger and X-Ray Photo-electron Spectroscopy, D. Briggs and M. P. Seah, eds., John Wiley and Sons, Chichester, U. K., Ch. 4, 141-180 (1983).

32. H. E. Bishop, et al, Surf. Sci. 24: 1-17 (1971).

33. M. C. Burrell and N. R. Armstrong, J. Vac. Sci. Tech. A 1(4): 1831-1836 (1983).

34. L. E. Davis, et al, editors, Handbook of Auger Electron Spectroscopy, 2nd Edition, Perkin-Elmer Corp., Eden Prairie, Minn., (1978).

35. P. H. McBreen and M. Polak, Surf. Sci. 163: L666-L674 (1985).

36. P. H. Holloway and R. A. Outlaw, Surf. Sci. 111: 300-316 (1981).

37. N. P. Suh, Wear 25: 111 (1973).

38. S. Jahanmir, N. P. Suh, and E. P. Abrahamson, Wear 28: 235 (1974).

39. J. Breznak, E. Breval, and N. H. MacMillan, Jour. Mat. Sci. 20: 4657 (1985).

40. H. C. Sin and N. P. Suh, J. App. Mech. 51: 317 (1984).

41. Y. Yamamoto and D. H. Buckley, ASLE Trans. 26: 277 (1982).

42. D. H. Buckley, Surface Effects in Adhesion, Friction, Wear, and Lubrication, Tribology Series, 5, Elsevier Scientific Pub. Co., Amsterdam, (1984).

43. I. L. Singer, Appl. of Surf. Science 18: 28-62 (1984).

44. Y. Sato, "The Development of the Ceramic Turbocharger Rotor," Applications for and Designing with High Temperature Materials in Natural Gas Usage Seminar, Gas Research Institute and Center for Advanced Materials, Chicago, IL, April 6,7, 1989.

49

PRECEDING PAGE BLANK NOT FILMED

APPENDIX A

FIGURES
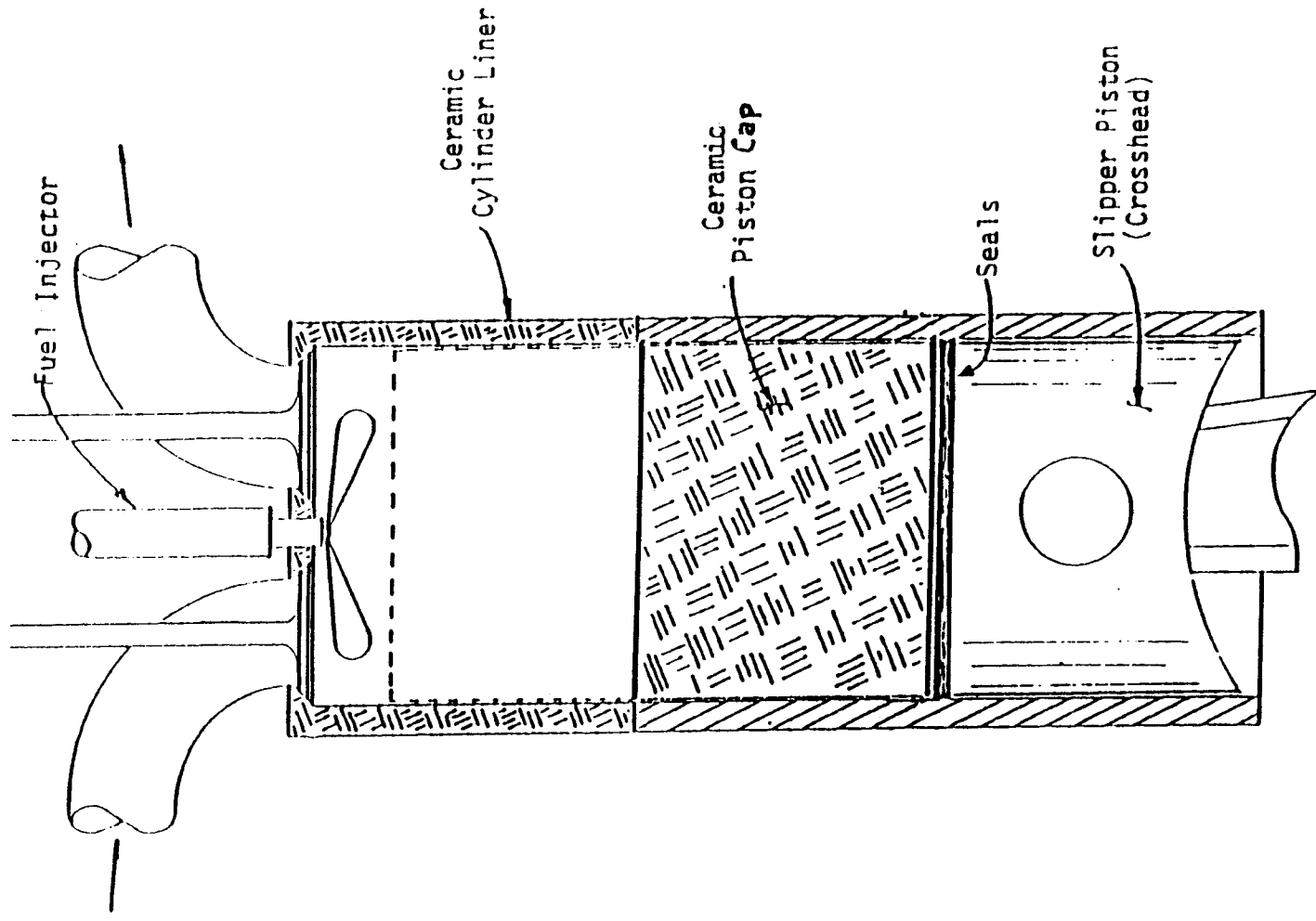
FIGURE 1. CROSSHEAD ENGINE SCHEMATIC

53
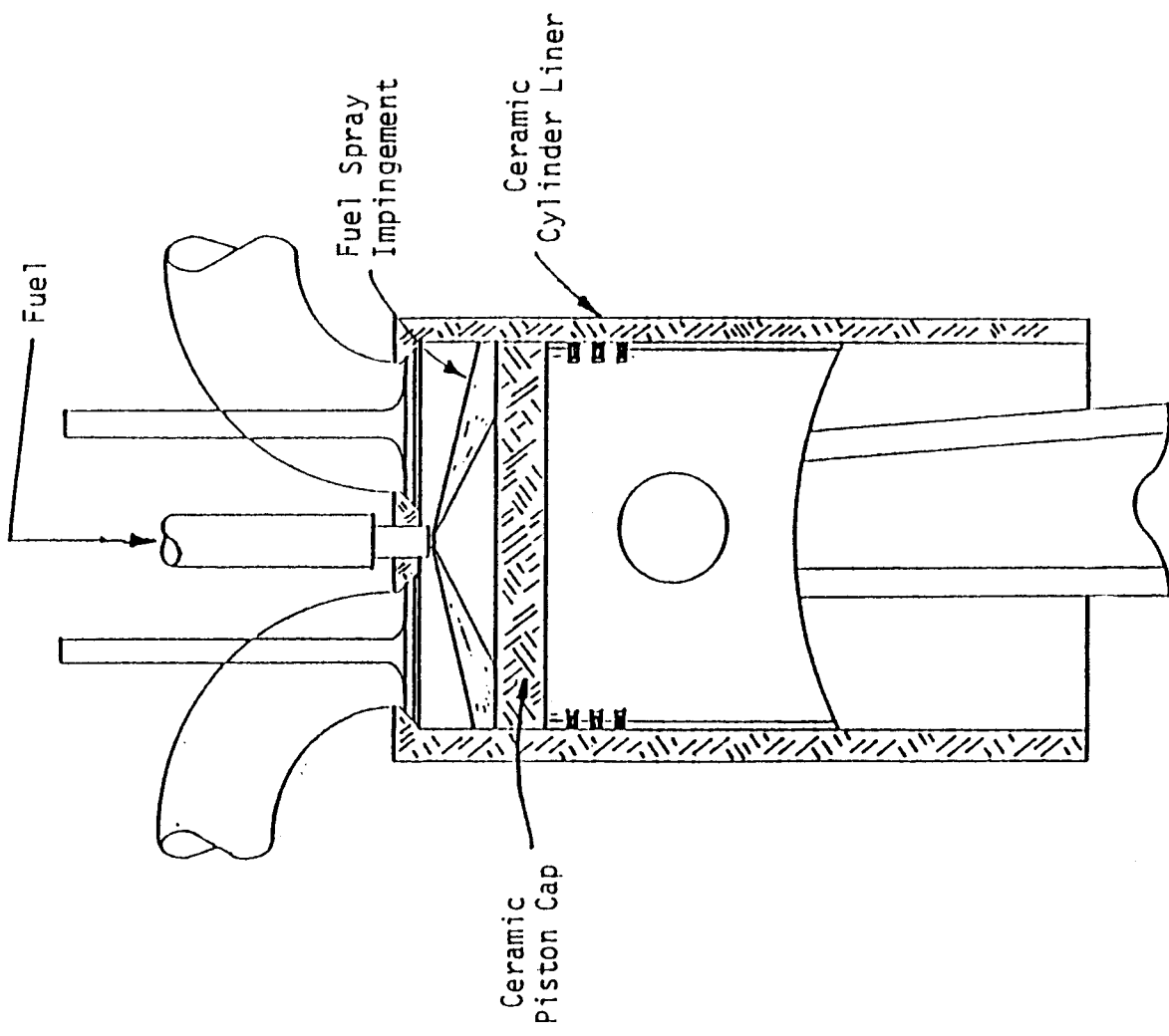
FIGURE 2. SCHEMATIC OF ENGINE WITH FULL-LENGTH
CERAMIC CYLINDER LINER

54
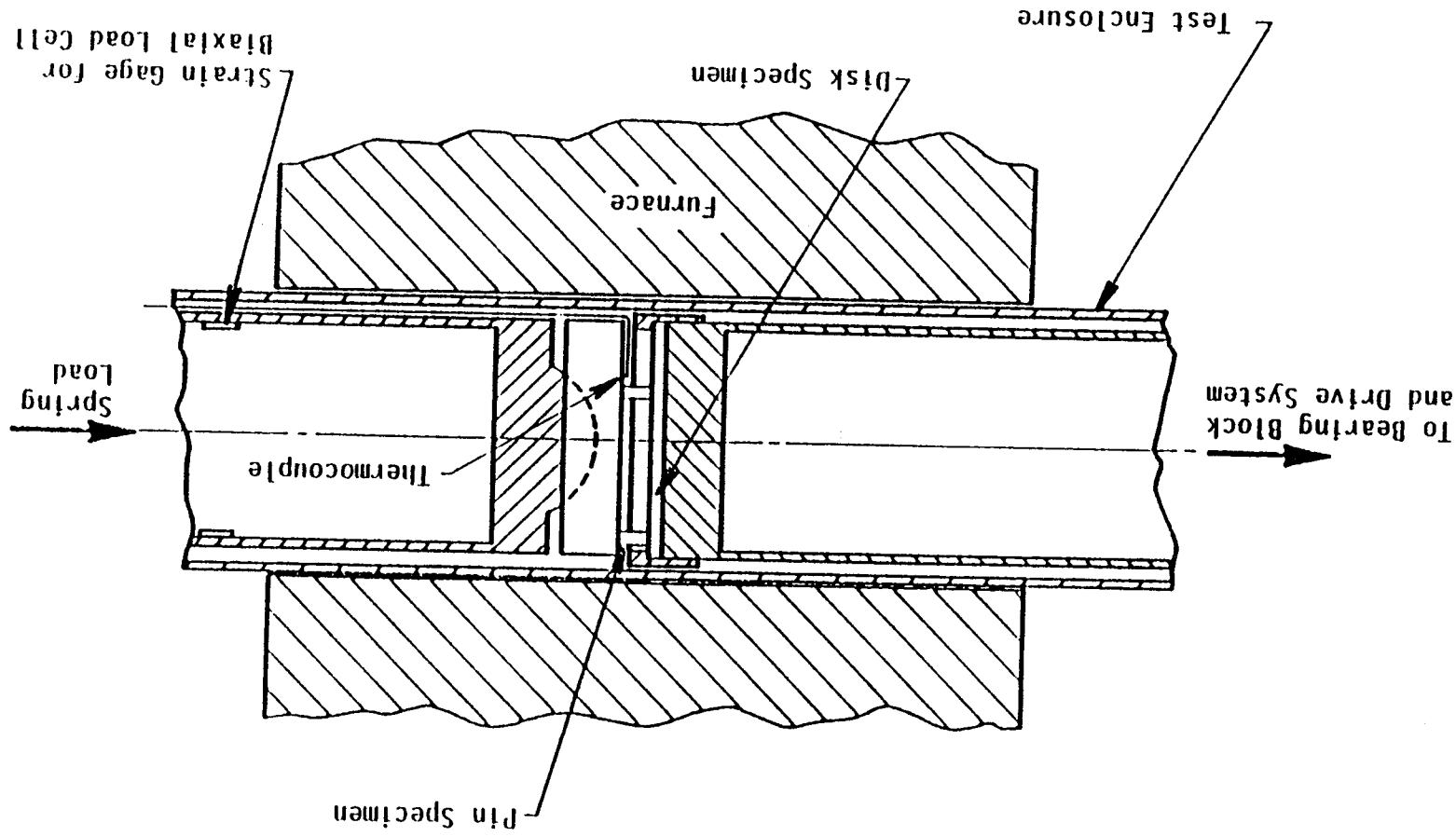
EXPERIMENTAL VARIABLES
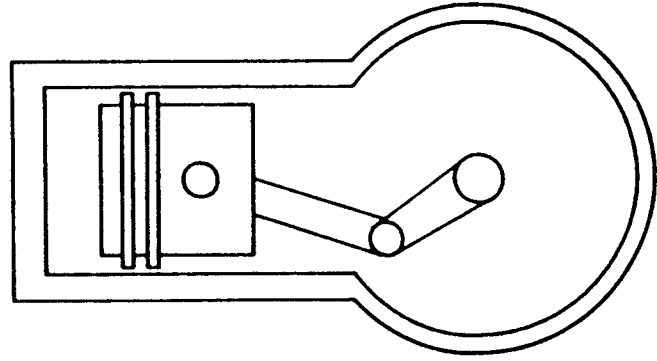
Cast Iron Ring
Cast Iron Liner
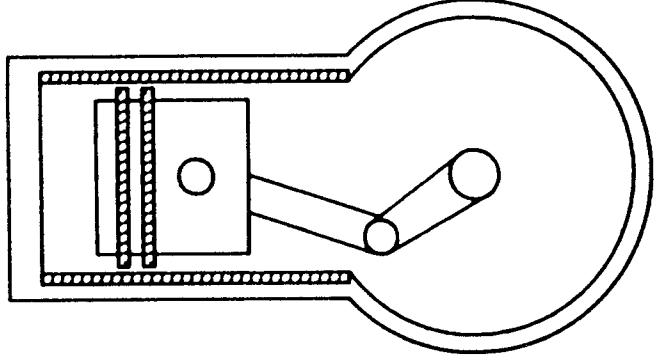
Ni-Mo-TiC Ring
PSZ Liner

Combination 1
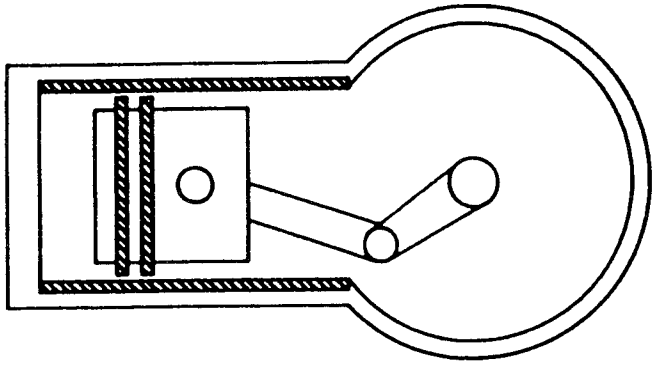
HP-TiC Ring
Si_3N_4

Combination 2

FIGURE 4. MATERIAL COUPLES USED FOR FRICTION
RIG AND ENGINE TESTS

56

MATERIAL COMBINATION NO. 1
(Ni-Moly Bonded TiC rings/PSZ liner)

RING TYPE	RING TENSION LEVEL	
	LOW	HIGH
TOP COMPRESSION	RING SET 1	RING SET 2
SECOND COMPRESSION	RING SET 3	RING SET 4

MATERIAL COMBINATION NO. 2
(Hot-Pressed TiC rings/Si$_3$N$_4$ liner)

RING TYPE	RING TENSION LEVEL	
	LOW	HIGH
TOP COMPRESSION	RING SET 1	N/A
SECOND COMPRESSION	RING SET 2	N/A

FIGURE 5. DESCRIPTION OF CERAMIC PISTON RINGS

57
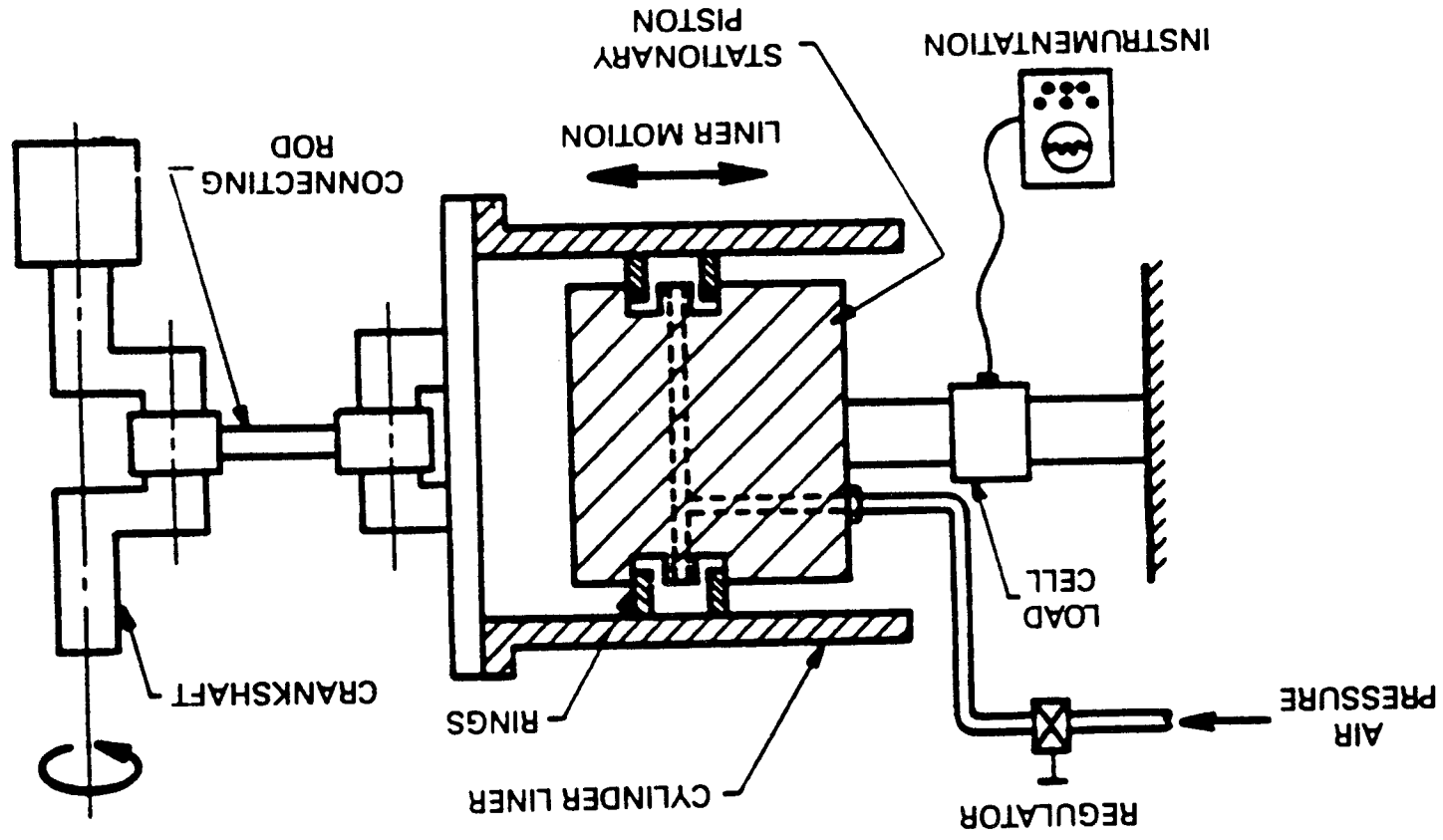
FIGURE 6. FRICTION TEST RIG SCHEMATIC

58
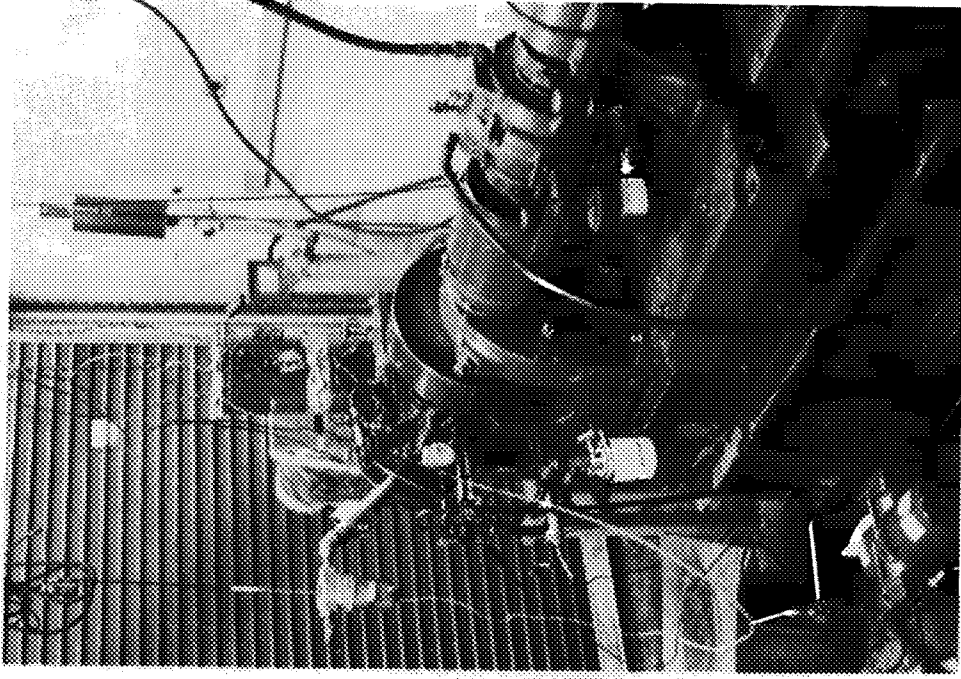
FIGURE 7. GENERAL VIEW OF FRICTION RIG

59
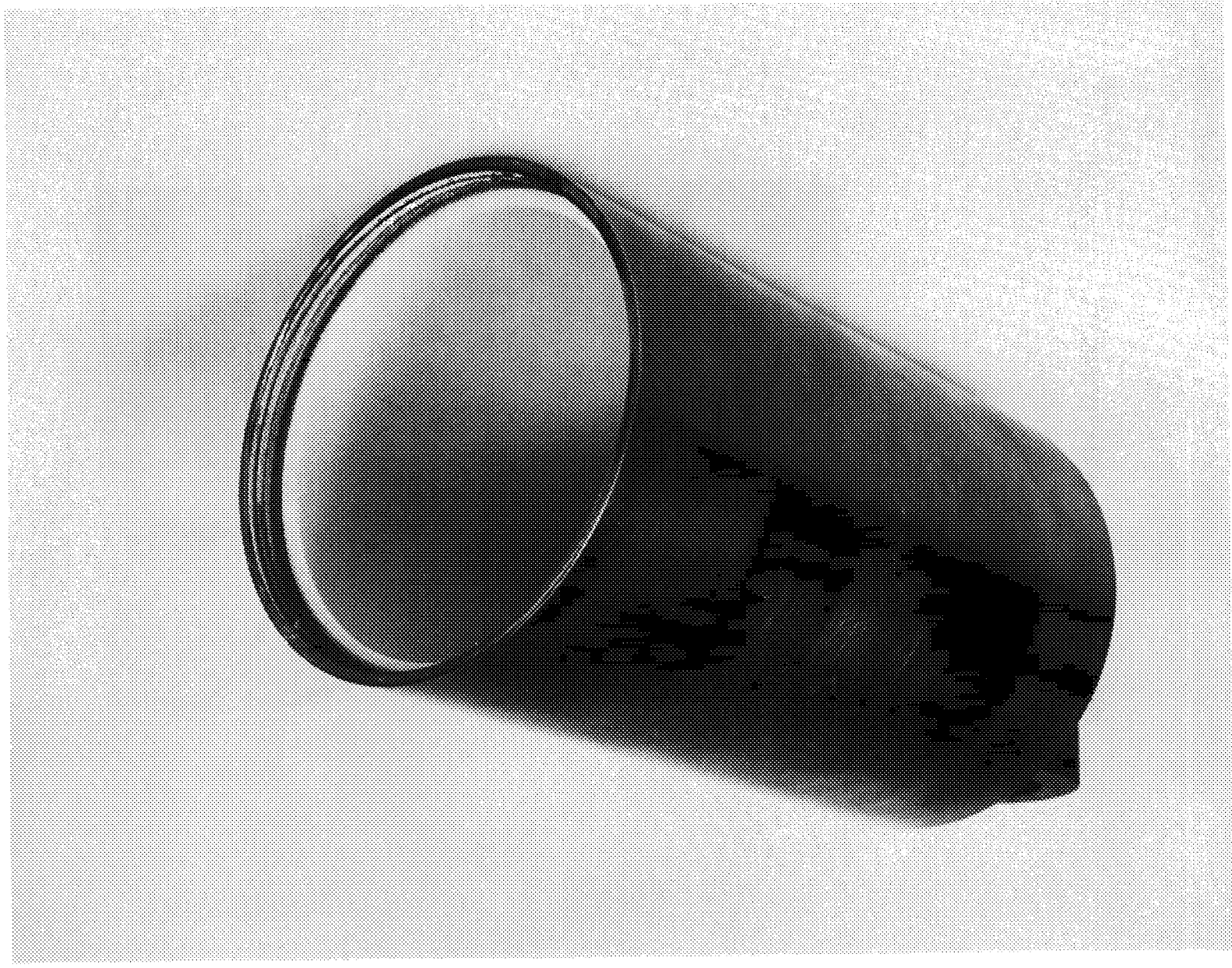
FIGURE 8. PHOTOGRAPH OF PSZ LINER BEFORE ION-IMPLANTATION
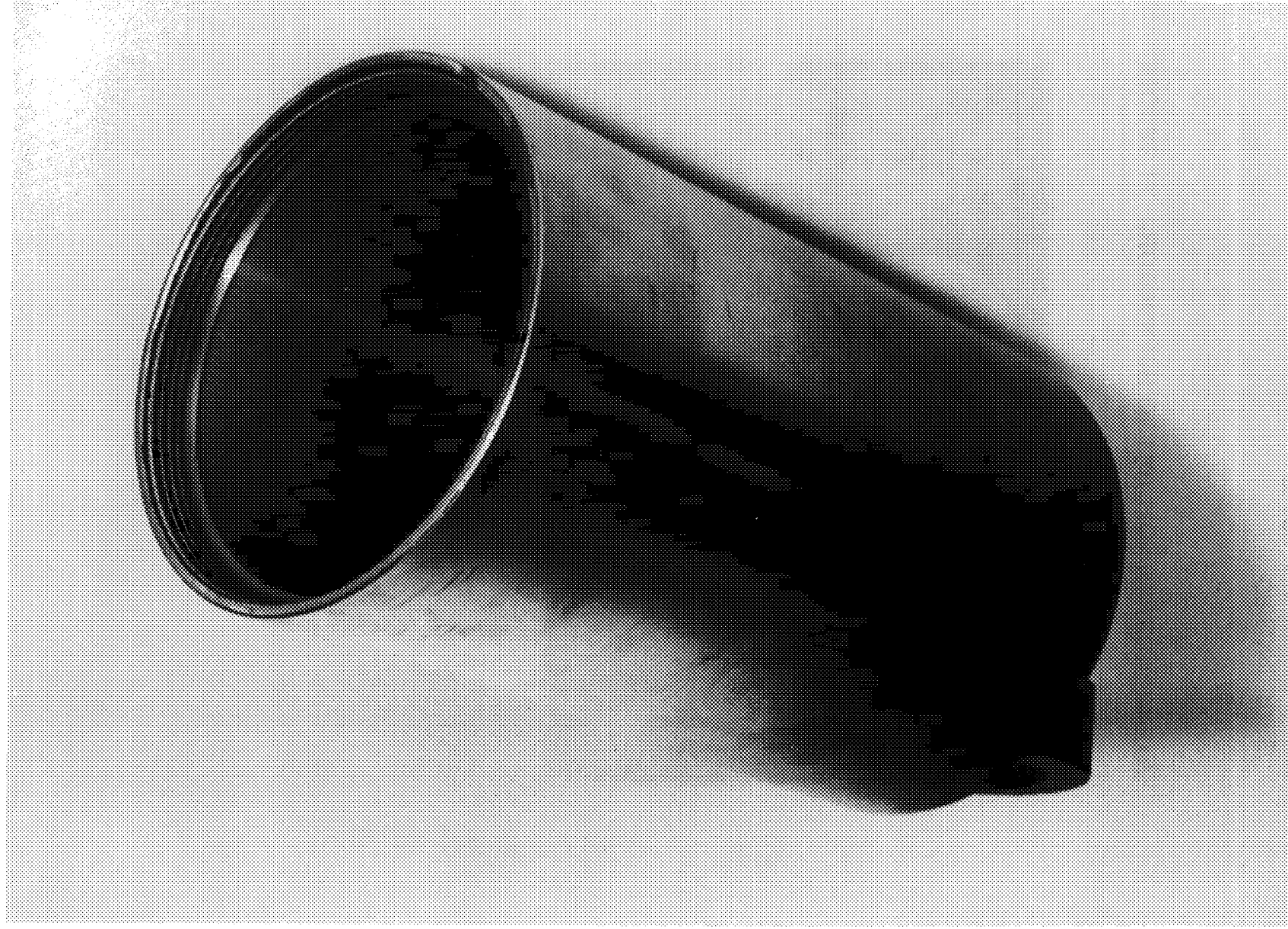
FIGURE 9. PHOTOGRAPH OF PSZ LINER WITH TiNi IMPLANTATION

61
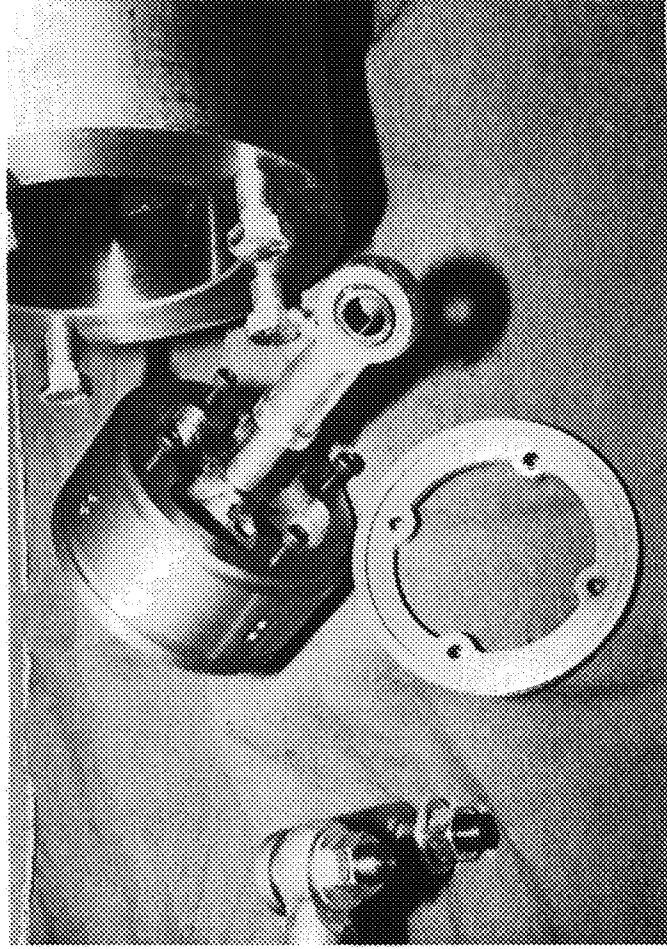
FIGURE 10. PHOTOGRAPH OF FRICTION TEST RIG PISTON
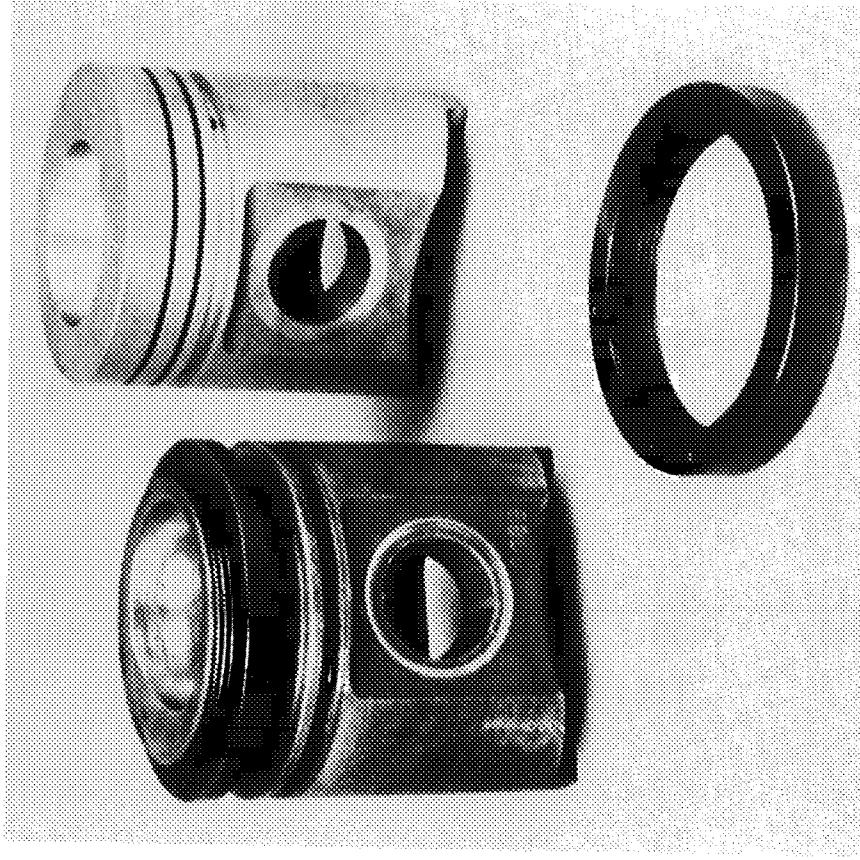
FIGURE 11. PHOTOGRAPH OF MODIFIED D-I DIESEL PISTON

63
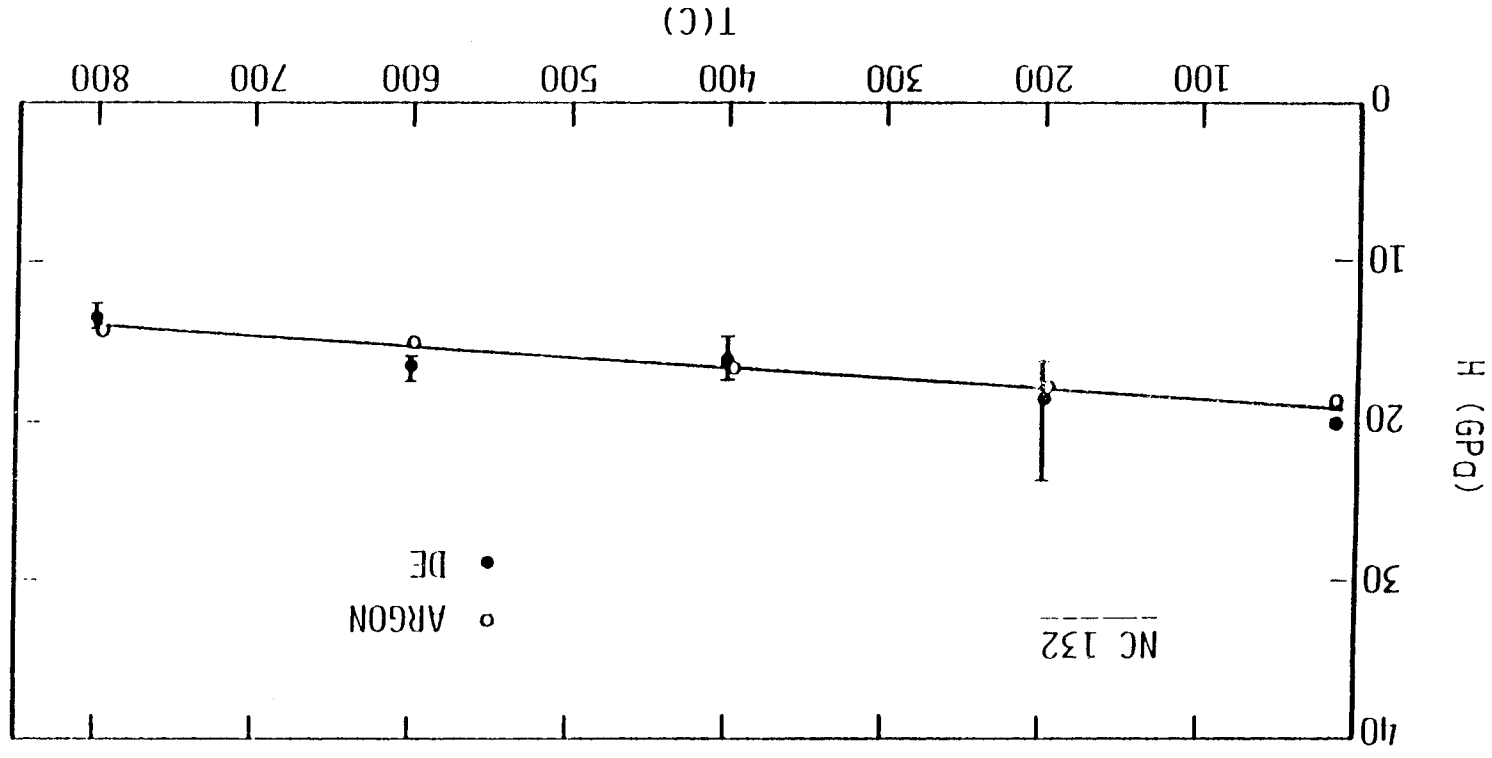
FIGURE 12. HARDNESS VERSUS TEMPERATURE FOR NC 132 IN DE AND Ar

T(C)

H (GPa)

DE •
o ARGON
NC 132
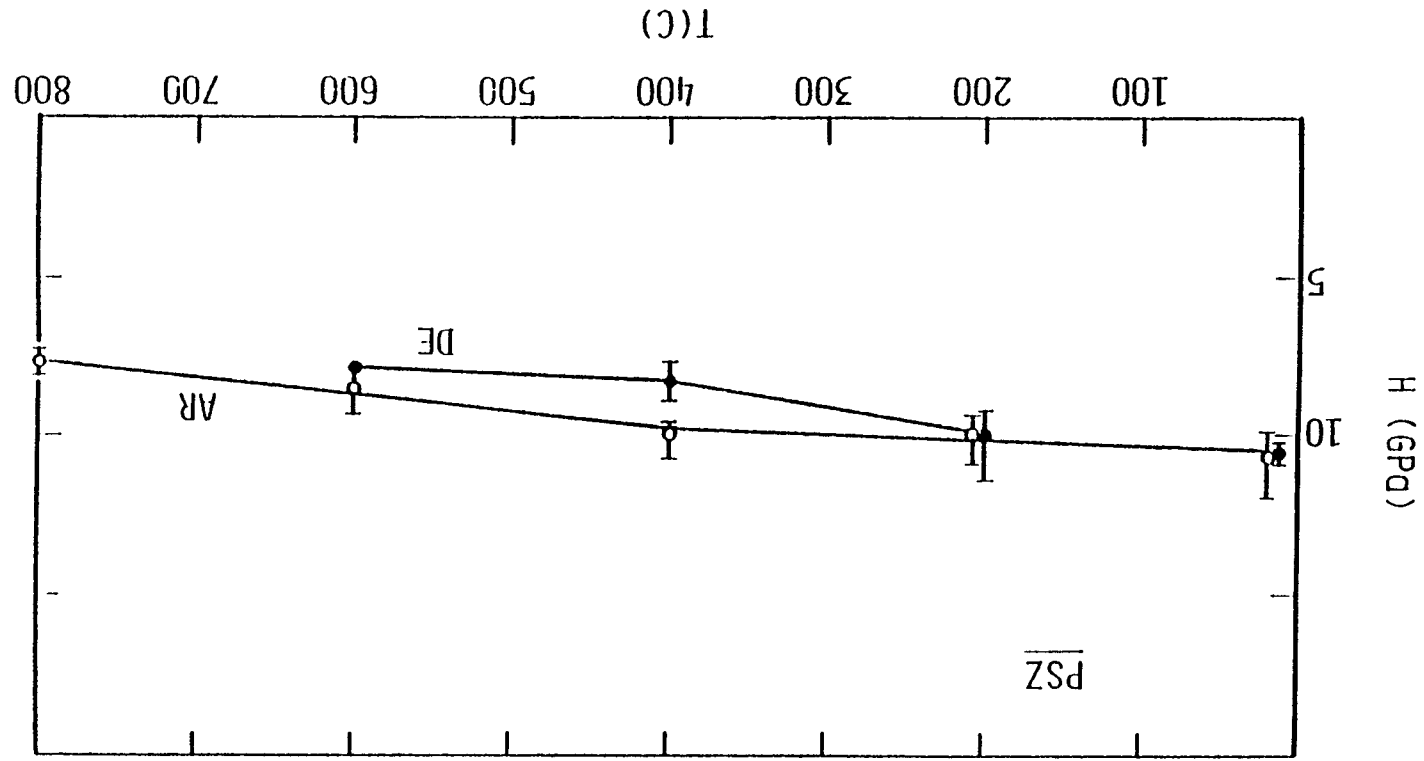
FIGURE 13. HARDNESS VERSUS TEMPERATURE FOR PSZ IN DE AND AF
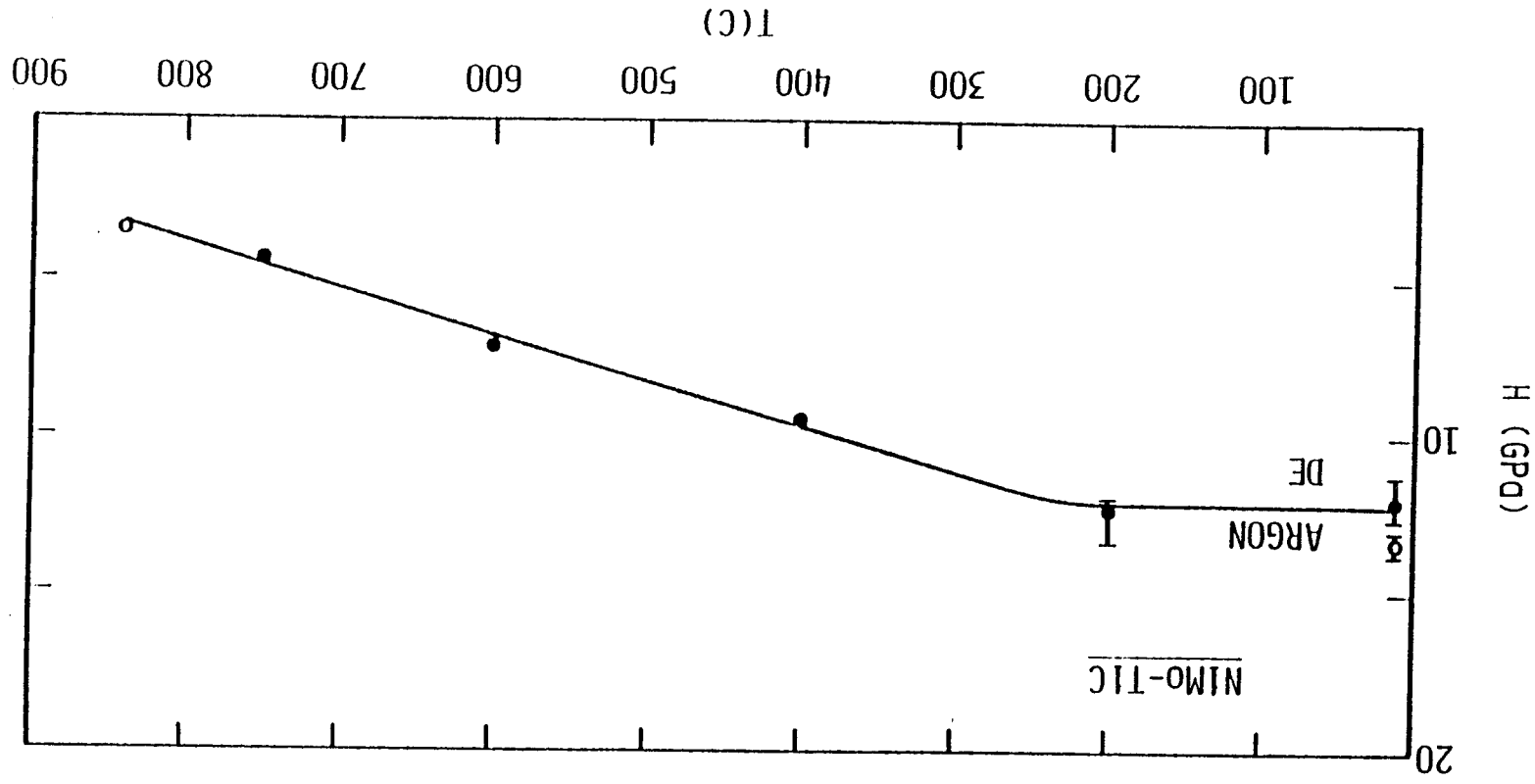
FIGURE 14. HARDNESS VERSUS TEMPERATURE FOR Ni-Mo-TiC IN DE AND Ar.
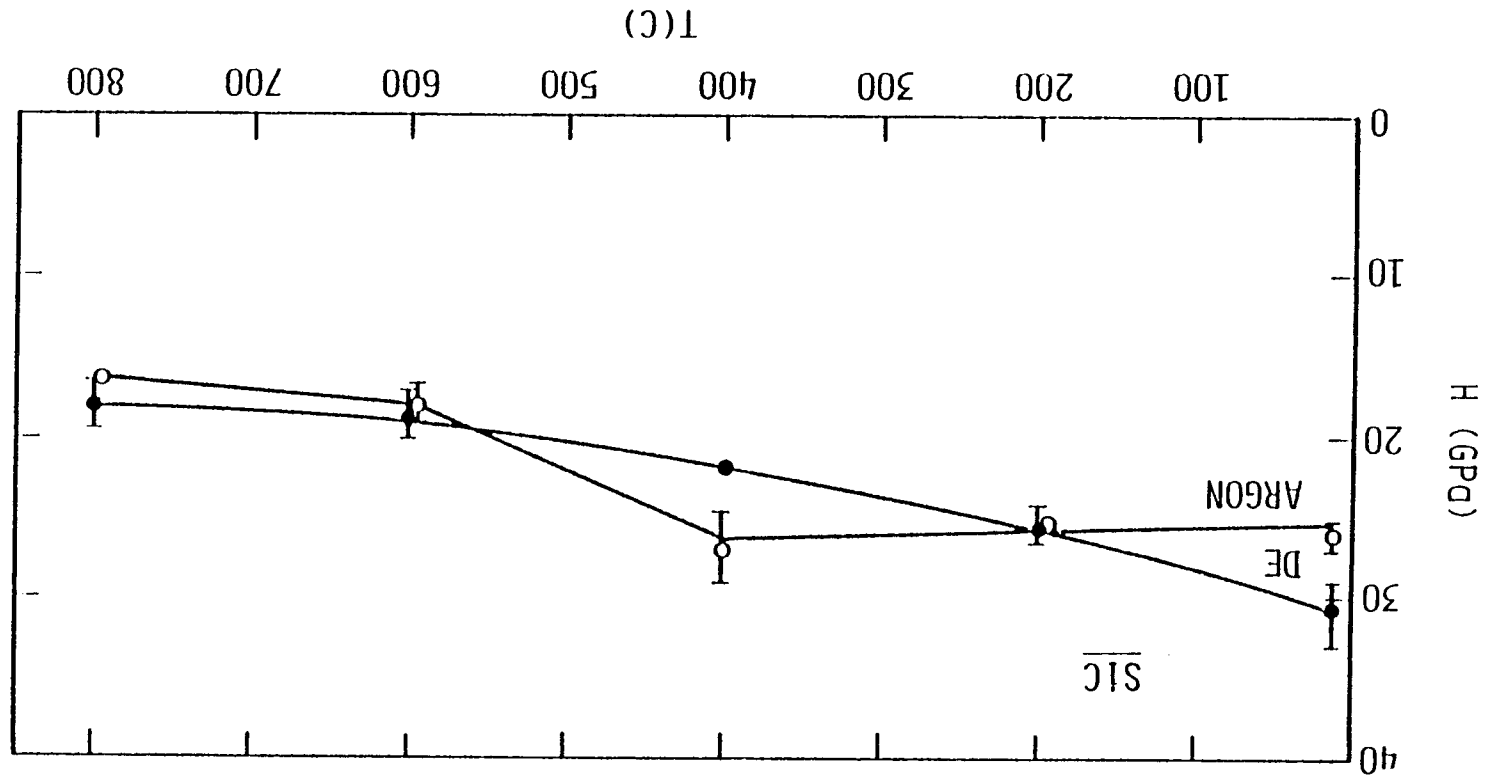
FIGURE 15. HARDNESS VERSUS TEMPERATURE FOR SiC IN DE AND Ar

67
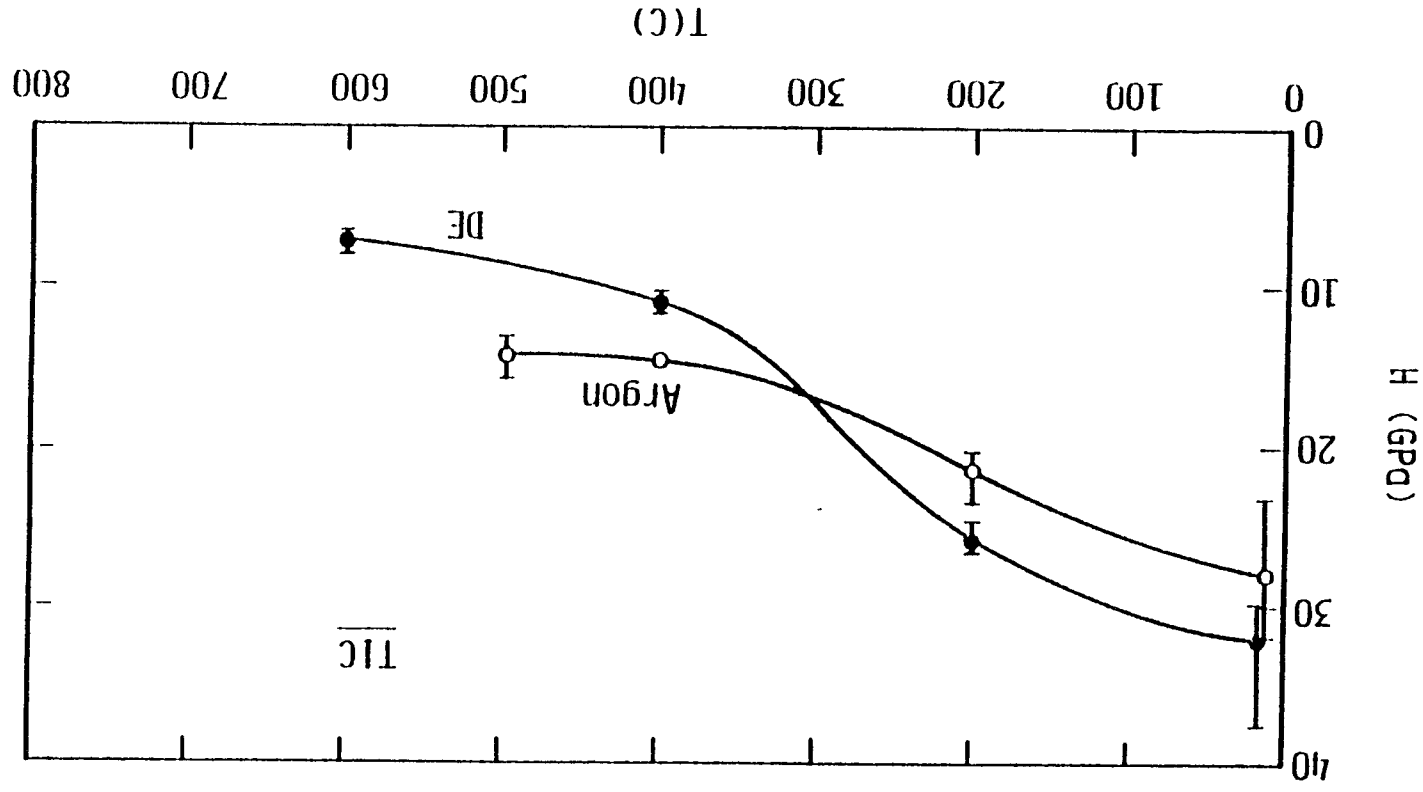
FIGURE 16. HARDNESS VERSUS TEMPERATURE FOR TiC IN DE AND Ar.

89
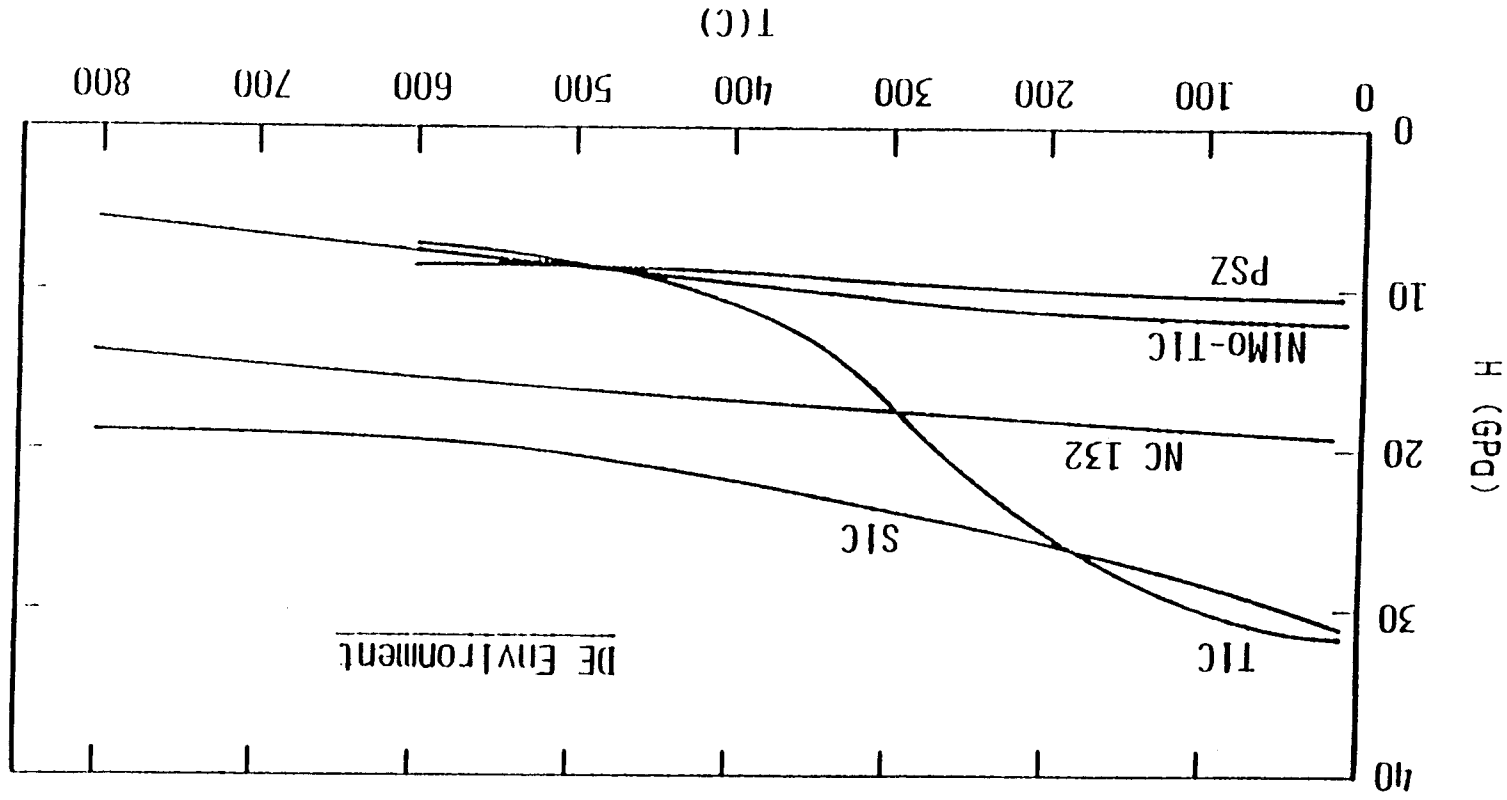
FIGURE 18. HARDNESS VERSUS APPLIED ELECTRICAL POTENTIAL
FOR SiC AT 23°C IN HUMID AIR

70
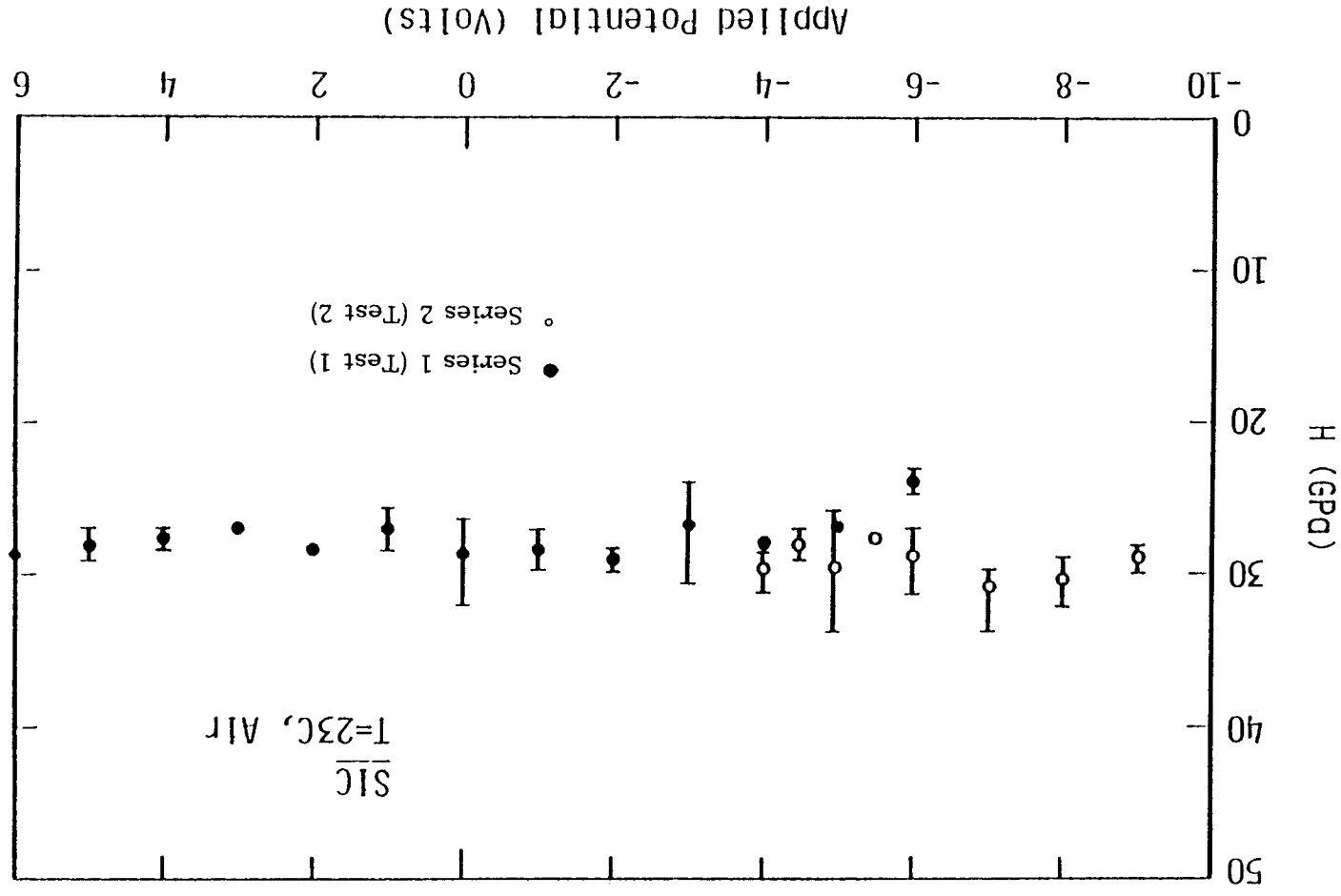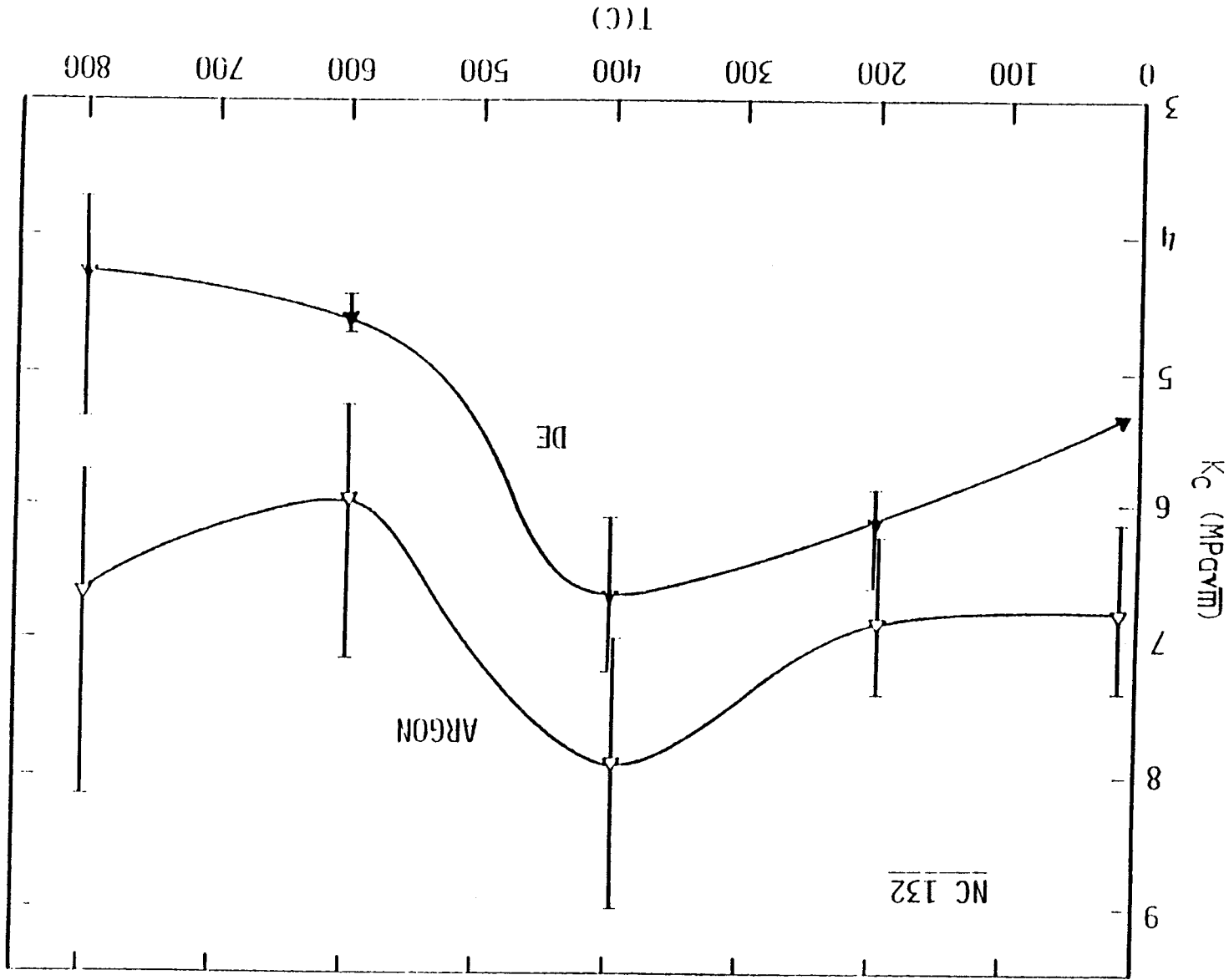
FIGURE 19. FRACTURE TOUGHNESS VERSUS
TEMPERATURE FOR NC 132 IN DE AND Ar.

T (C)

K_c (MPa$\sqrt{m}$)

DE

ARGON
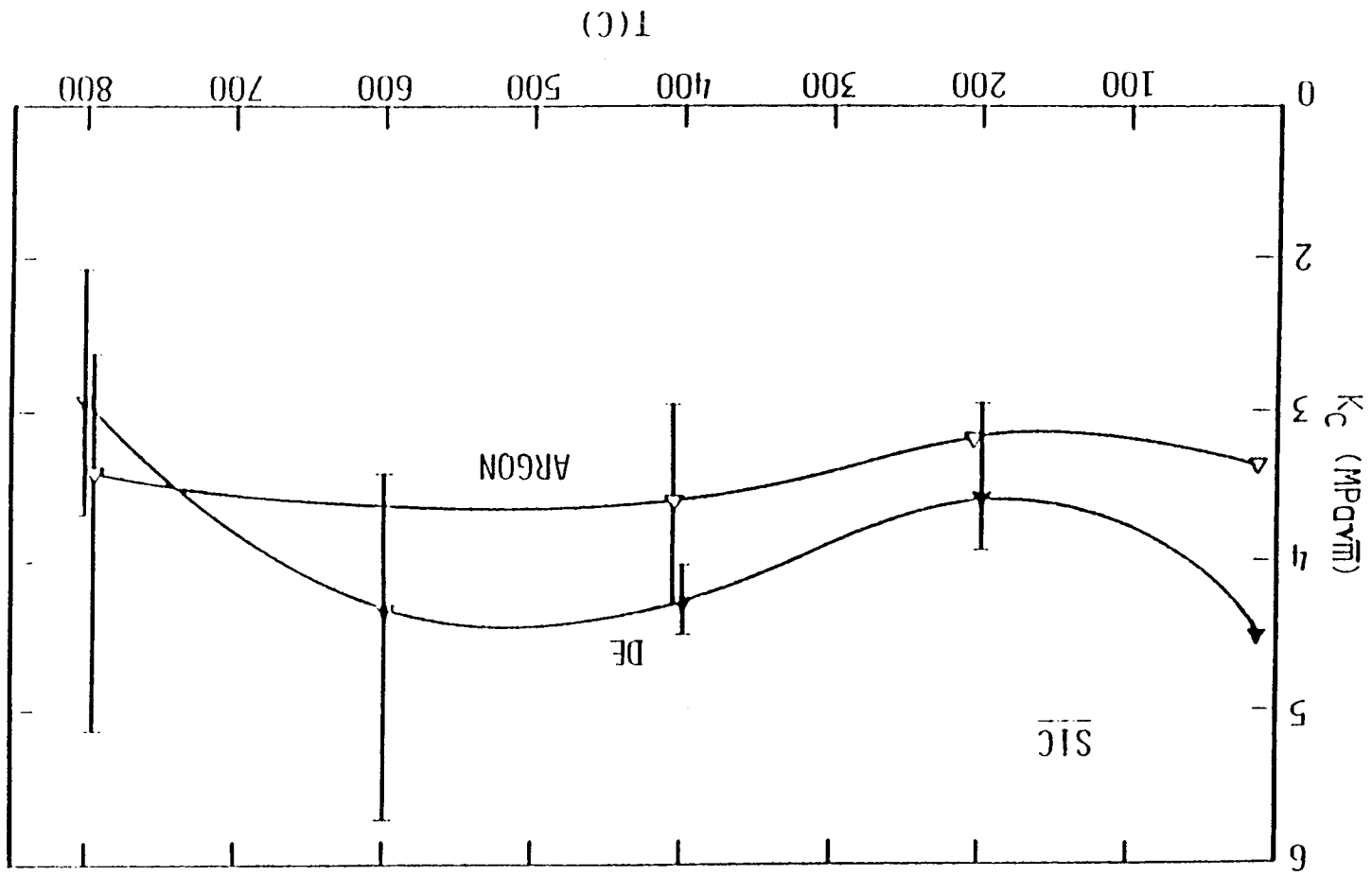
NC 132

FIGURE 20. FRACTURE TOUGHNESS VERSUS TEMPERATURE FOR SiC IN DE AND Ar.

T(C)

100 200 300 400 500 600 700 800

0

2

3

4

5

6

K_C (MPa√m)

ARGON

DE

SiC

FIGURE 22. FRACTURE TOUGHNESS VERSUS TEMPERATURE FOR NC 132, SiC, AND TiC IN DE

74
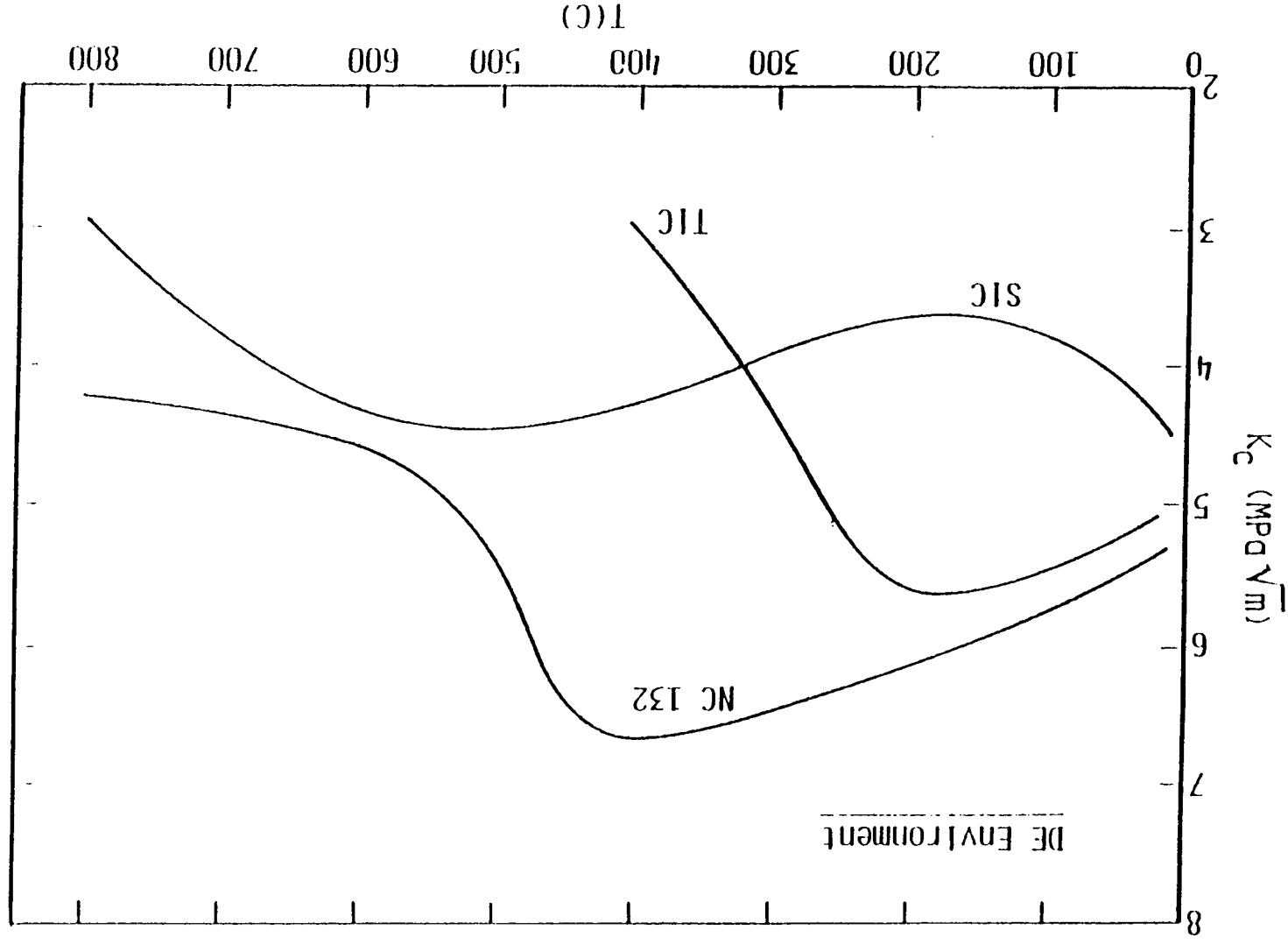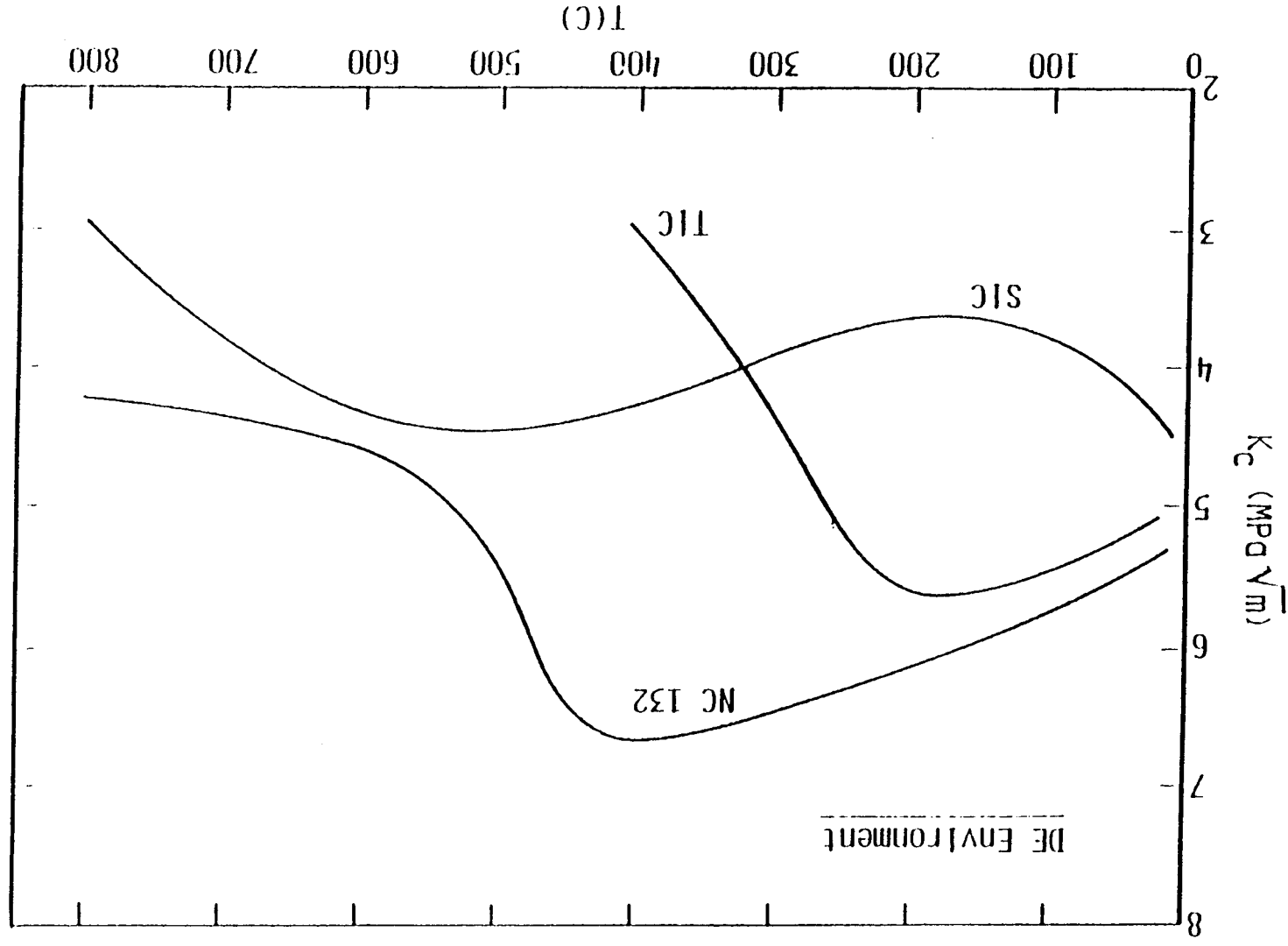
FIGURE 22. FRACTURE TOUGHNESS VERSUS TEMPERATURE FOR NC 132, SiC, AND TiC IN DE
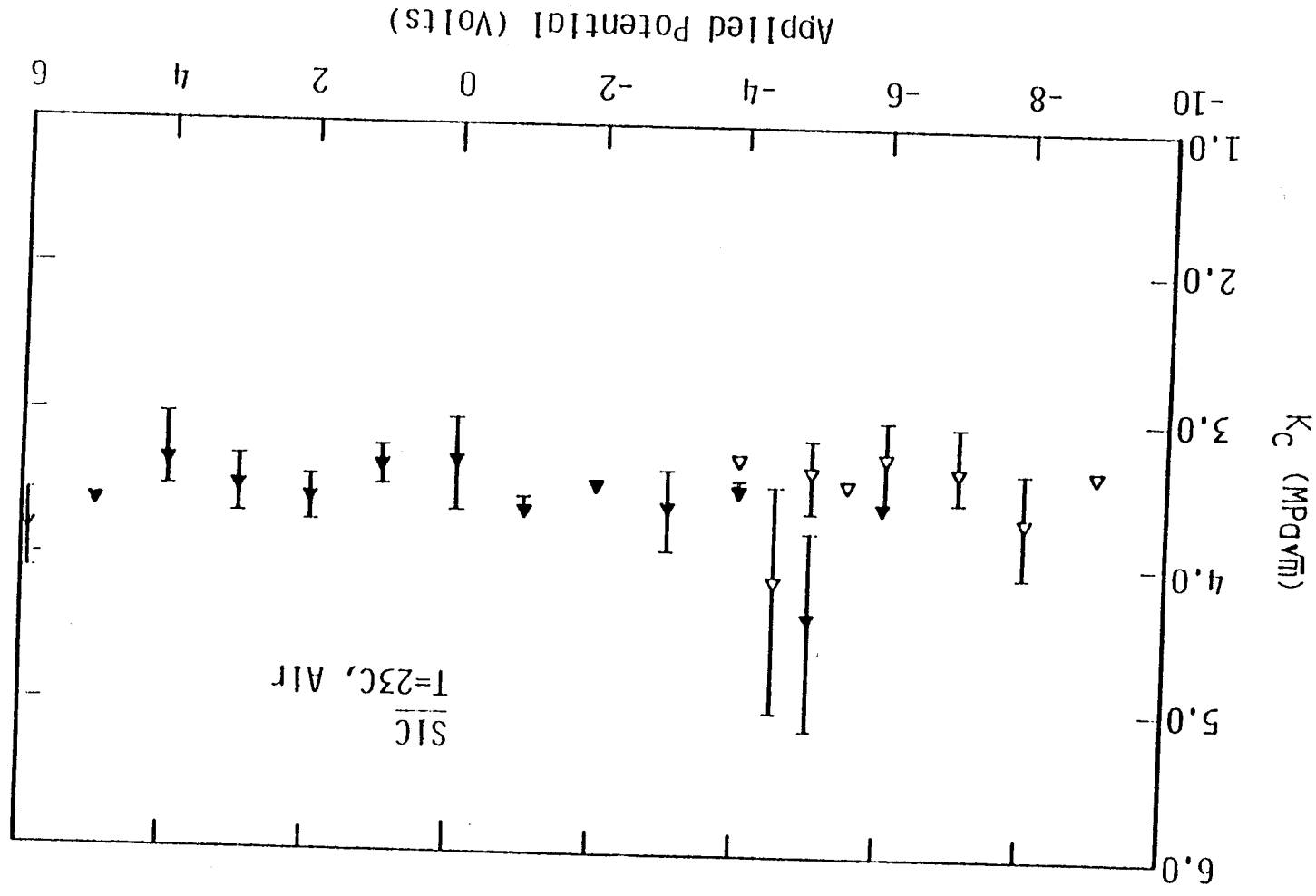
FIGURE 23. FRACTURE TOUGHNESS VERSUS APPLIED ELECTRICAL POTENTIAL FOR SiC AT 23°C IN HUMID AIR

FIGURE 24. FRICTION COEFFICIENT VERSUS TEMPERATURE FOR
K162B PINS/PSZ DISK IN DE AND Ar.

76
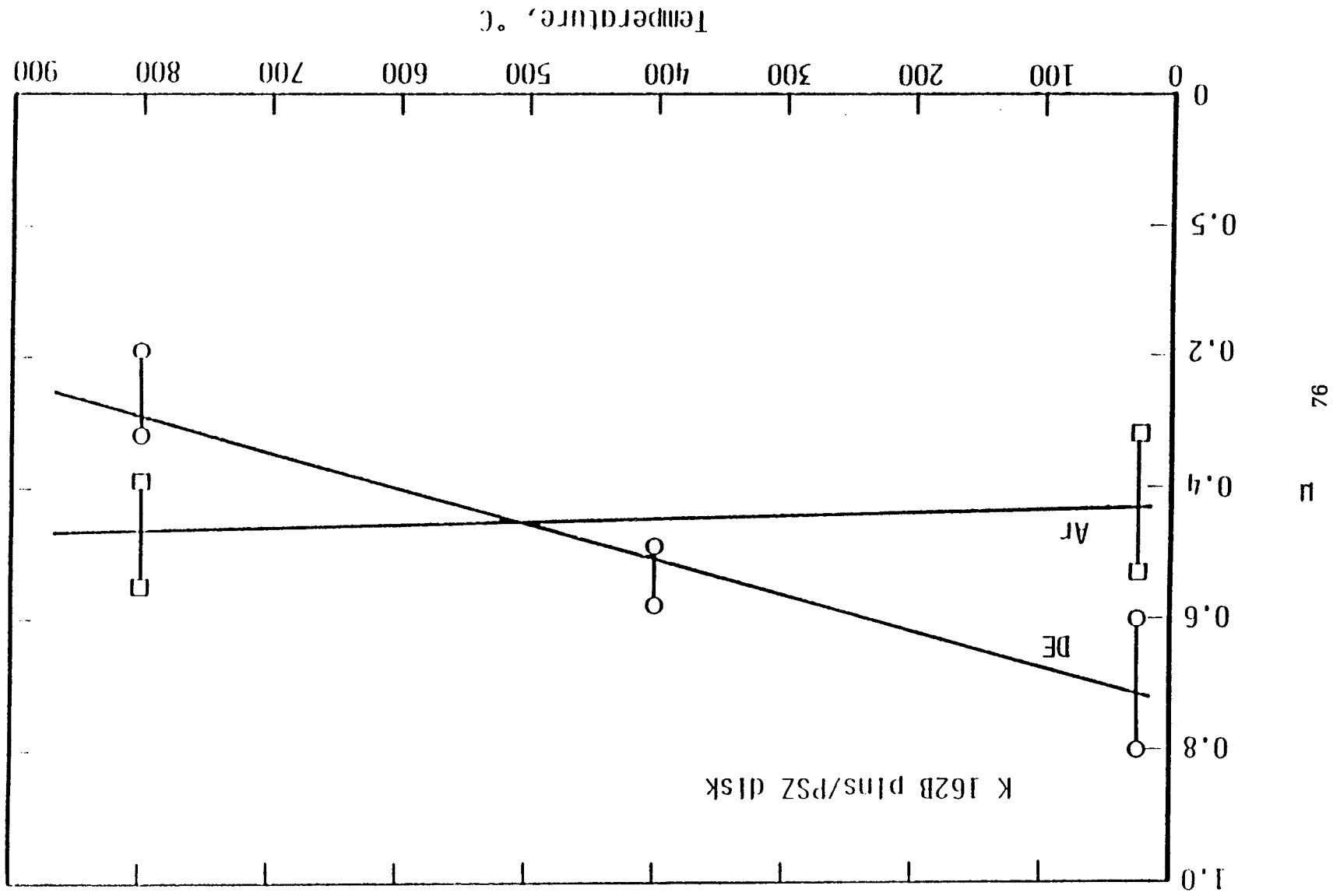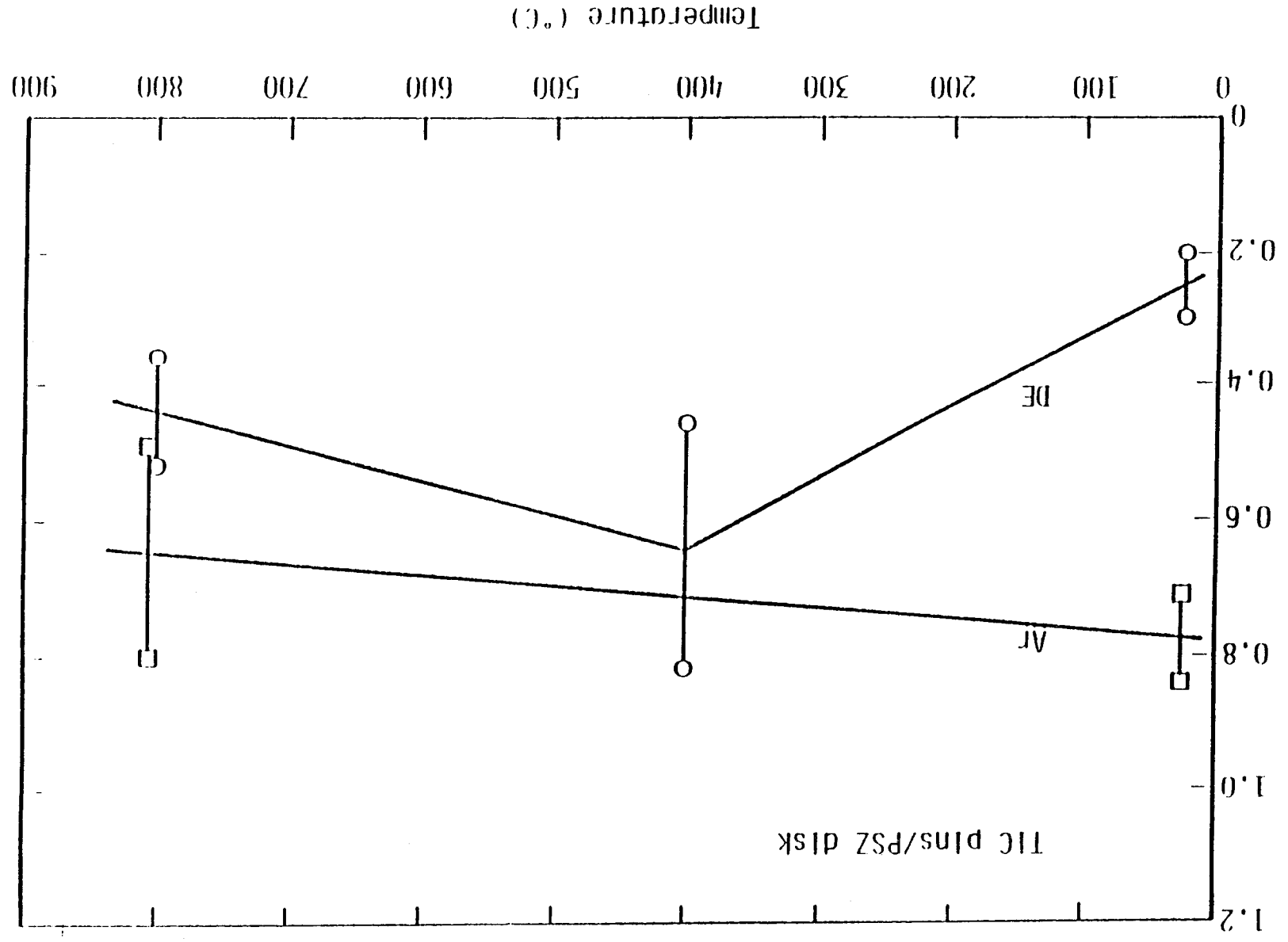
FIGURE 26. FRICTION COEFFICIENT VERSUS TEMPERATURE FOR
TiC PINS/PSZ DISK IN DE AND Ar.

FIGURE 26. FRICTION COEFFICIENT VERSUS TEMPERATURE FOR
TiC PINS/PSZ DISK IN DE AND Ar.

78
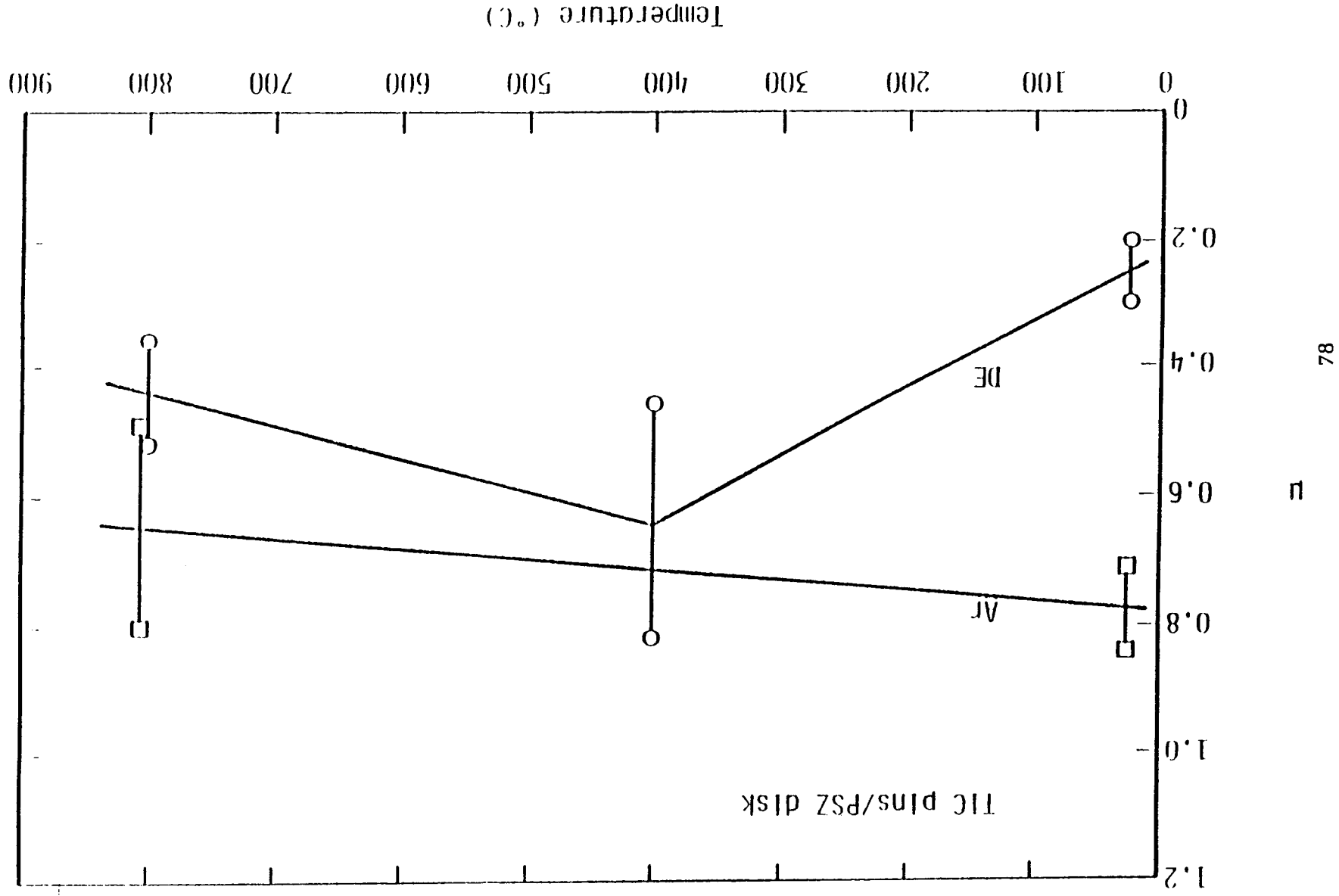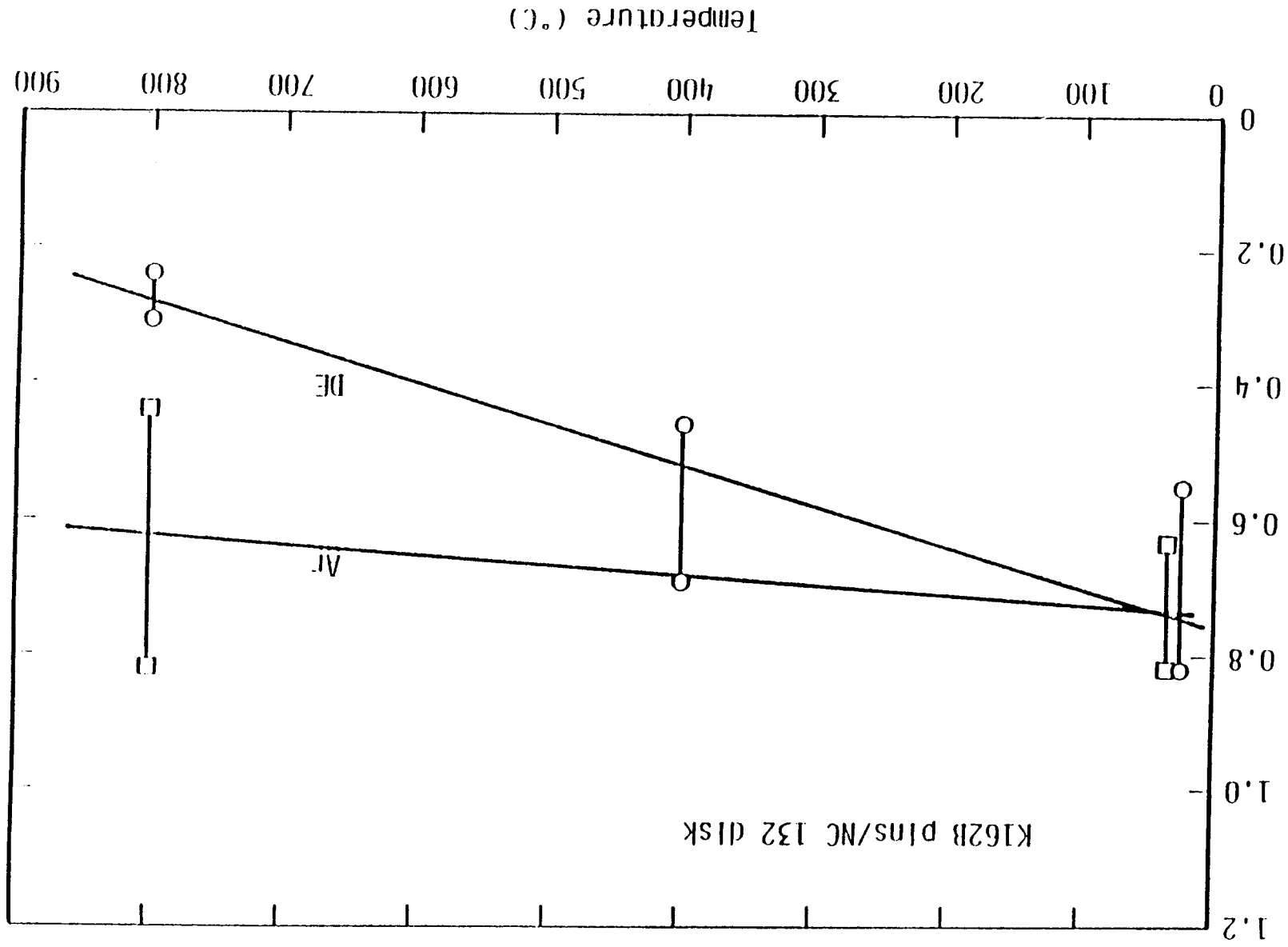
FIGURE 27. FRICTION COEFFICIENT VERSUS TEMPERATURE FOR
K162B PINS/NC 132 DISK IN DE AND Ar

FIGURE 28. FRICTION COEFFICIENT VERSUS TEMPERATURE FOR
SiC PINS/NC 132 DISK IN DE AND Ar.

Temperature (°C)

0   100   200   300   400   500   600   700   800   900

μ

0

0.2

0.4

SiC   0.6

K 162B

TiC

0.8

1.0

PSZ disk, Ar.

1.2
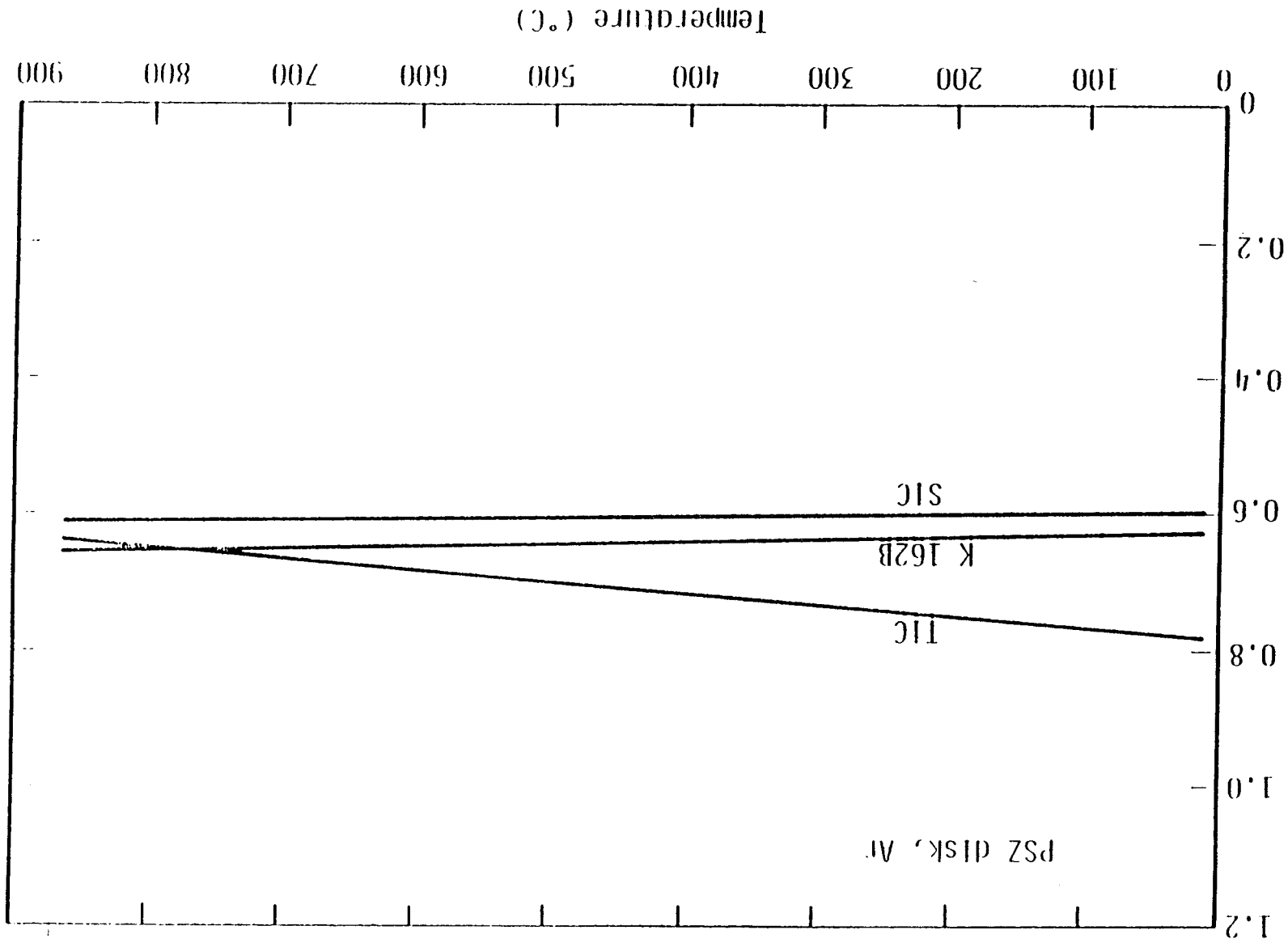
FIGURE 30. FRICTION COEFFICIENT VERSUS TEMPERATURE FOR ALL PIN
MATERIALS ON PSZ DISKS IN Ar.
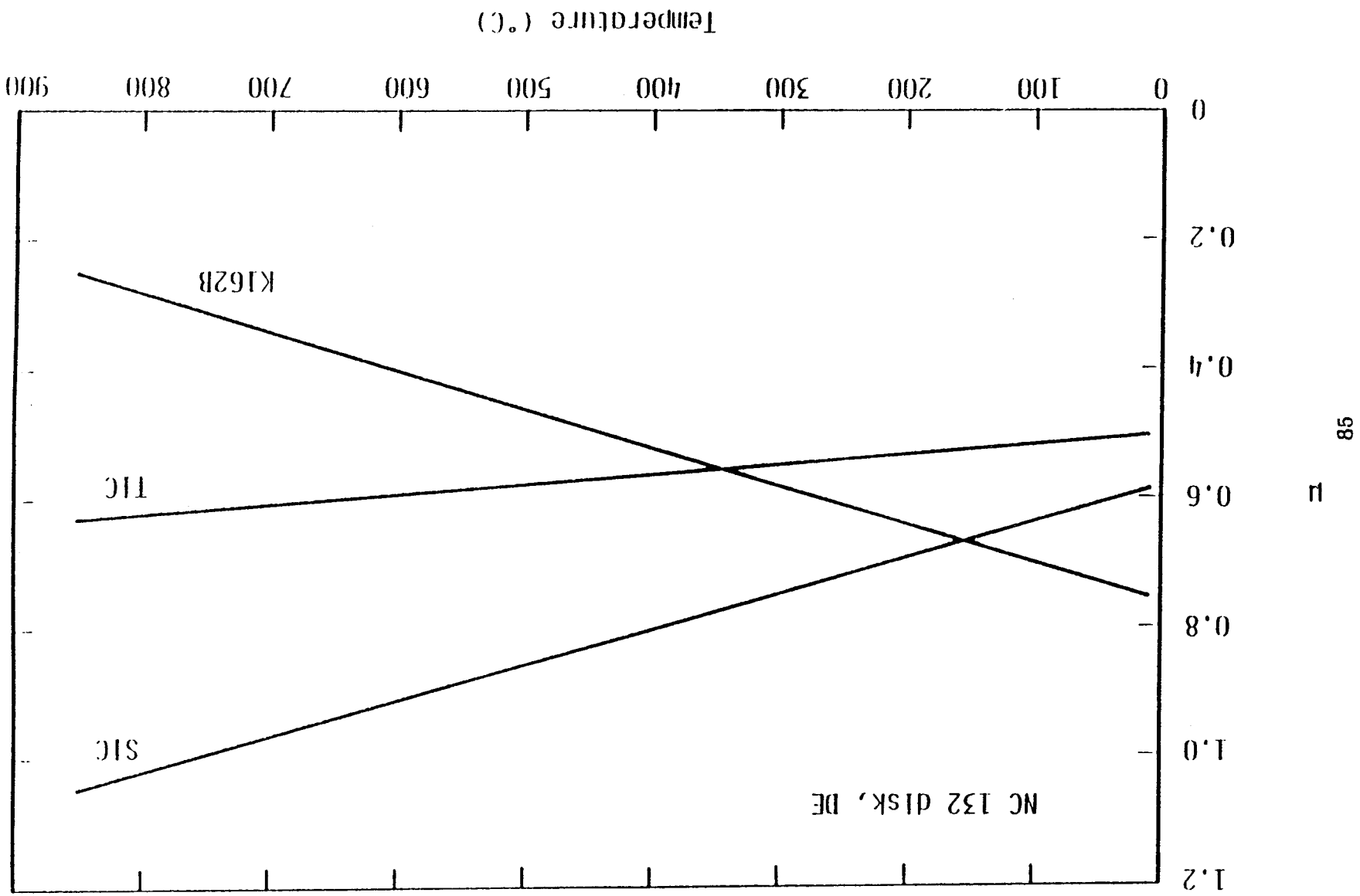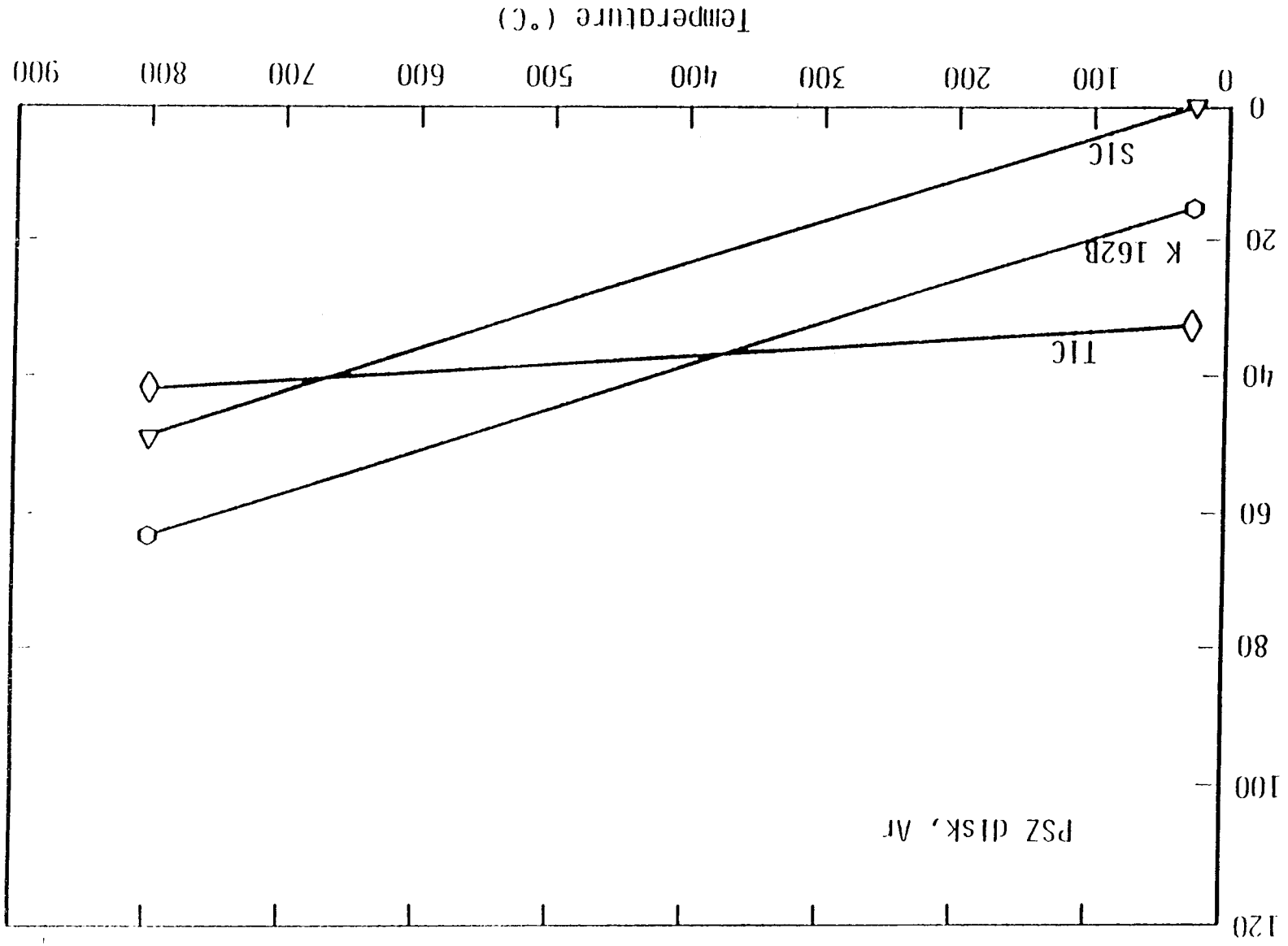
FIGURE 34. WEAR RATE VERSUS TEMPERATURE FOR PSZ DISKS IN Ar.

Temperature (°C)

0   100   200   300   400   500   600   700   800   900

0
20
40
60
80
100
120

SiC

K 162B

TiC

PSZ disk, Ar

Disc Ẇ
N x 10-4
gms/min

FIGURE 35. WEAR RATE VERSUS TEMPERATURE FOR PSZ DISKS IN DE

87

NC 132 disk

SiC, DE

SiC, Ar ▼

TiC, Ar ◆

TiC, DE

K 162B, DE

K 162B, Ar

Disc W
N × 10-4
gms/min

Temperature (°C)

0   100   200   300   400   500   600   700   800   900

0   20   40   60   80   100   120
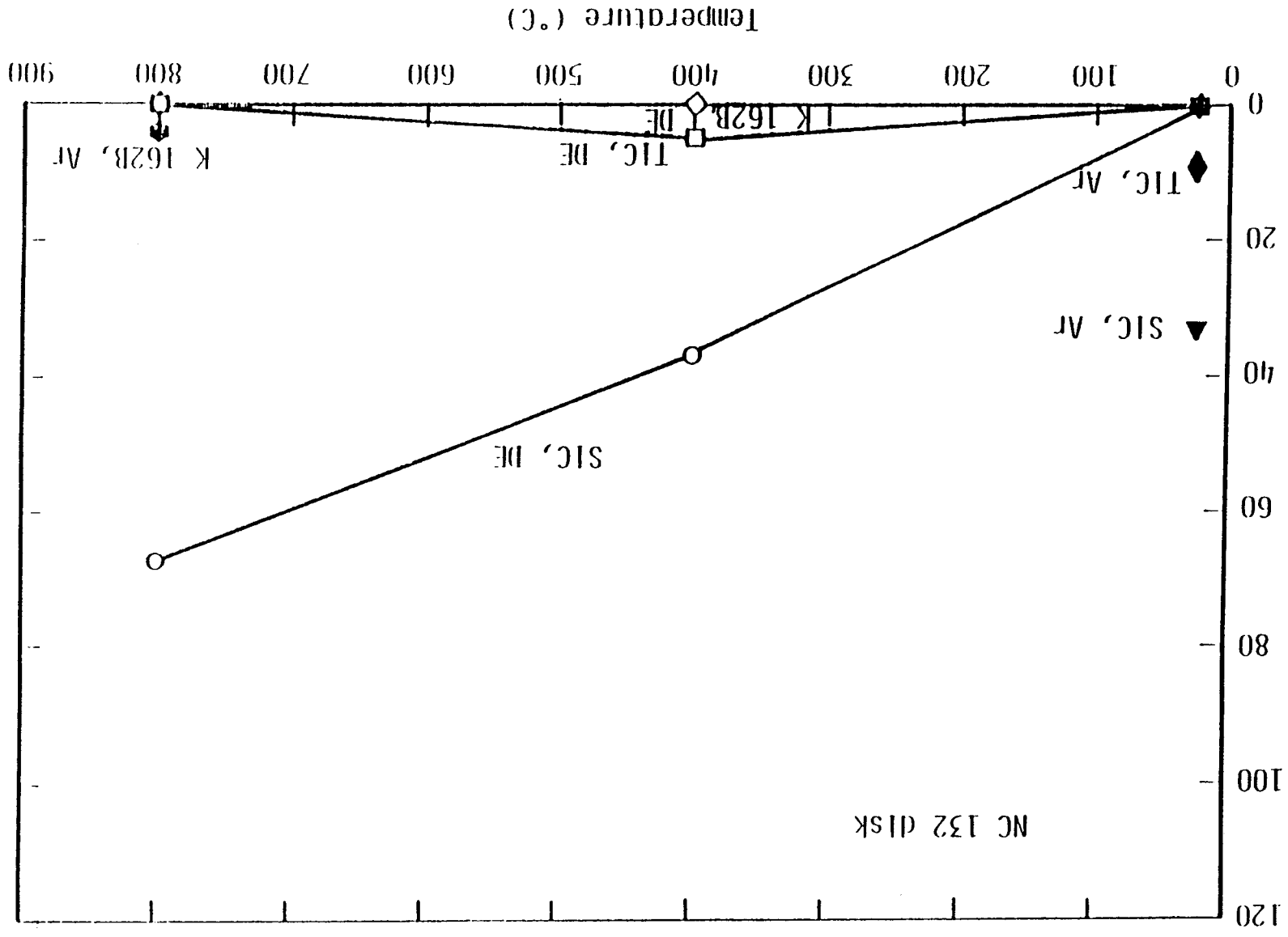
FIGURE 36. WEAR RATE VERSUS TEMPERATURE FOR NC 132 DISKS IN DE AND Ar
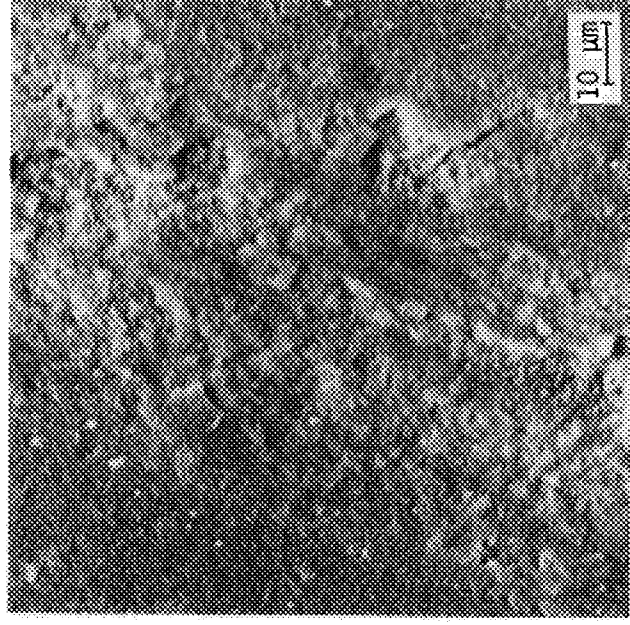
(a) Early wear, NC 132 disk
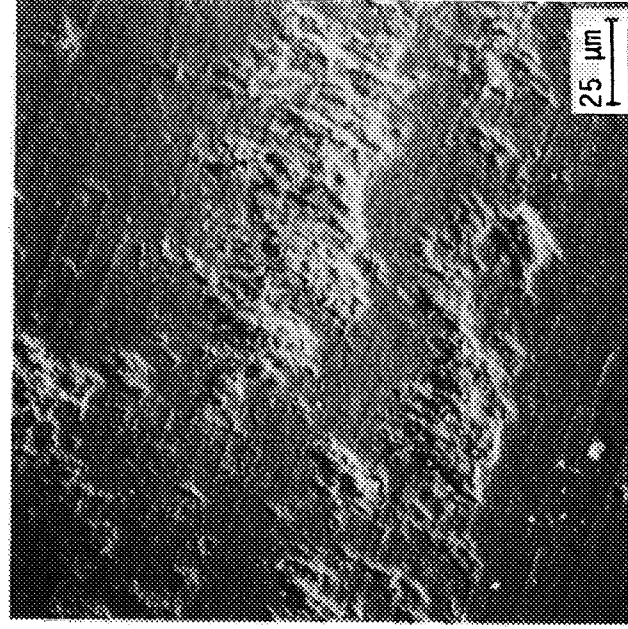
(b) Initial wear, SiC pin
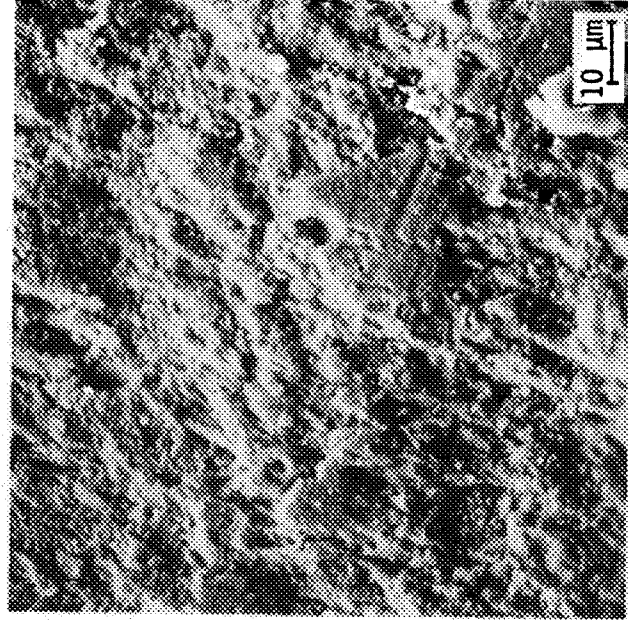
(c) Equilibrium wear, SiC pin

FIGURE 37. SiC PIN/NC 132 DISK, 23°C IN DE, SHOWING EARLY STAGE OF
DELAMINATION IN NC 132 DISK, AND RADIAL OR CONE-CRACK
WEAR PARTICLE FORMATION IN SiC PINS

89
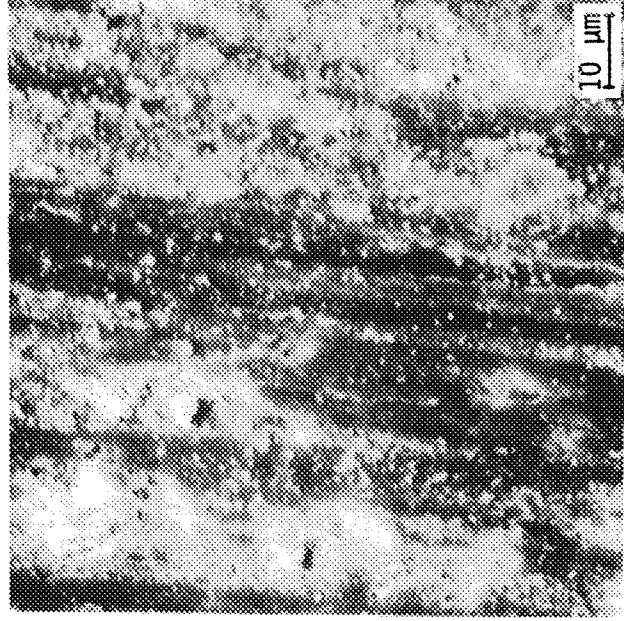
(a) NC 132 disk (SiC pins)
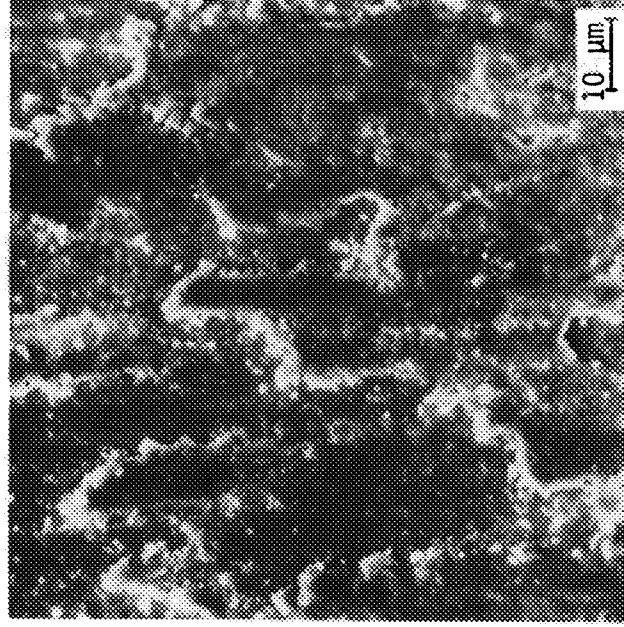
(b) PSZ disk (SiC pins)
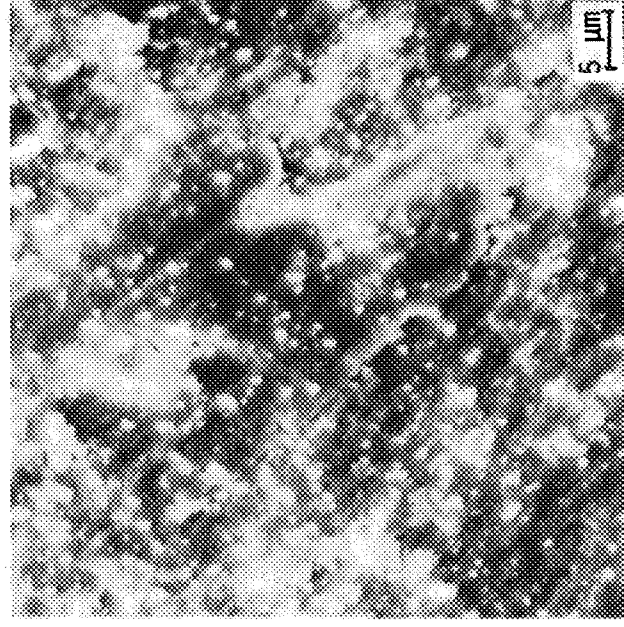
(c) PSZ disk (TiC pins)

FIGURE 38. EXAMPLES OF DELAMINATION IN NC 132 AND PSZ DISKS
DURING EQUILIBRIUM STAGE OF WEAR, 23°C IN DE

90
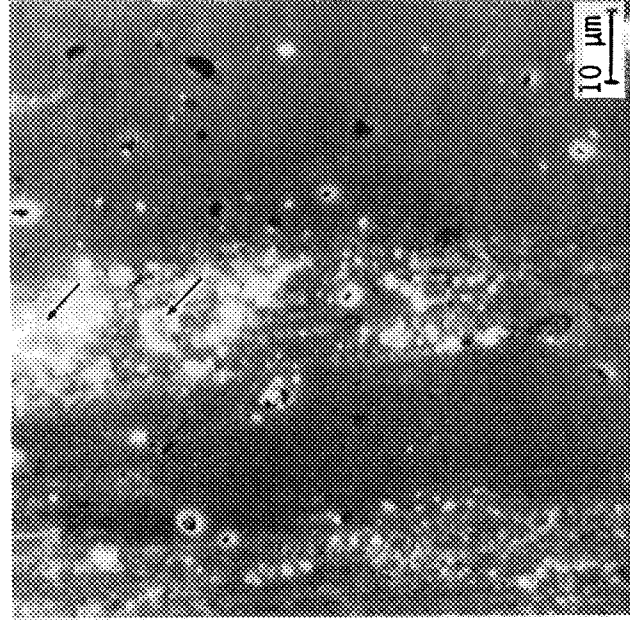
(a) Early damage, disk; arrows
    indicate delamination
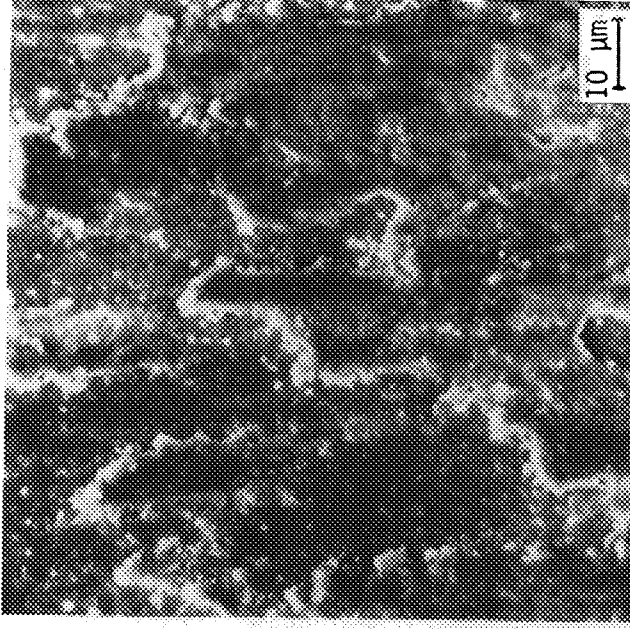
(b) Equilibrium damage, disk
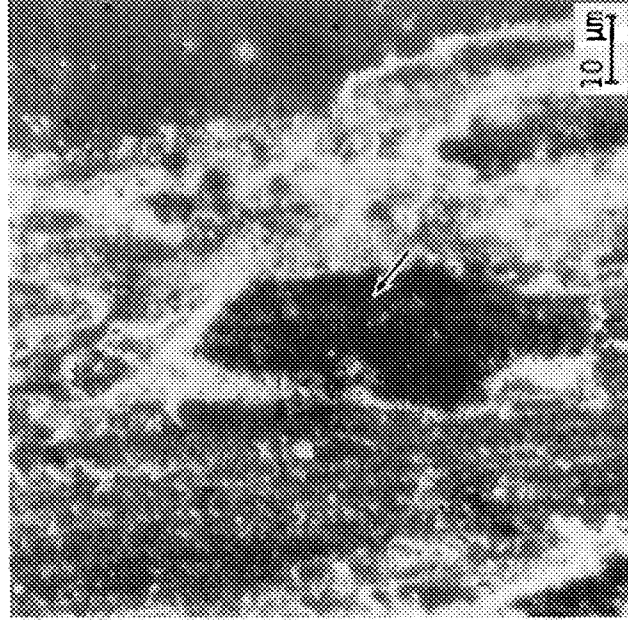
(c) Thin sheet (arrow) in
    process of delamination,
    disk
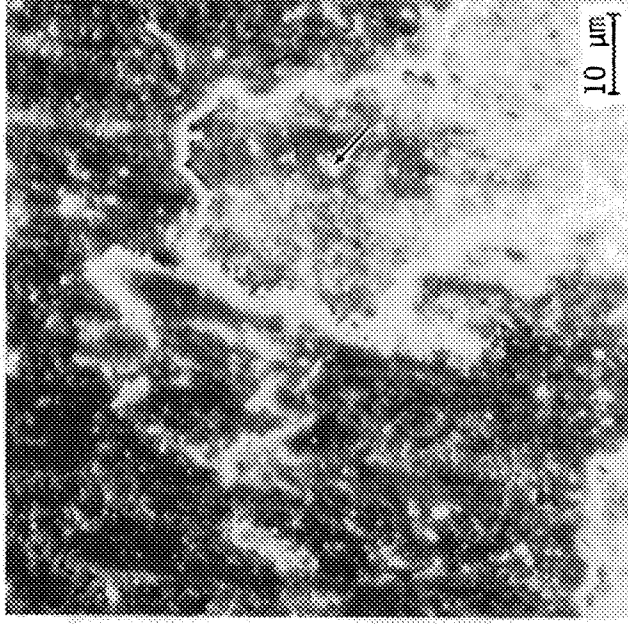
(d) Delaminated zone (arrow),
    disk

FIGURE 39. DELAMINATION DEVELOPMENT IN PSZ DISKS DURING
SLIDING OF SiC PINS AT 23°C IN DE

91
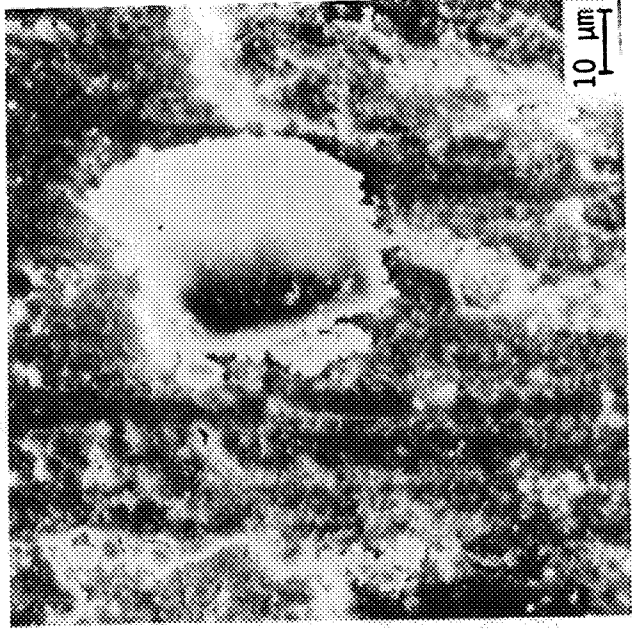
(a) Delaminated sheet on disk
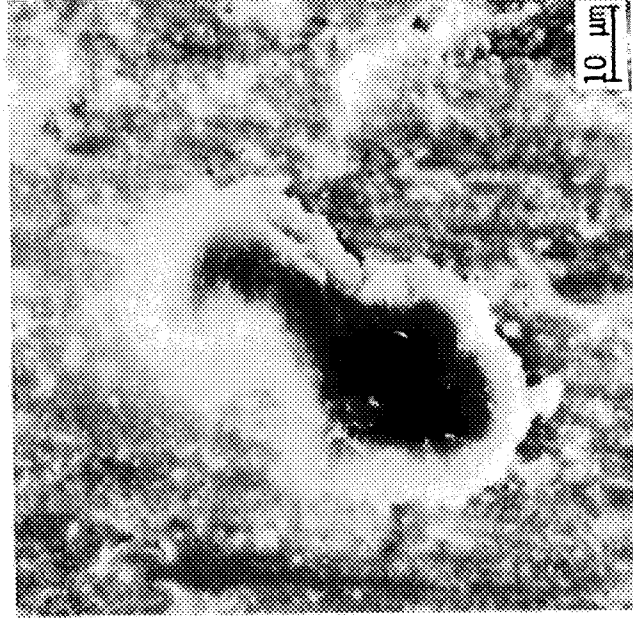
(b) Delaminated sheet on disk

FIGURE 40. PSZ DELAMINATE SHEETS LYING ON THE SURFACE OF THE PSZ DISK; SiC PINS AT 23°C IN DE

92

(a) PSZ delaminated sheet on SiC pin
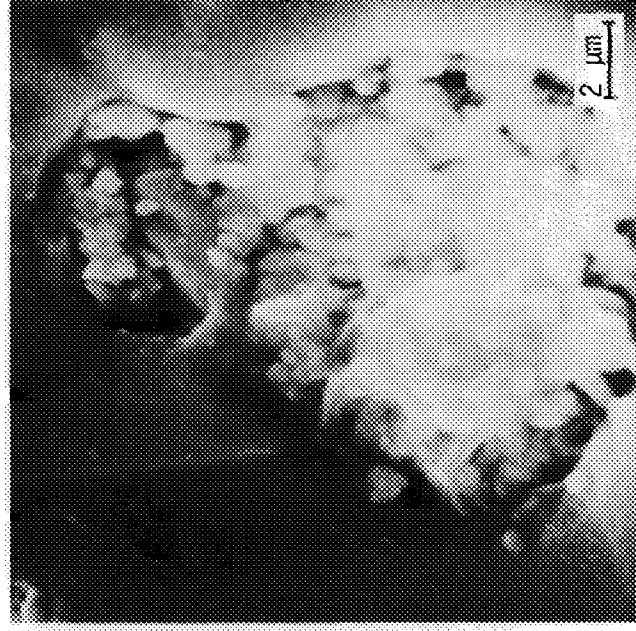
(b) Deposit within pore in SiC pin

FIGURE 41. PSZ DEPOSITED ONTO SiC PINS
AT 23°C IN DE

93
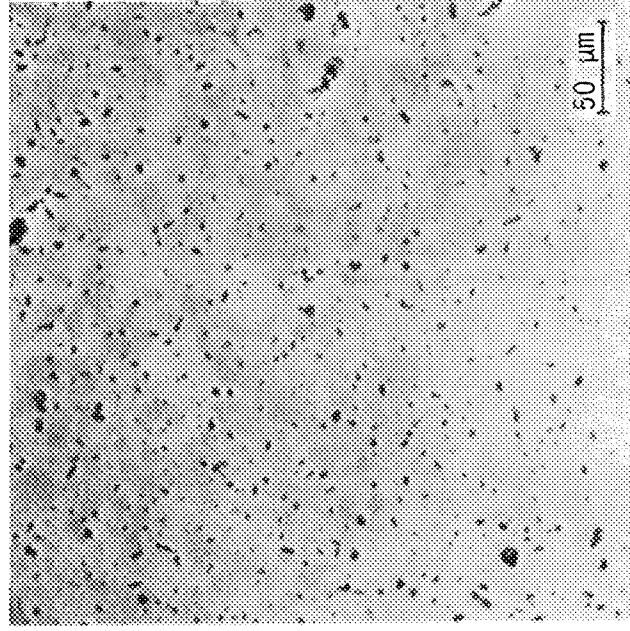
(a) Unworn pin, uncoated
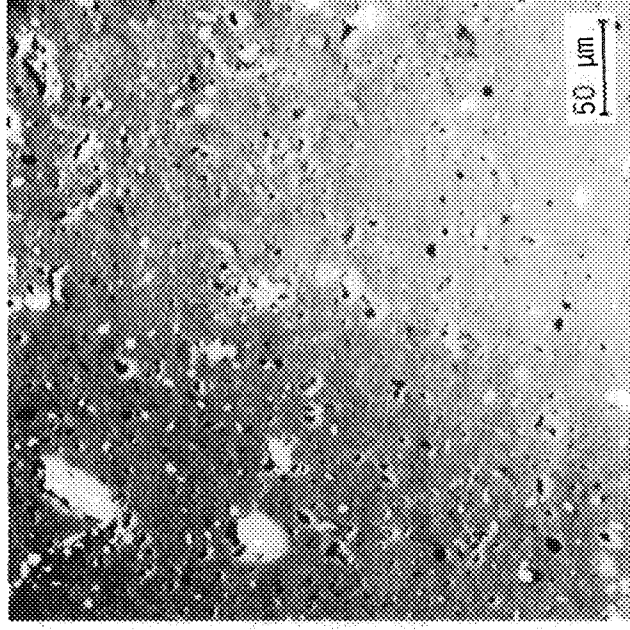
(b) Early wear pin, uncoated
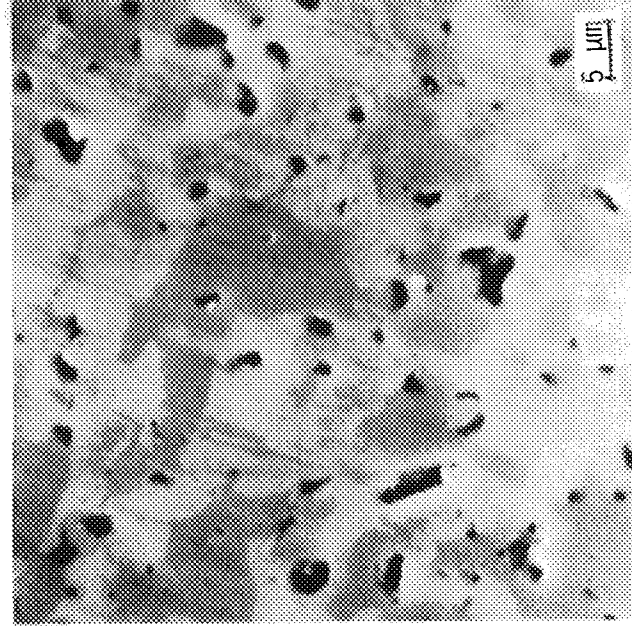
(c) Unworn pin, uncoated
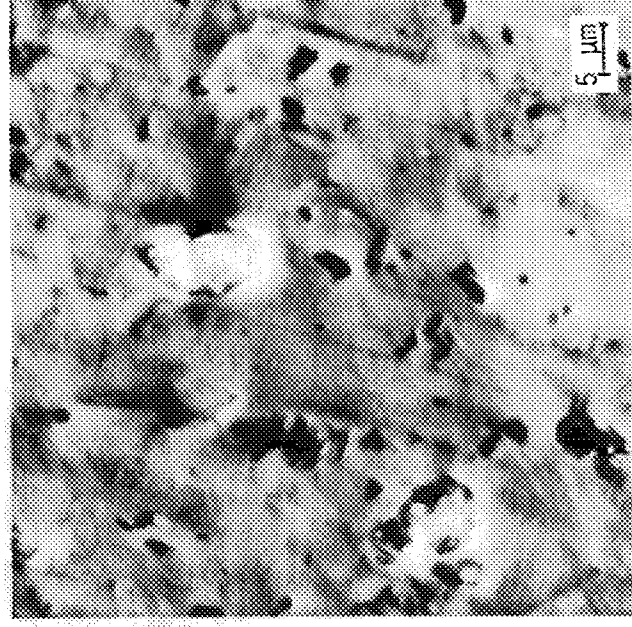
(d) Moderate wear pin, uncoated

FIGURE 42. TRANSFER OF PSZ DISK MATERIAL TO, AND PLASTIC
DEFORMATION OF, SiC PIN MATERIAL.

94
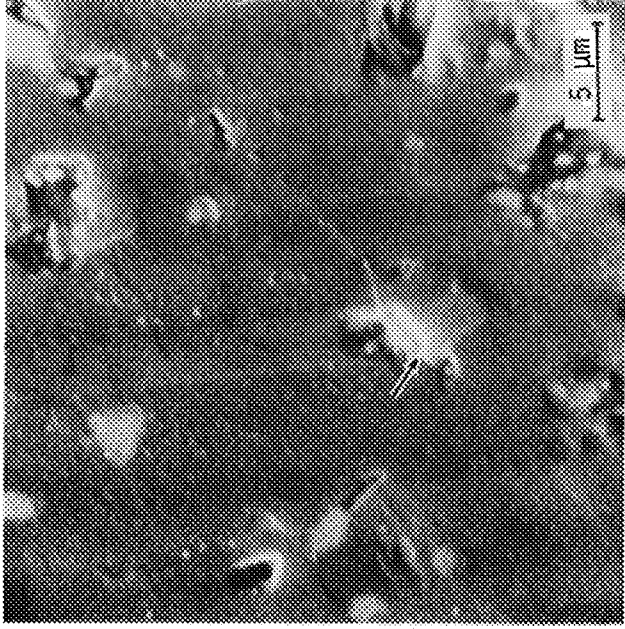
(a) Early wear, carbides come into relief (arrow) due to plastic flow in surrounding matrix
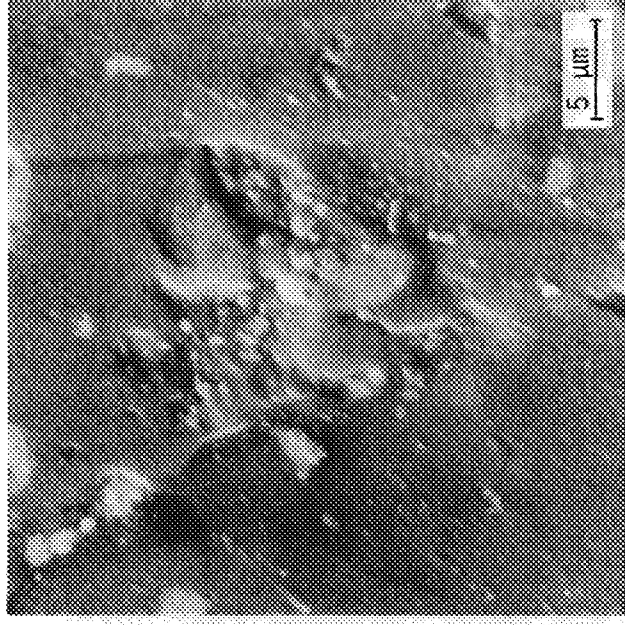
(b) Later wear, particle relief
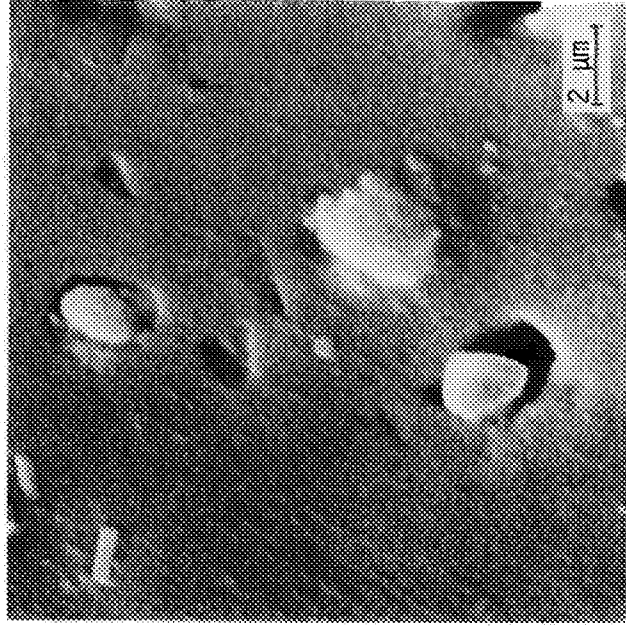
(c) Later wear, erosion of pits around particles
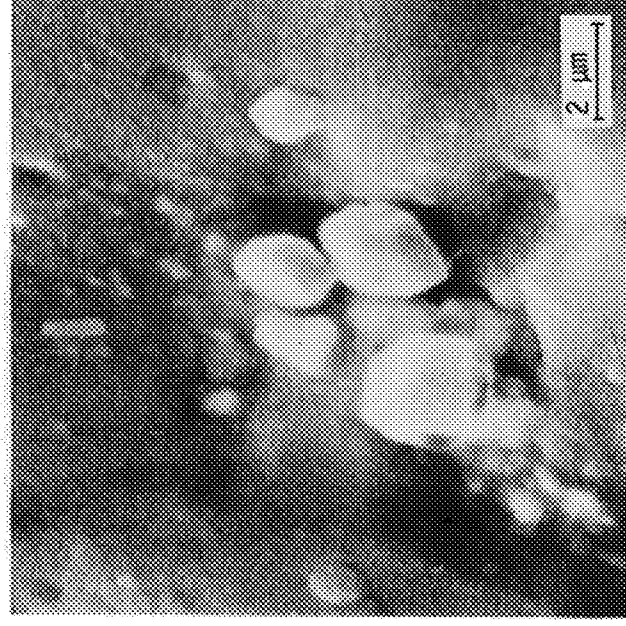
(d) Final wear, particles fully exposed

FIGURE 43. SiC PIN WEAR DUE TO PLASTIC DEFORMATION INDUCED BY A PSZ DISK, 23°C, DE

95

(a) Equilibrium wear, pin
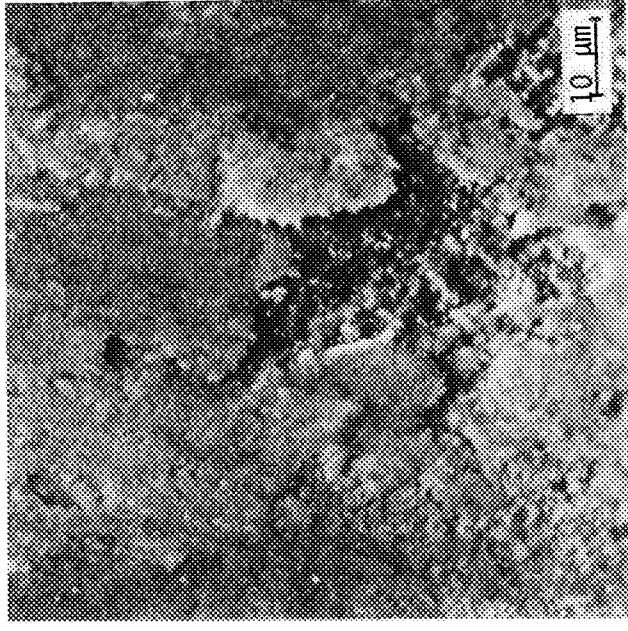
(c) Delamination of NiMoX deposit, disk

(b) NiMoX deposit, disk

FIGURE 44. WEAR OF K162 PINS/NC 132 DISK IN DE AT 23°C
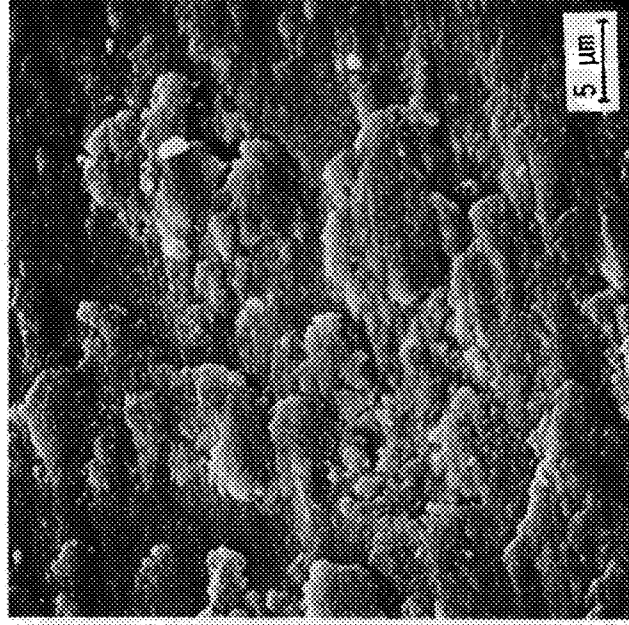
(a) Equilibrium wear, pin
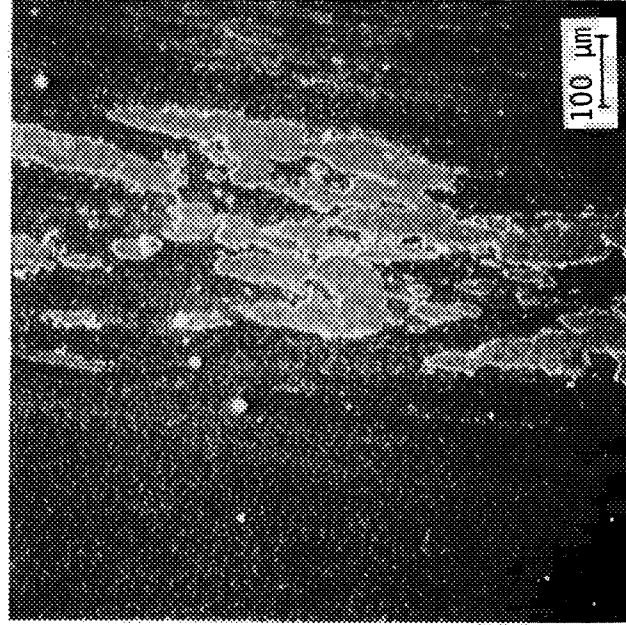
(b) NiMo deposit, disk
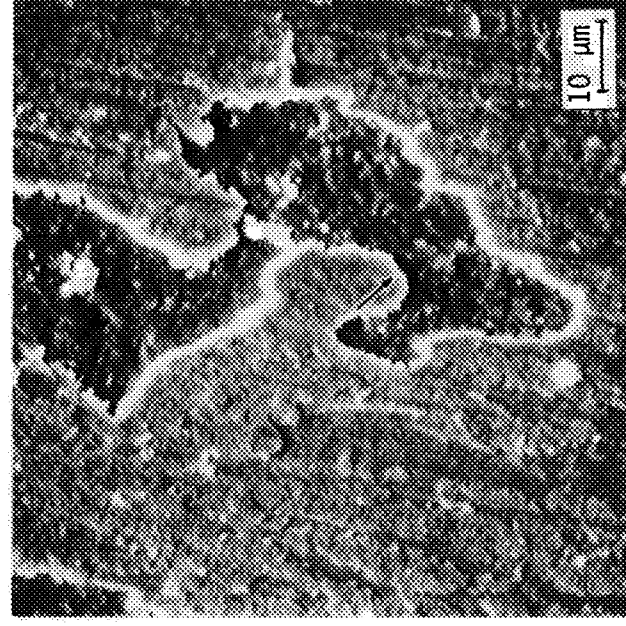
(c) Delamination NiMo deposit, disk. Flexure (arrow) of the coating is evident

FIGURE 45. WEAR OF K162B PINS/NC 132 DISK IN Ar AT 23°C

97
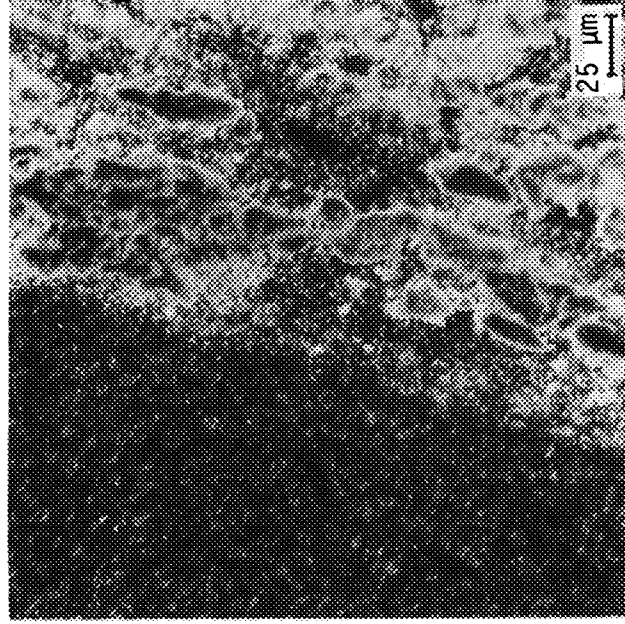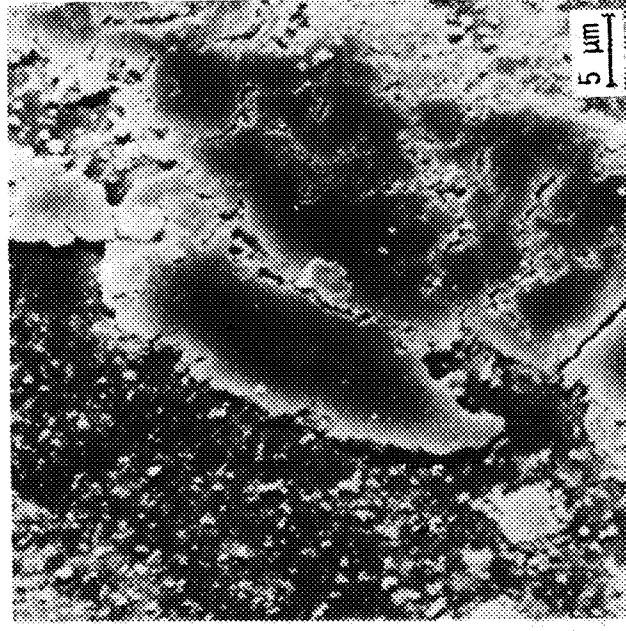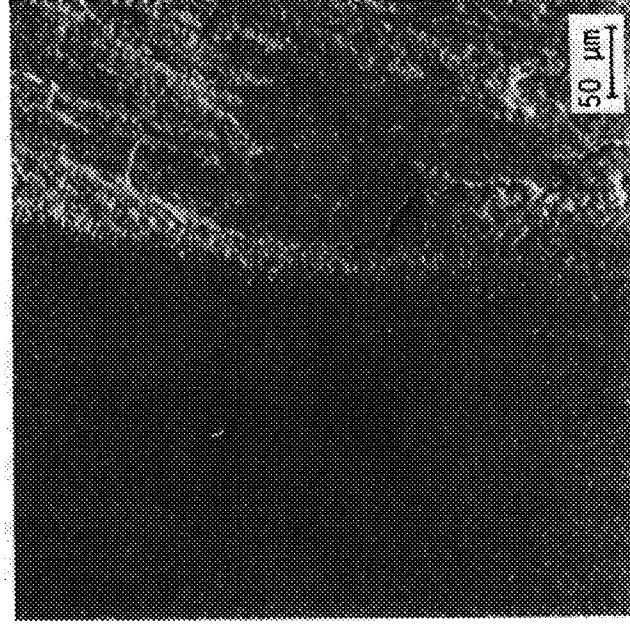
(b) Details TiO$_2$ deposit, disk, 23°C

(d) Details TiO$_2$ deposit, disk 800°C

(a) TiO$_2$ deposit, disk, 23°C

(c) TiO$_2$ deposit, disk, 800°C

FIGURE 46. TiO$_2$ DEPOSITS ON NC 132 DISKS RUN AGAINST TiC PINS IN DE

98
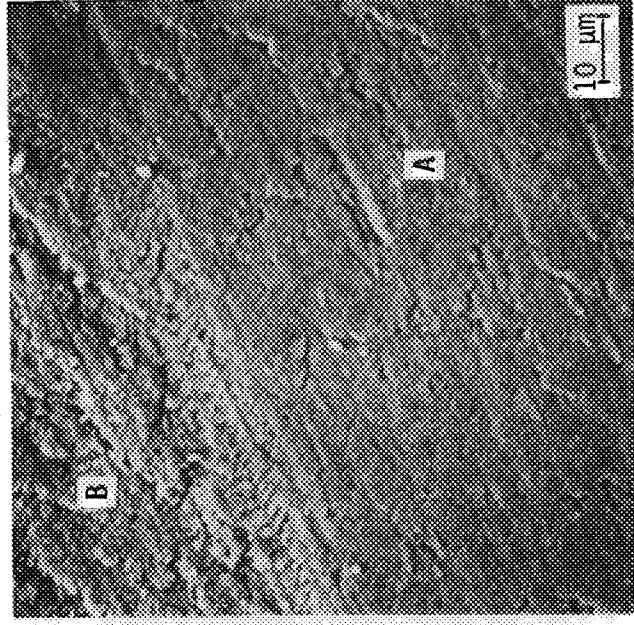
(a) Transition wear
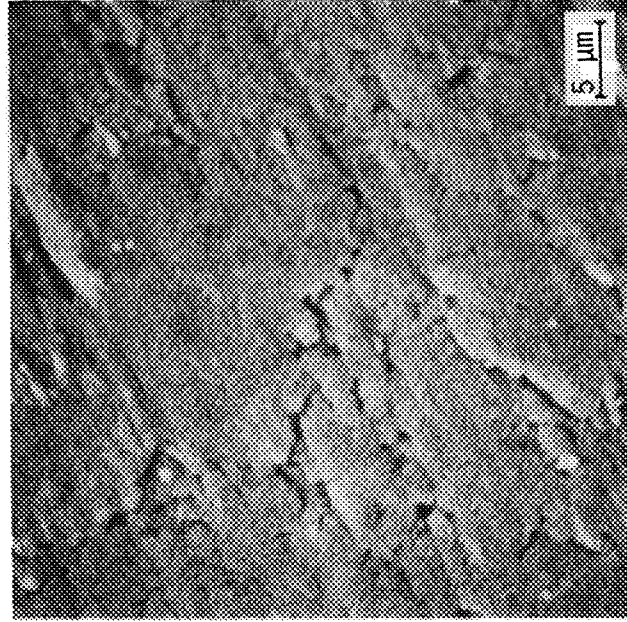
(b) Initial wear, Region A

(c) Equilibrium wear, Region B

FIGURE 47. K162B PIN, AFTER WEAR TEST AGAINST
NC 132 DISK AT 800°C IN Ar

99
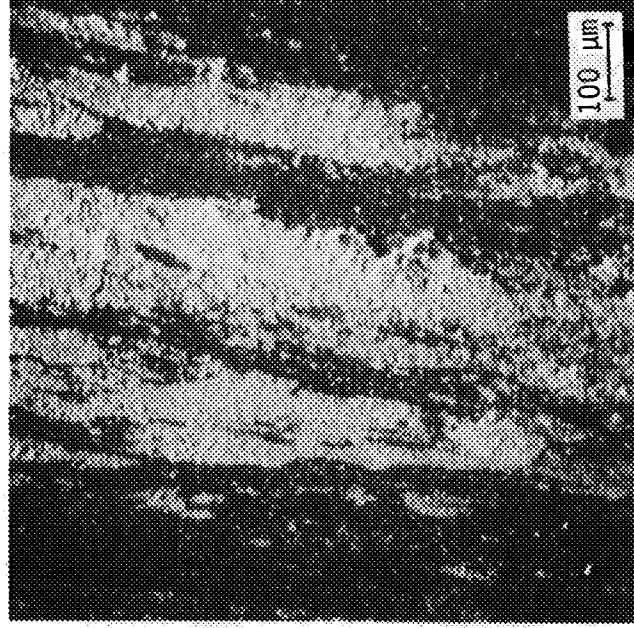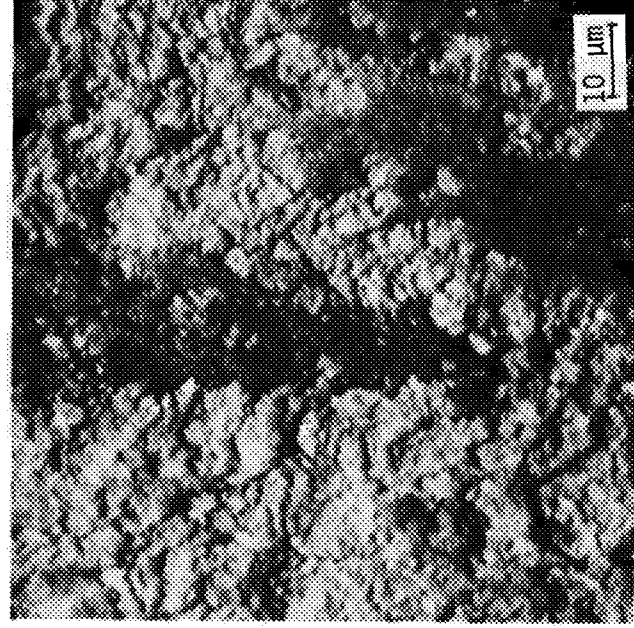
(a) NiMo deposit

(b) Microstructure NiMo deposit

FIGURE 48. NC 132 WEAR TRACK, AFTER WEAR TEST
AGAINST K162B PINS AT 800°C IN Ar
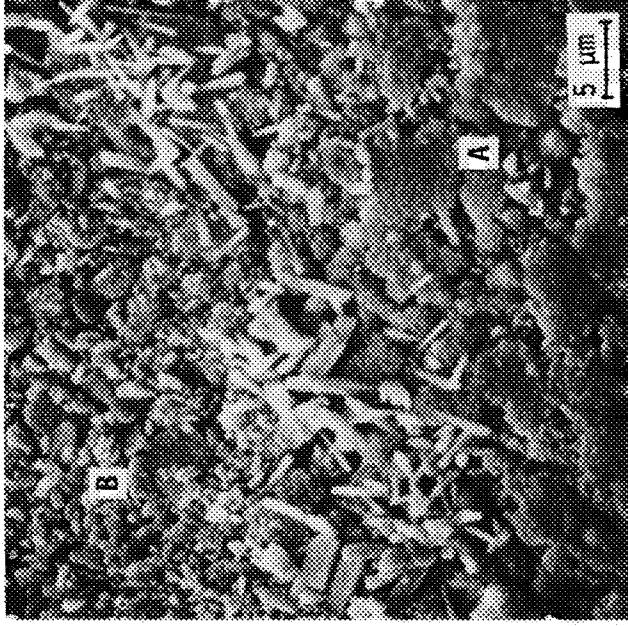
(a) Transition wear, pin
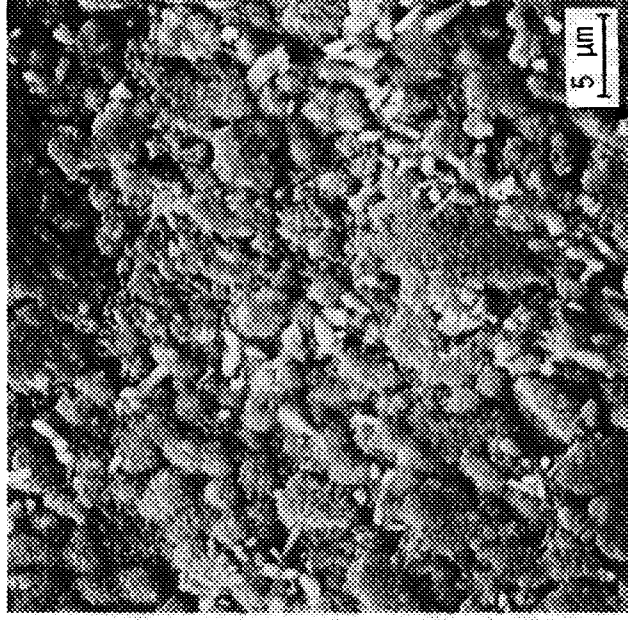
(b) Initial Wear, Region A
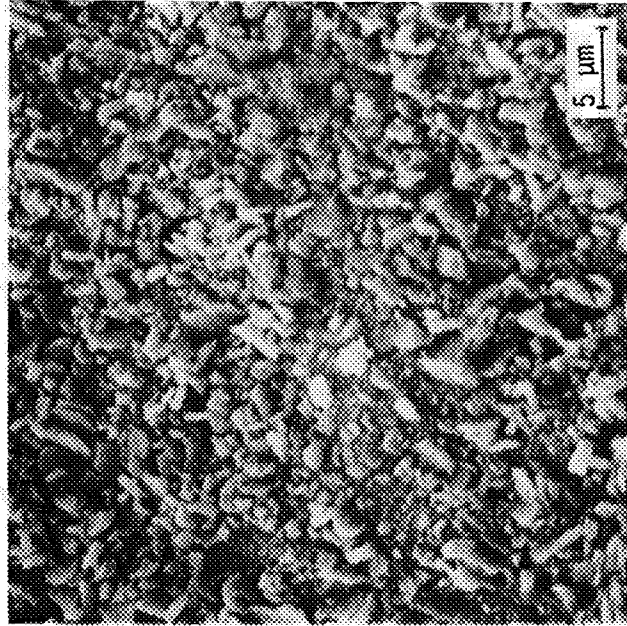
(c) Equilibrium wear, Region B
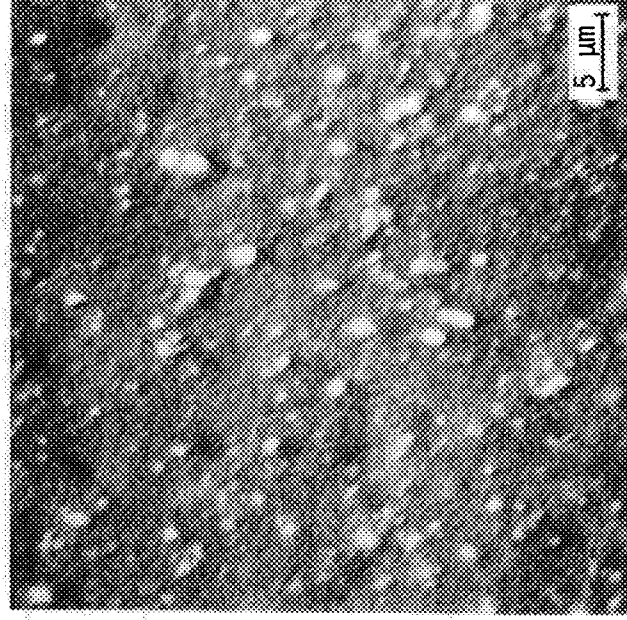
(d) Disk wear surface

**FIGURE 49. K162B PIN/NC 132 DISK WEAR SURFACES
AFTER TESTING AT 800°C IN DE**

101
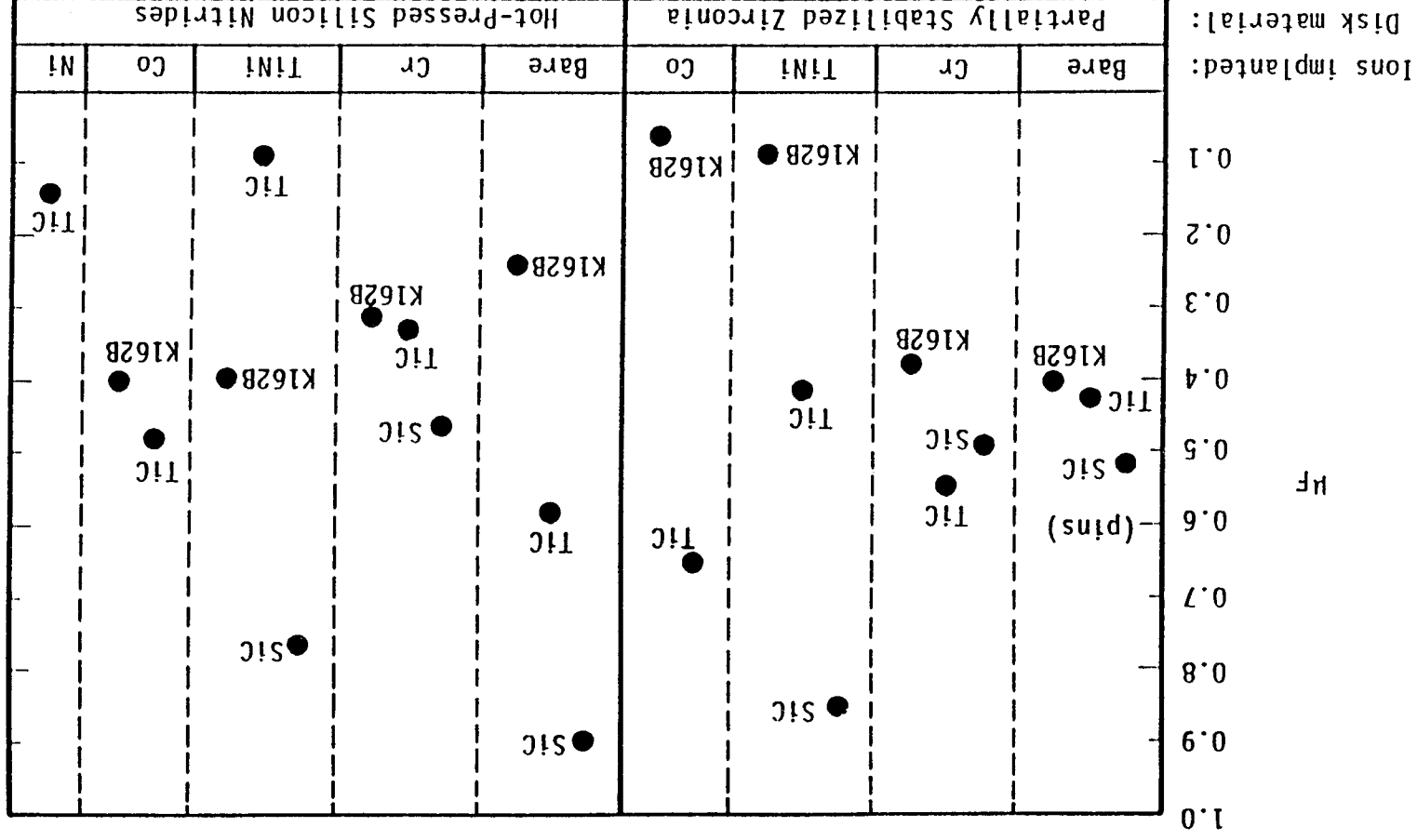
FIGURE 50. STEADY-STATE COEFFICIENT OF FRICTION AT 800°C IN DE

Disk material:

Partially Stabilized Zirconia				Hot-Pressed Silicon Nitrides				
Bare	Cr	TiNi	Co	Bare	Cr	TiNi	Co	Ni

Ions implanted:

μF

- 0.1
- 0.2
- 0.3
- 0.4
- 0.5
- 0.6
- 0.7
- 0.8
- 0.9
- 1.0

(pins)

Partially Stabilized Zirconia:
- Co: K162B (0.1), TiC (0.6)
- TiNi: K162B (0.1), TiC (0.4), SiC (0.8)
- Cr: K162B (0.4), TiC (0.55), SiC (0.5)
- Bare: K162B (0.4), TiC (0.45), SiC (0.5)

Hot-Pressed Silicon Nitrides:
- Ni: TiC (0.15)
- Co: TiC (0.1), K162B (0.4), TiC (0.45)
- TiNi: K162B (0.4), SiC (0.75)
- Cr: K162B (0.3), TiC (0.35), SiC (0.45)
- Bare: K162B (0.25), TiC (0.6), SiC (0.9)

(a) As-implanted elemental distribution
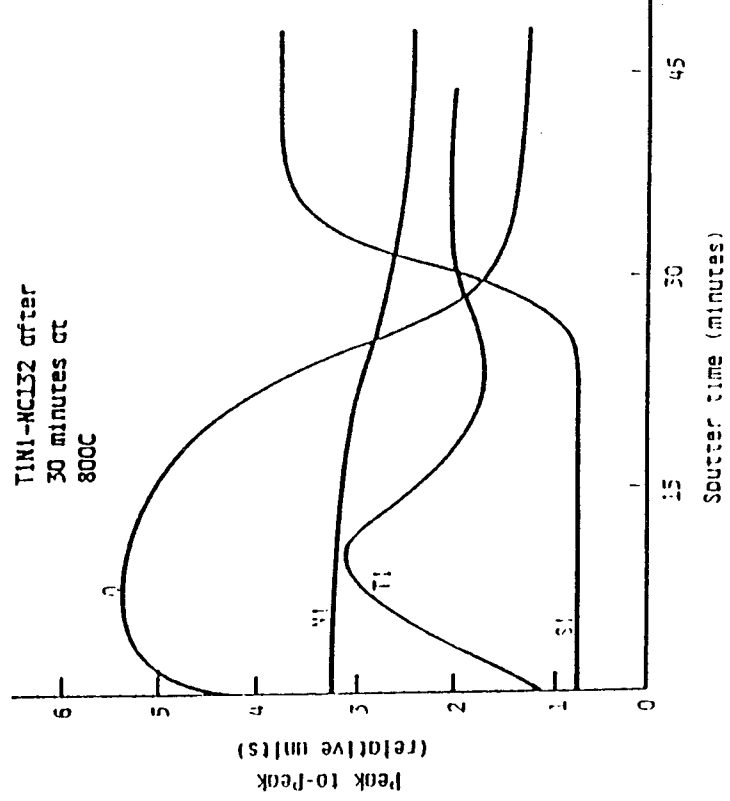
(b) Elemental distribution after 30 minutes at 800°C in DE

FIGURE 51. SCANNING AUGER ANALYSIS OF TiNi ION-IMPLANTATION IN NC 132

103
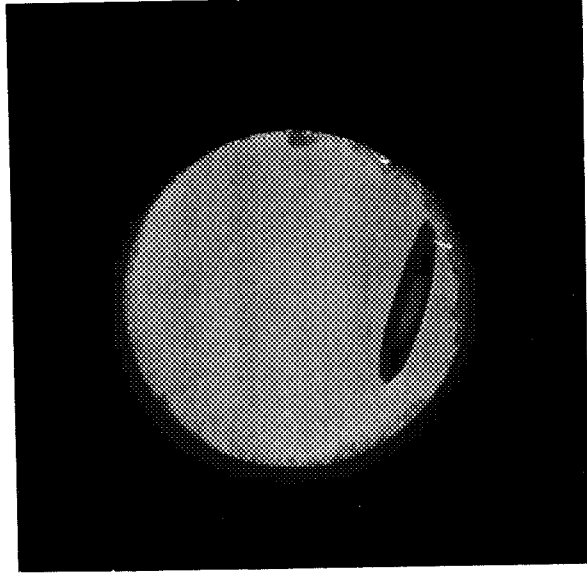
FIGURE 52. WEAR ZONE (DEPOSITS) ON K162B PIN RUN AGAINST TiNi-PSZ
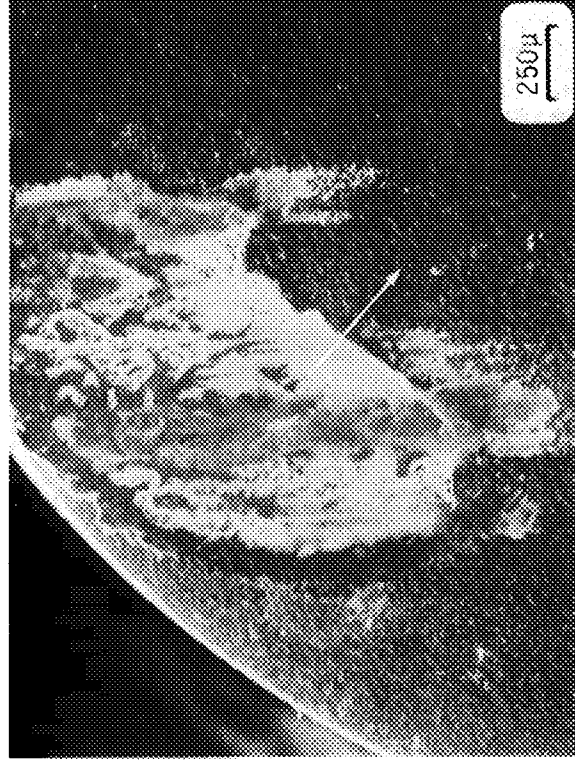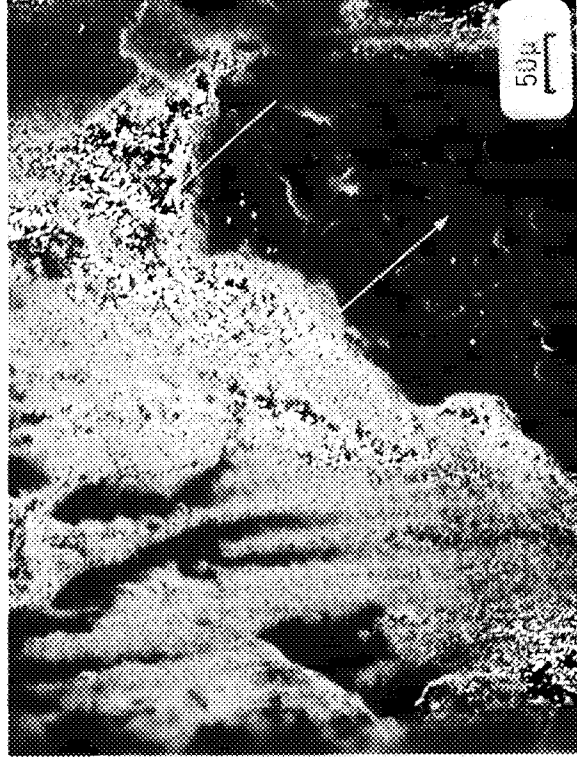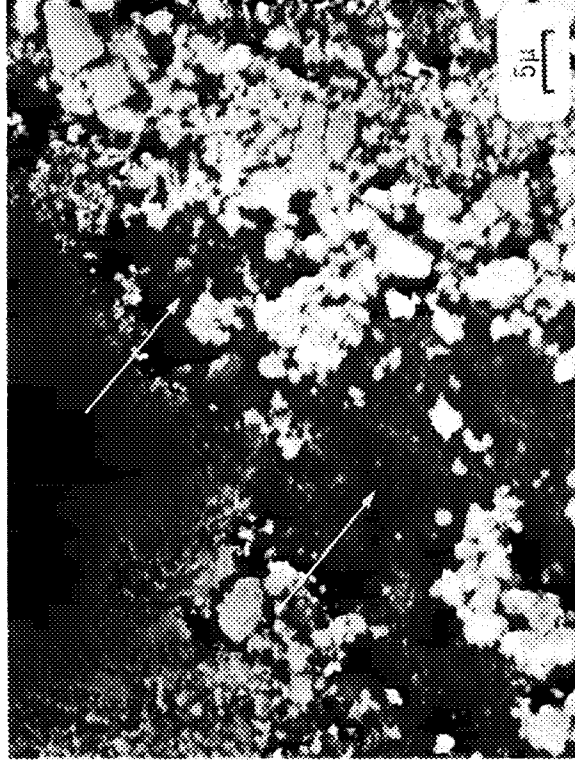
104

(a)

(b)

(c)

FIGURE 54. TRANSFER LAYER ON A TiC PIN RUN AGAINST A TiNi-IMPLANTED DISK IN A DIESEL ENVIRONMENT AT 800°C. ARROWS INDICATE PIN "BASE" MATERIAL.

250μ

50μ

5μ

(a)

(b)

(c)

FIGURE 54. TRANSFER LAYER ON A TiC PIN RUN AGAINST A TiNi-IMPLANTED DISK IN A DIESEL ENVIRONMENT AT 800°C. ARROWS INDICATE PIN "BASE" MATERIAL.

106
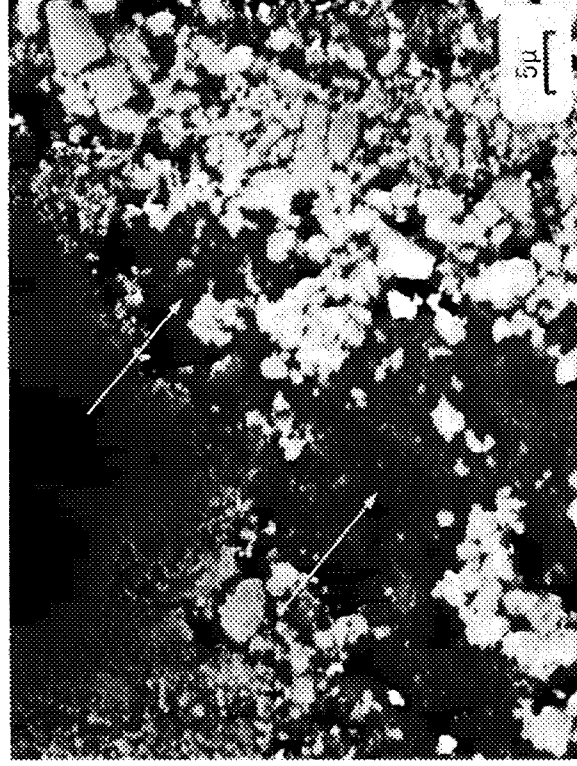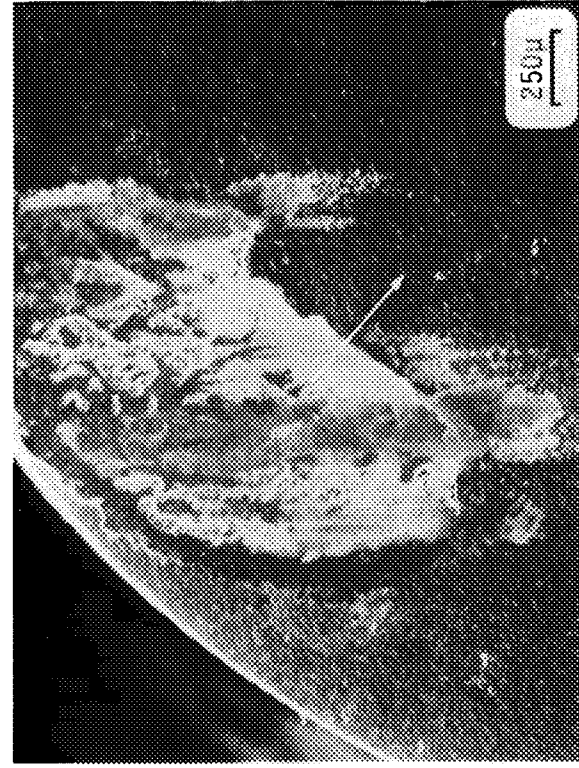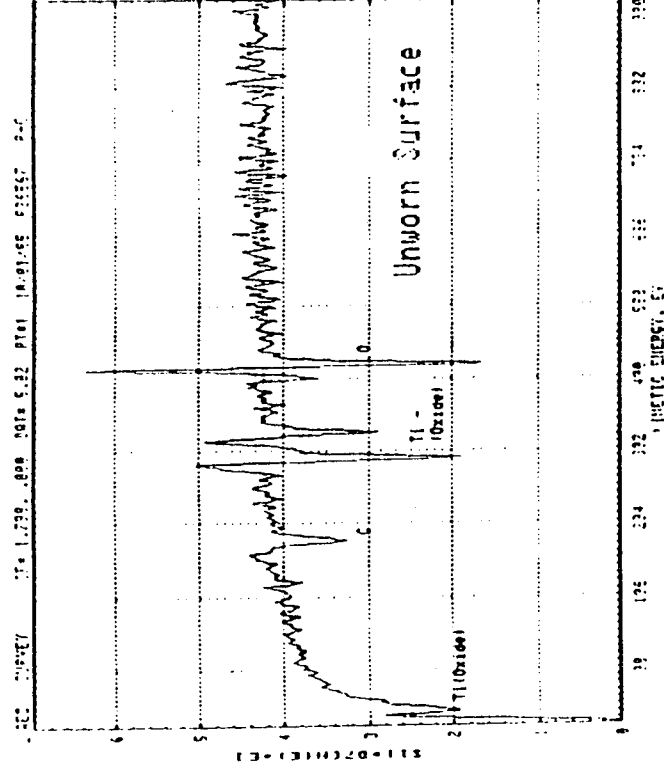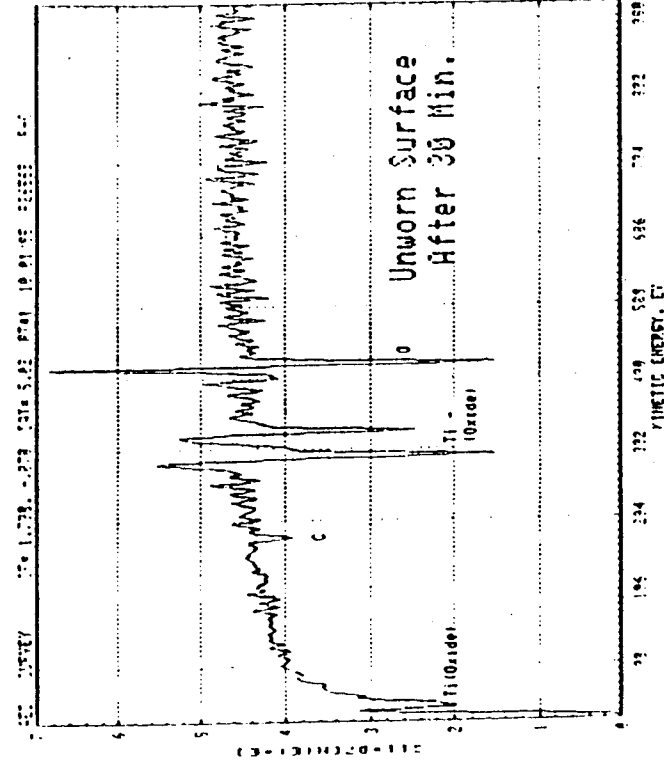
(a) Unworn surface

(b) Unworn surface after 30 minute sputter

FIGURE 55. AUGER SPECTRA TAKEN FROM A TiC PIN RUN AGAINST A Ti,
Ni-IMPLANTED SI_3N_4 DISK IN A DIESEL ENVIRONMENT AT 800°C

107
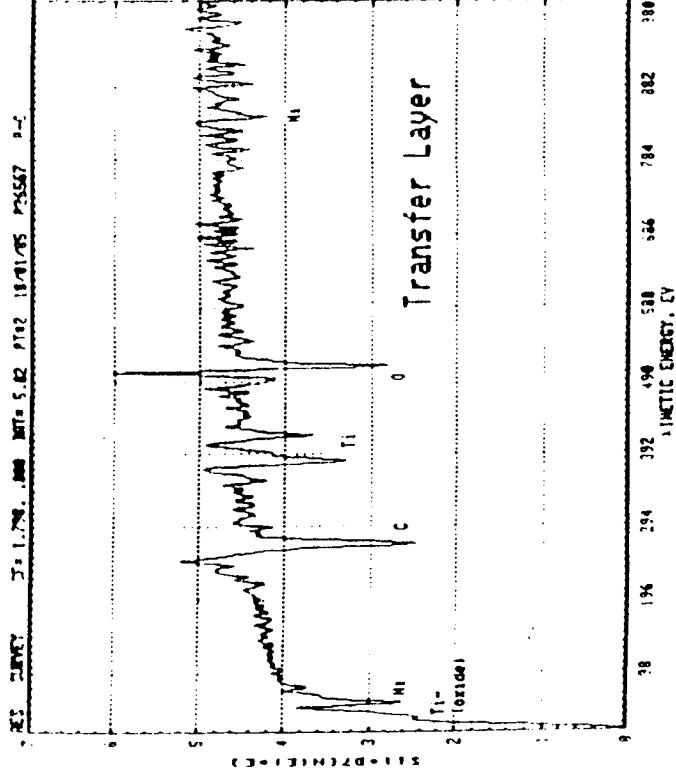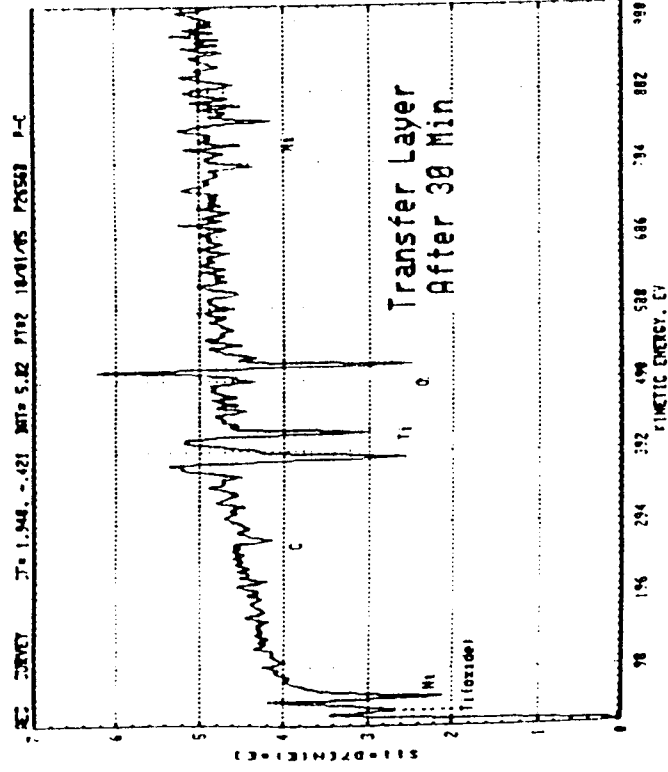
(c) Transfer layer

(d) Transfer layer after 30 minute sputter

FIGURE 55 (cont'd.). AUGER SPECTRA TAKEN FROM A TiC PIN RUN
AGAINST A Ti, Ni-IMPLANTED Si_3N_4 DISK IN A DIESEL
ENVIRONMENT AT 800°C

108
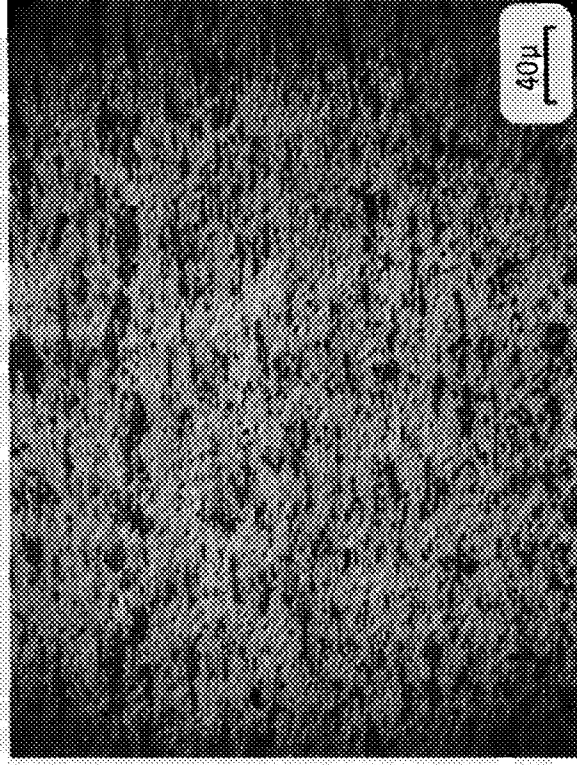
FIGURE 56. WEAR TRACK OF Si_3N_4 (TiNi) DISK RUN
AGAINST A TiC PIN ($\mu_F = 0.09$) IN A DIESEL
ENVIRONMENT AT 800°C
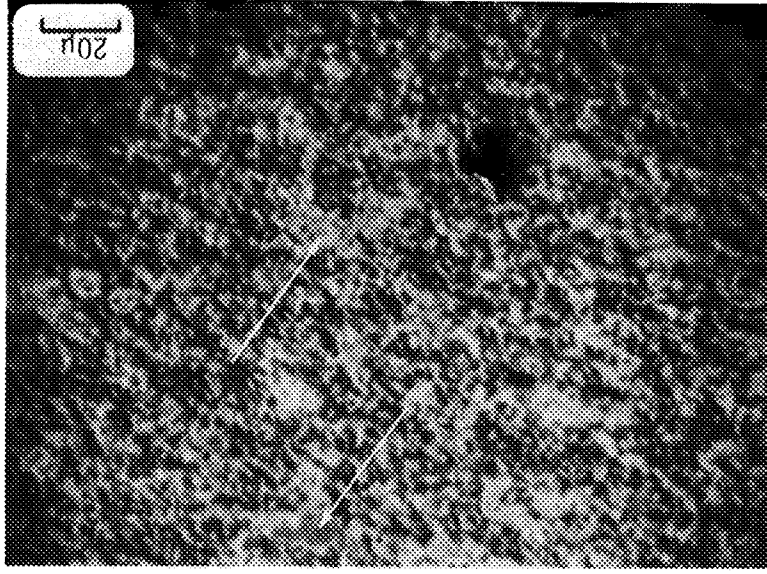
(c) Zr (147 eV) Auger map.
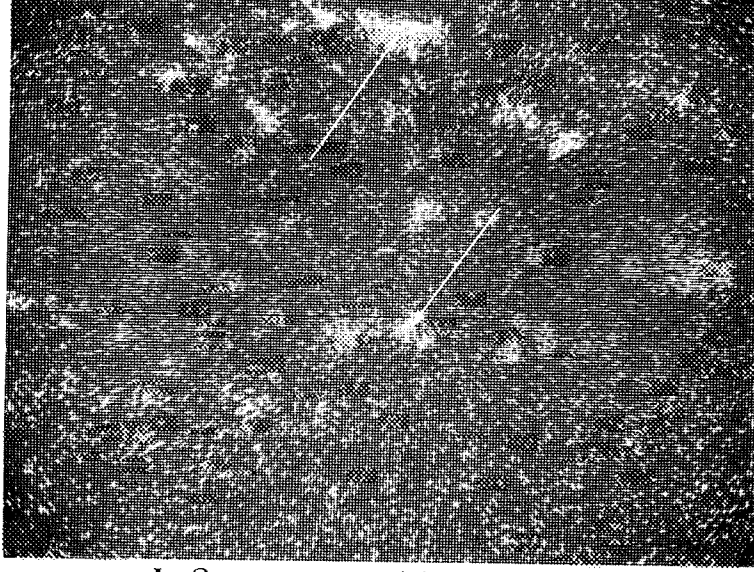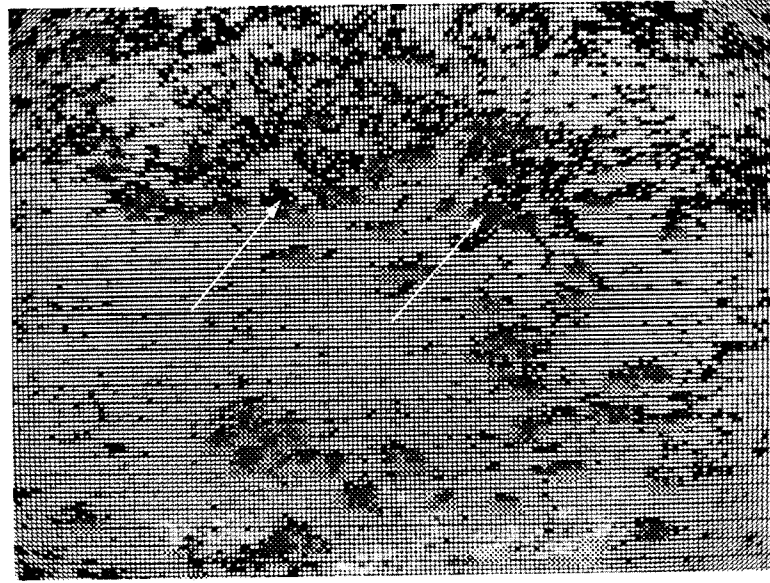
(b) Ti (387 eV) Auger map.

(a) SEM micrograph.
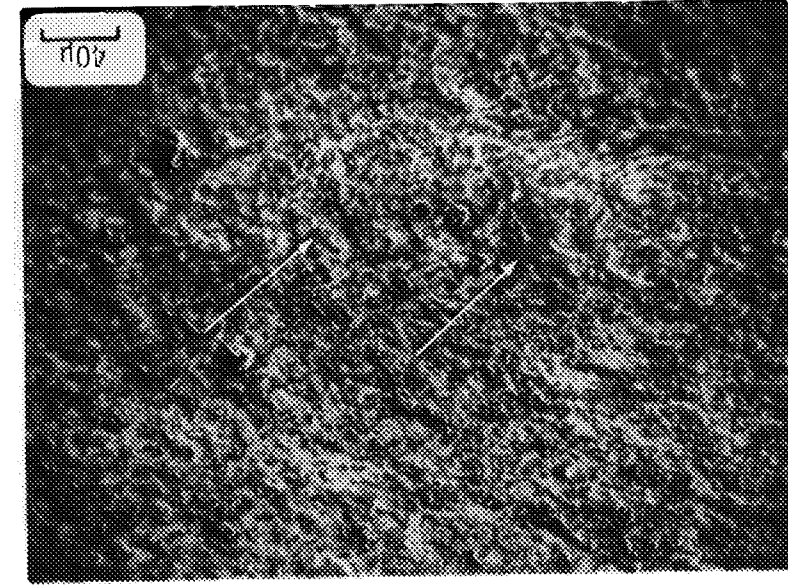
FIGURE 58. WEAR TRACK
OF PSZ (TiNi) DISK RUN
AGAINST A Ni-Mo-TiC PIN
(μ_r = 0.09) IN A DIESEL
ENVIRONMENT AT 800°C.

111
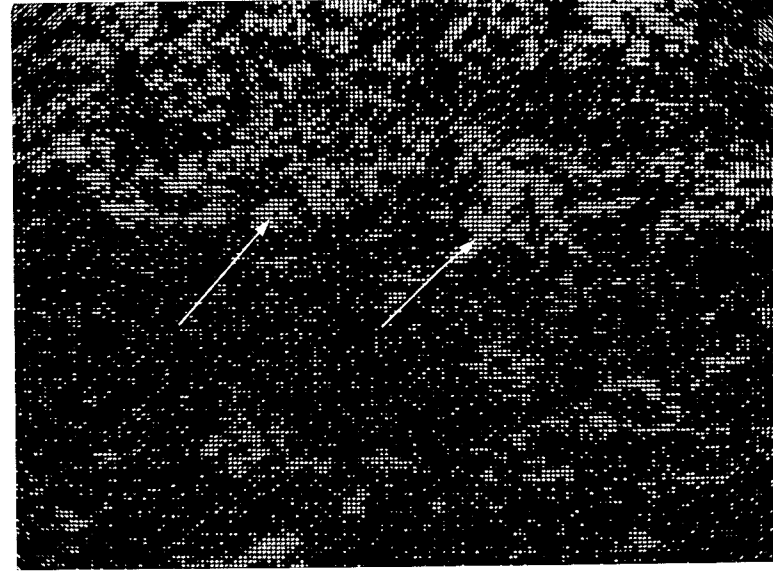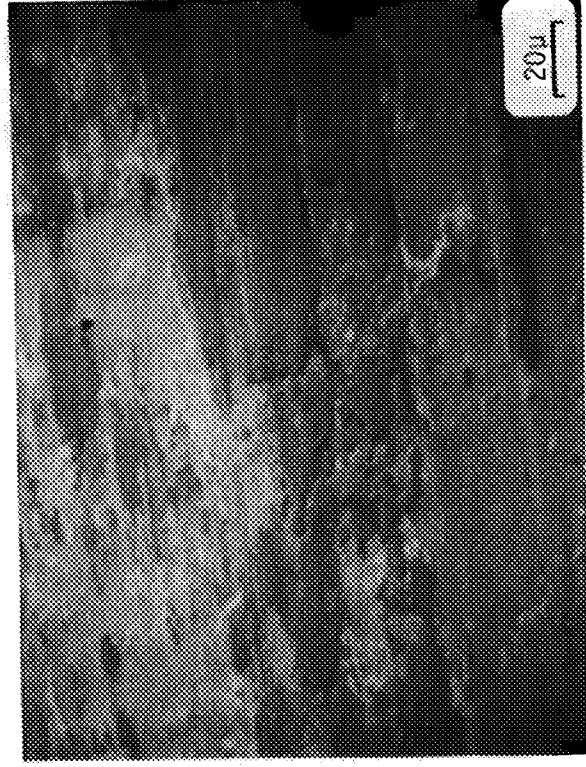
FIGURE 59. WEAR TRACK OF PSZ (TiNi) DISK RUN AGAINST A Ni-Mo-TiC PIN (μ_F = 0.25) IN A DIESEL ENVIRONMENT AT 800°C

112
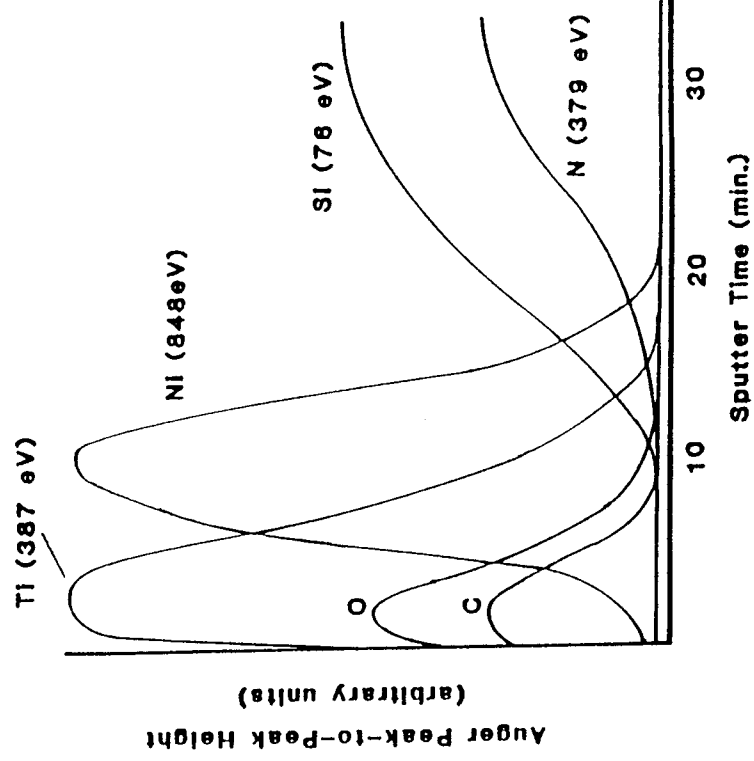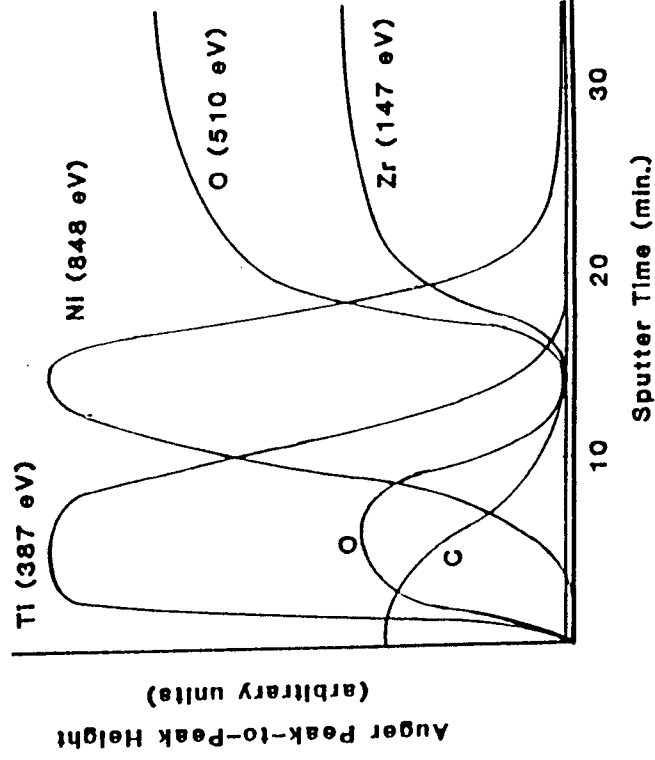
(a) Si_3N_4 (Ti, Ni)

(b) Partially stabilized zirconia (Ti, Ni)

FIGURE 60. ELEMENTAL DEPTH PROFILES OF ION-IMPLANTED DISKS BEFORE TESTING

113
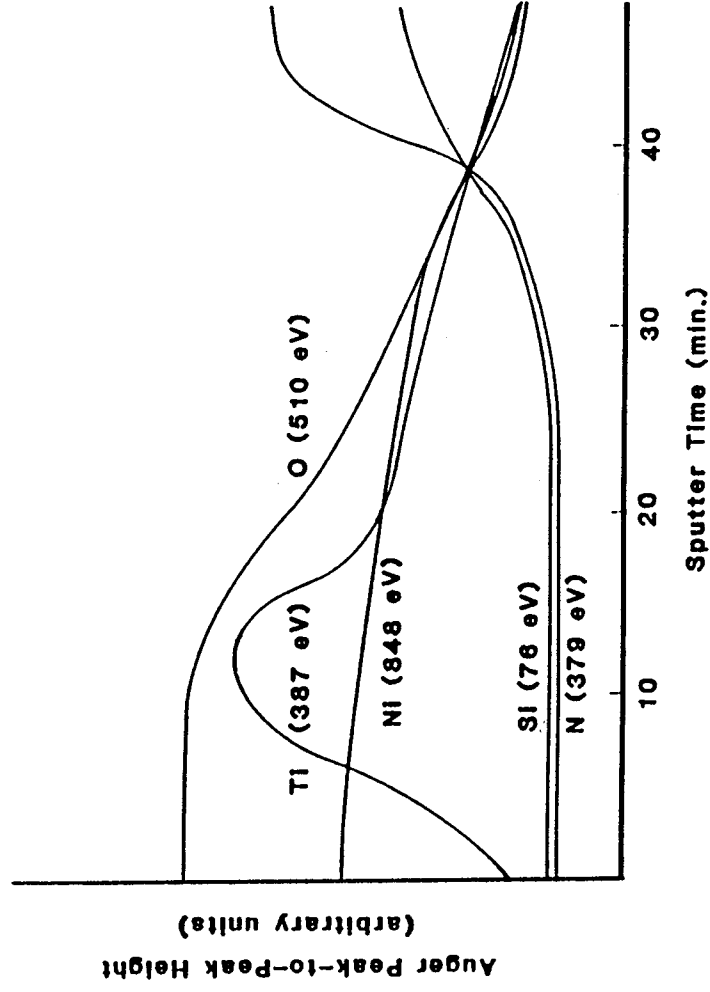
(a) Si_3N_4, (Ti, Ni)
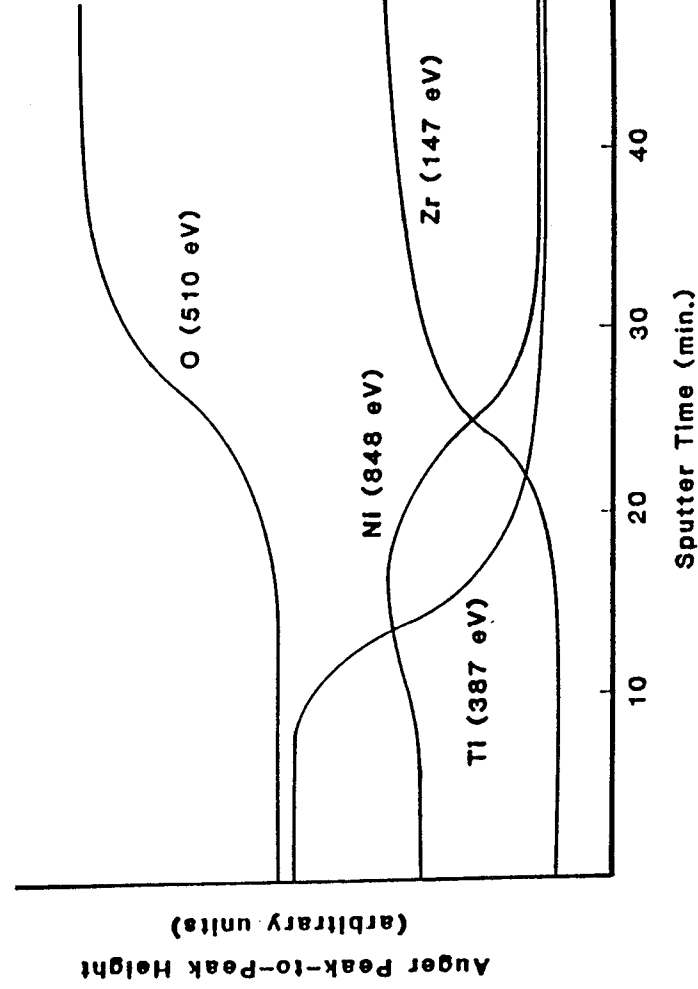
(b) Partially stabilized zirconia (Ti, Ni)

FIGURE 61. ELEMENTAL DEPTH PROFILES TAKEN AWAY FROM THE WEAR TRACK

114
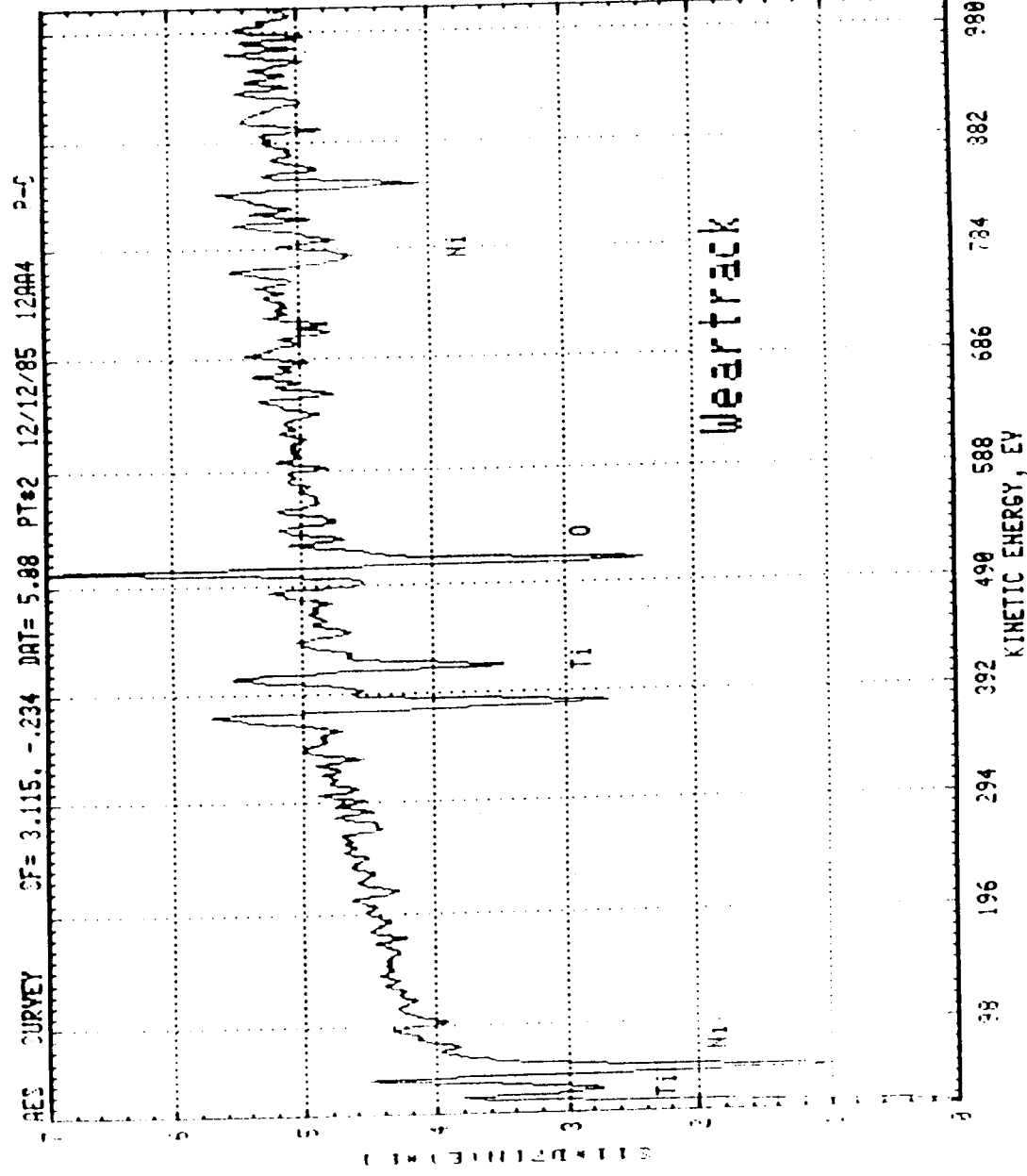
FIGURE 62. TYPICAL AUGER SPECTRUM TAKEN AFTER PARTIAL SPUTTER
REMOVAL OF THE IMPLANTED (TiNi) LAYER FROM A DISK

115

Auger Peak-to-Peak Height
(arbitrary units)

O (510 eV)

Ti (387 eV)

Ni (848 eV)

Si (76 eV)

N (379 eV)

Sputter Time (min.)
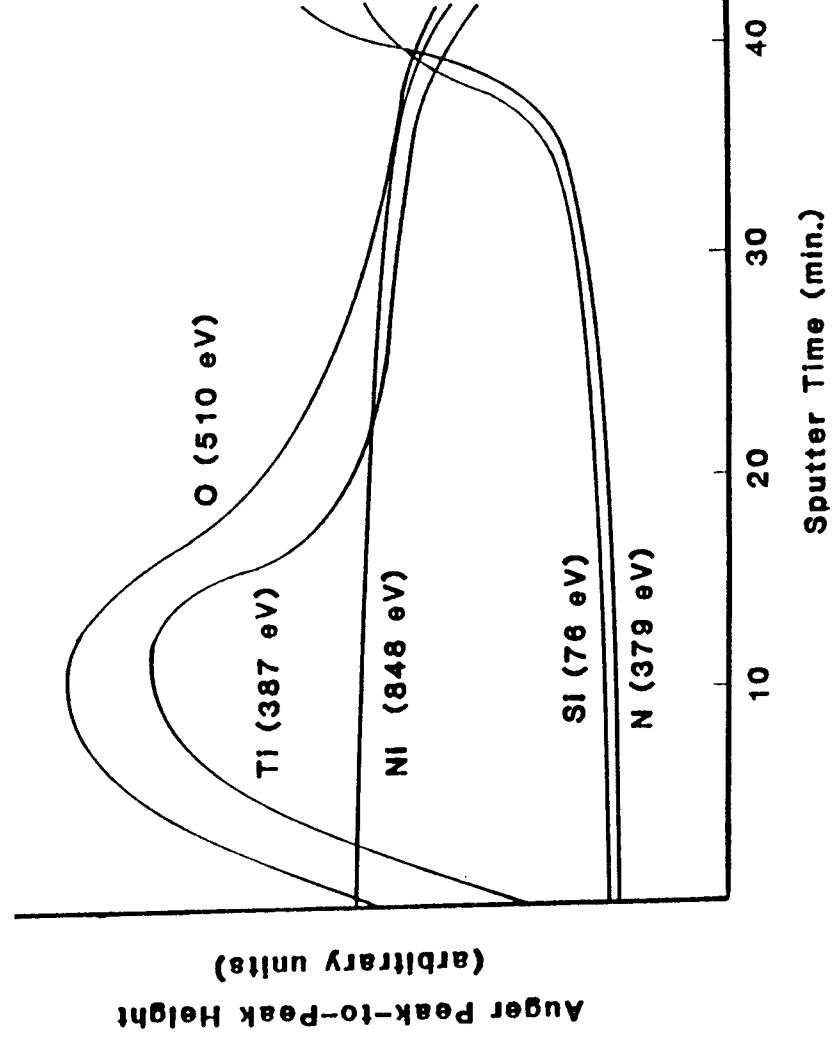
FIGURE 63. ELEMENTAL DEPTH PROFILE ON AN IMPLANT LAYER
LAMINATE LEFT ON THE WEAR TRACK OF A Si_3N_4 DISK

116
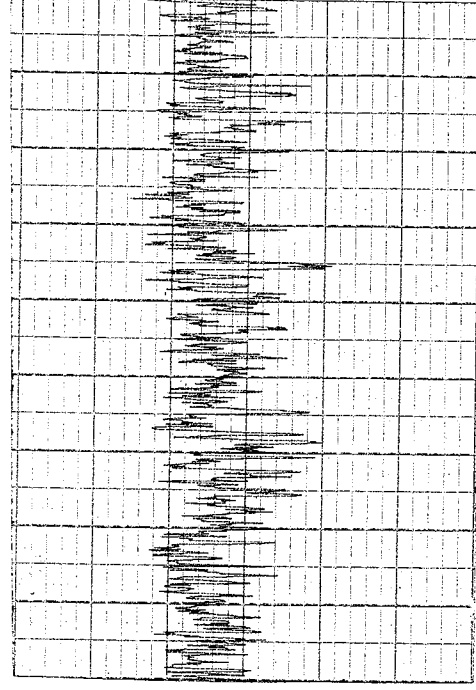
a.) 0 Hours (25 μ in)
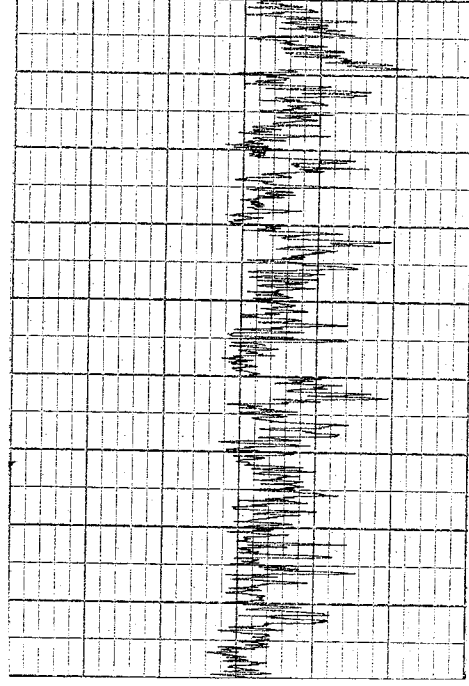
b.) 30 Hours, Metallic Region (24 μ in)
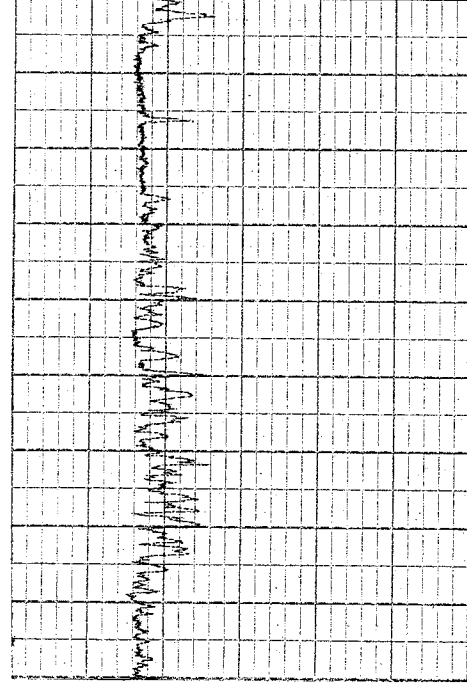
c.) 30 Hours, Light Region (7 μ in)

FIGURE 76. SURFACE FINISH MEASUREMENTS OF
TiNi IMPLANTED PSZ CYLINDER LINER

125

FIGURE 64. TYPICAL FRICTION FORCE TRACES FOR
HYDRODYNAMIC CAST IRON COMPONENTS

800 RPM

FRICTION FORCE

DOWNWARD STROKE | UPWARD STROKE

TDC   BDC   TDC

1200 RPM

FRICTION FORCE

DOWNWARD STROKE | UPWARD STROKE

TDC   BDC   TDC
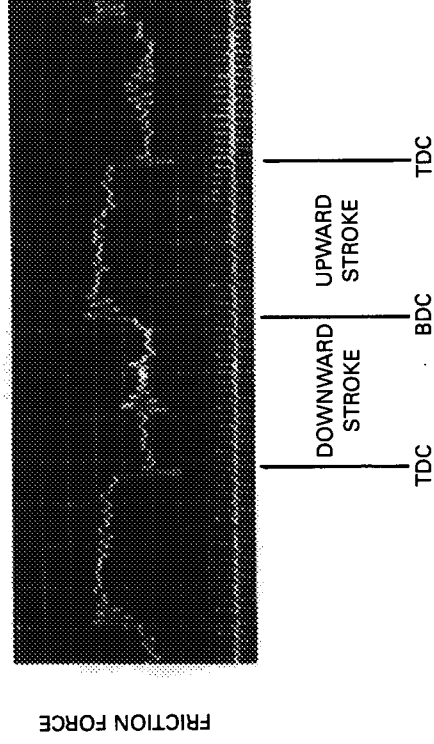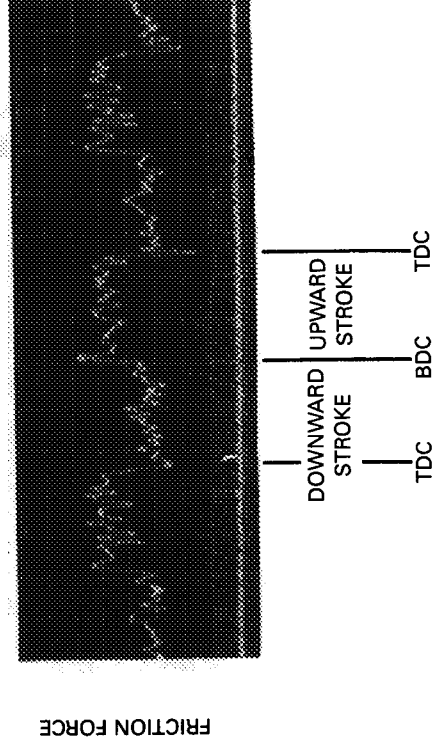
PSZ/Ni-MOLY BONDED TiC
RING SET 1
RING GAS LOAD = 200 PSI

FIGURE 65. TYPICAL FRICTION FORCE TRACES FOR
BOUNDARY LUBRICATED CERAMICS
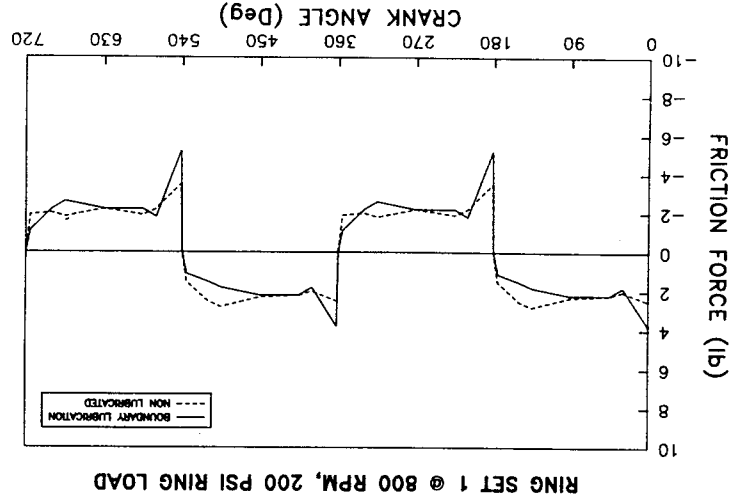
OUTER RING SURFACE

FRACTURE SURFACE

INNER RING SURFACE
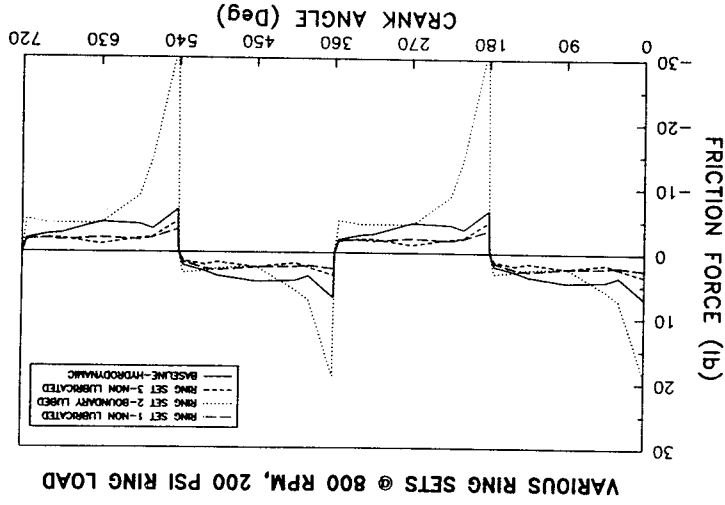
SEM PHOTO MICROGRAPH OF FRACTURE SURFACE
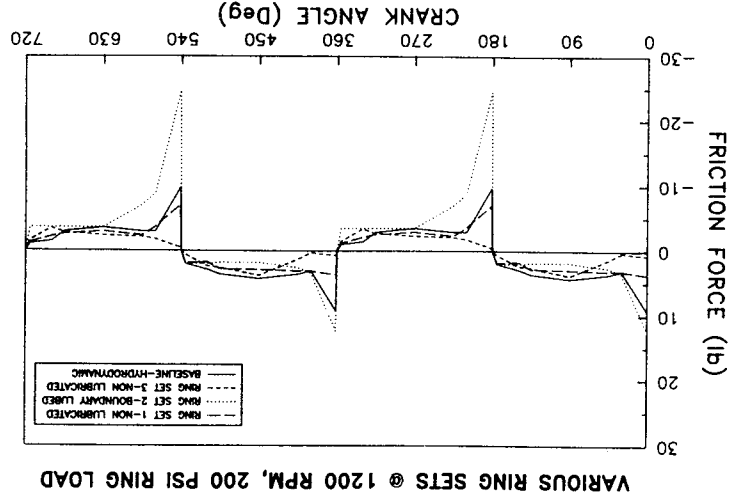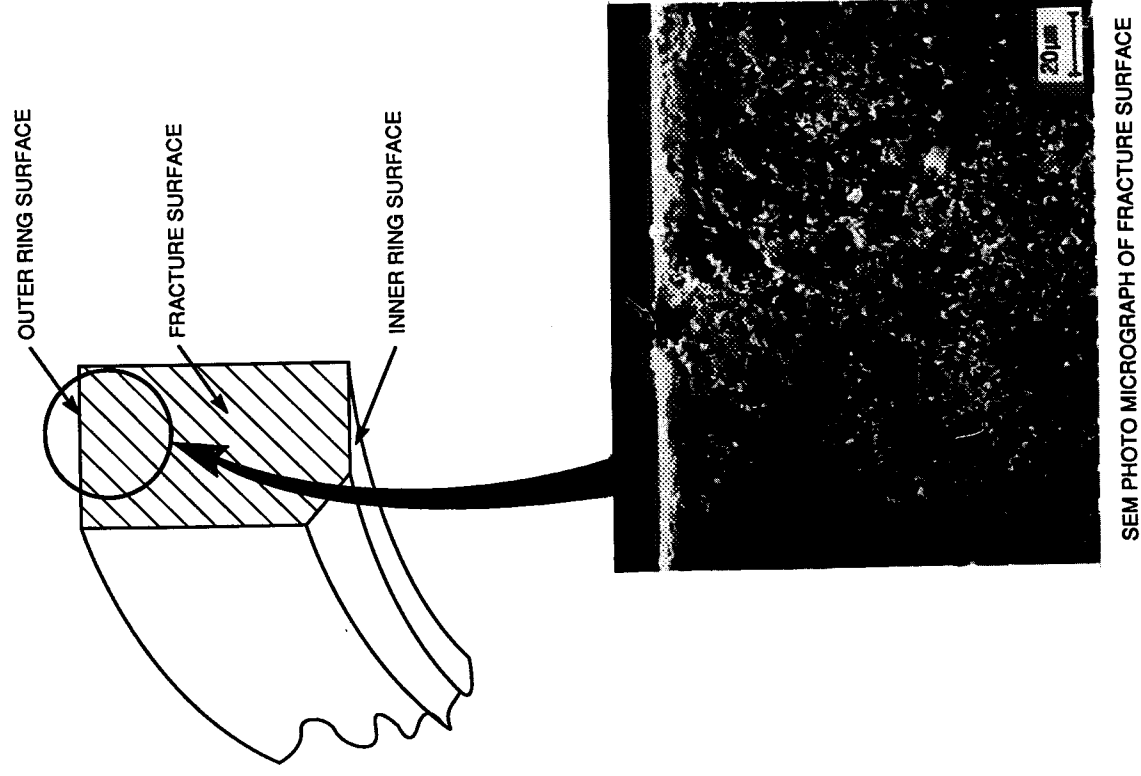
**FIGURE 69. Ni-Mo-TiC RING SET 4
FRACTURE SURFACE ANALYSIS**

FIGURE 72. PHOTOGRAPH OF SCUFFED PISTON SKIRT
AND TiNi ION-IMPLANTED PSZ LINER AFTER
INITIAL ENGINE TEST
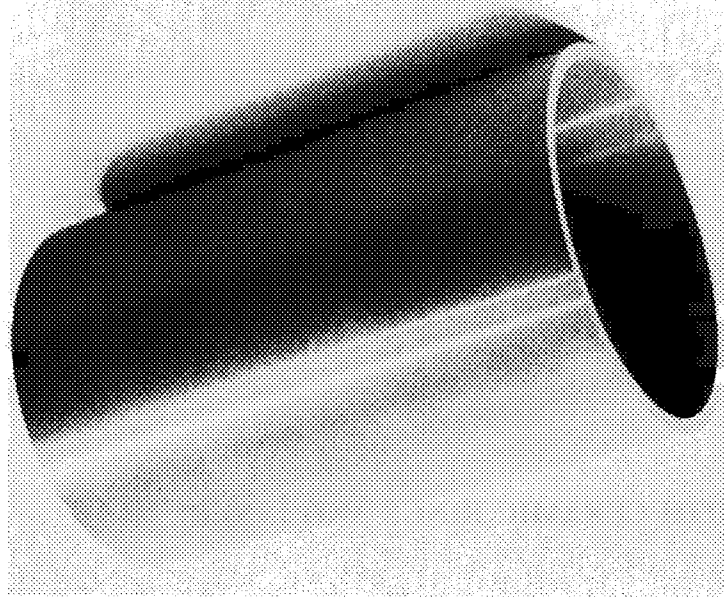
FIGURE 71. PHOTOGRAPH OF Si_3N_4
CYLINDER LINER

FIGURE 70. 3000x MAGNIFICATION OF
Ni-Mo-TiC RING SET 4 SURFACE CAVITY

121
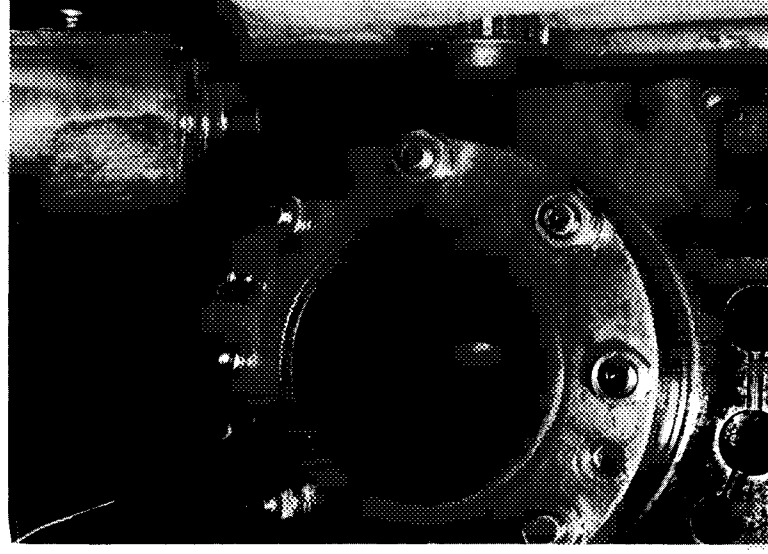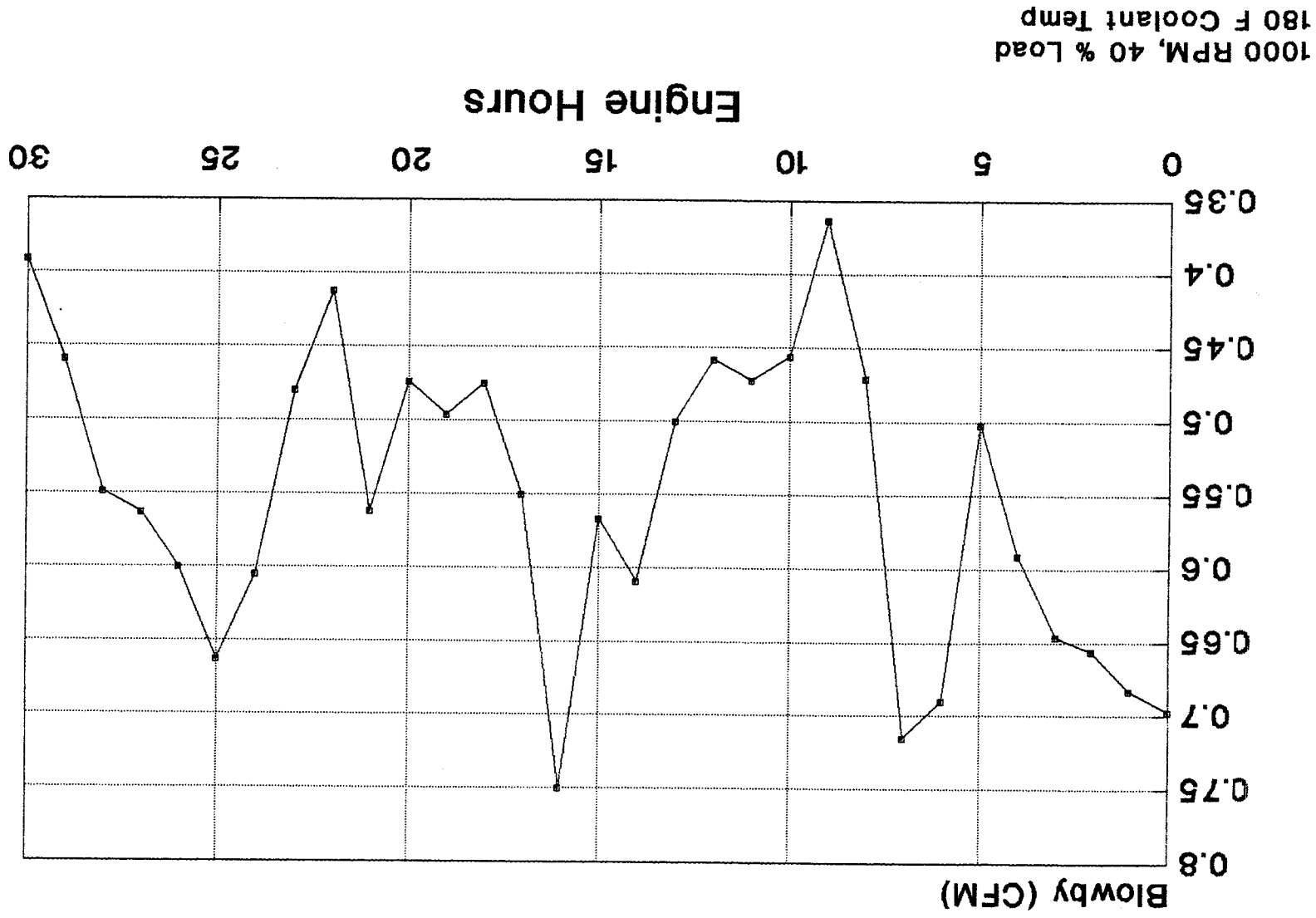
FIGURE 73. BLOWBY VERSUS ENGINE HOURS WITH CERAMIC RINGS AND LINER

1000 RPM, 40 % Load
180 F Coolant Temp

122

FIGURE 74. BSFC VERSUS ENGINE HOURS WITH CERAMIC RINGS AND LINER

1000 RPM, 40 % Load
180 F Coolant Temp

123
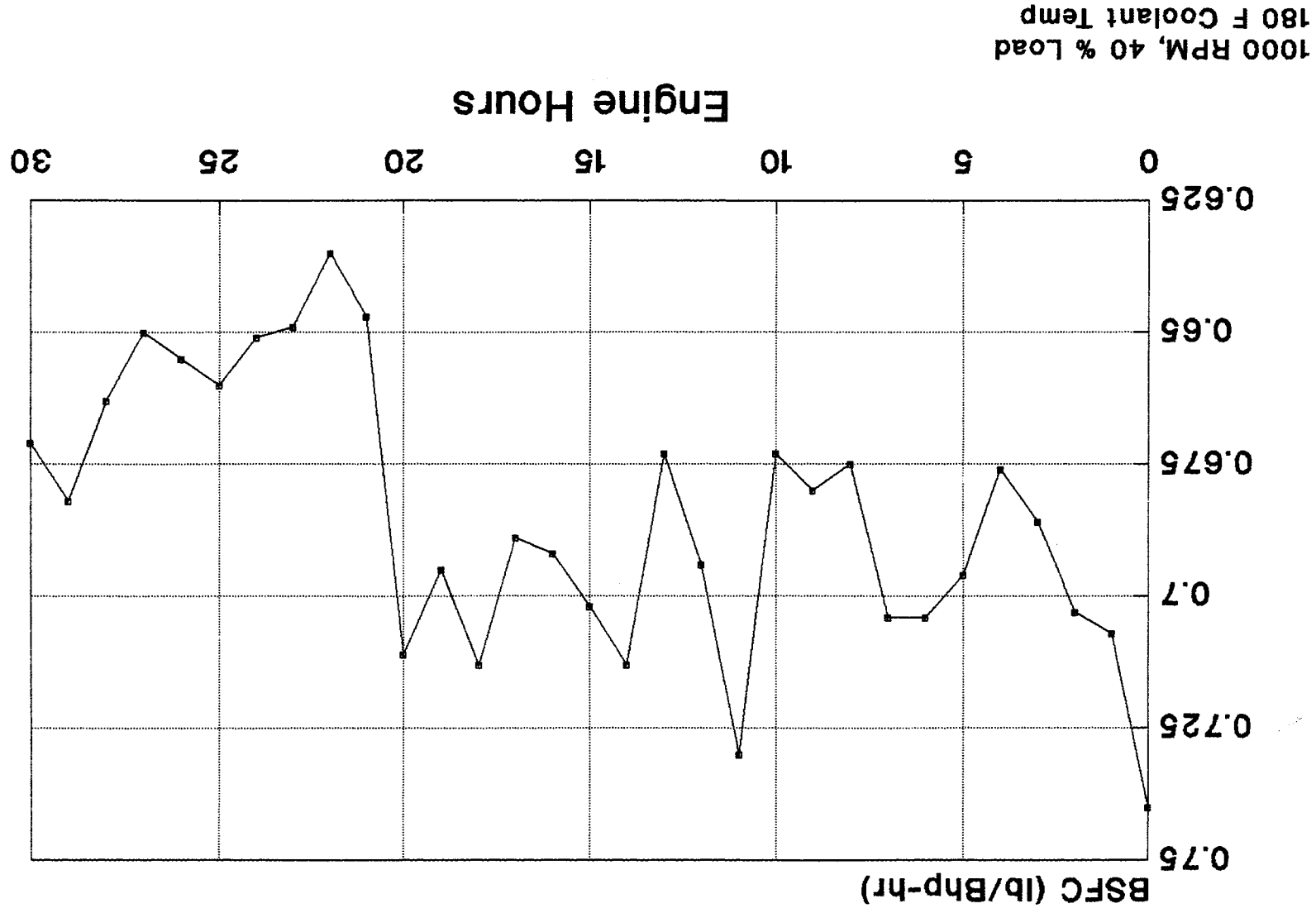
FIGURE 75. MOTORING FRICTION VERSUS ENGINE HOURS WITH CERAMIC RINGS AND LINER

124

1000 RPM, 40 % Load
180 F Coolant Temp

Legend:
- Cast Iron Baseline
- 10 hr Ceramics
- 0 hr Ceramics
- 25 hr Ceramics

Engine Speed (RPM)

Friction Torque (ft-lb)

126

FIGURE 78. ENGINE PERFORMANCE TEST RESULTS, CAST IRON AND CERAMIC DATA
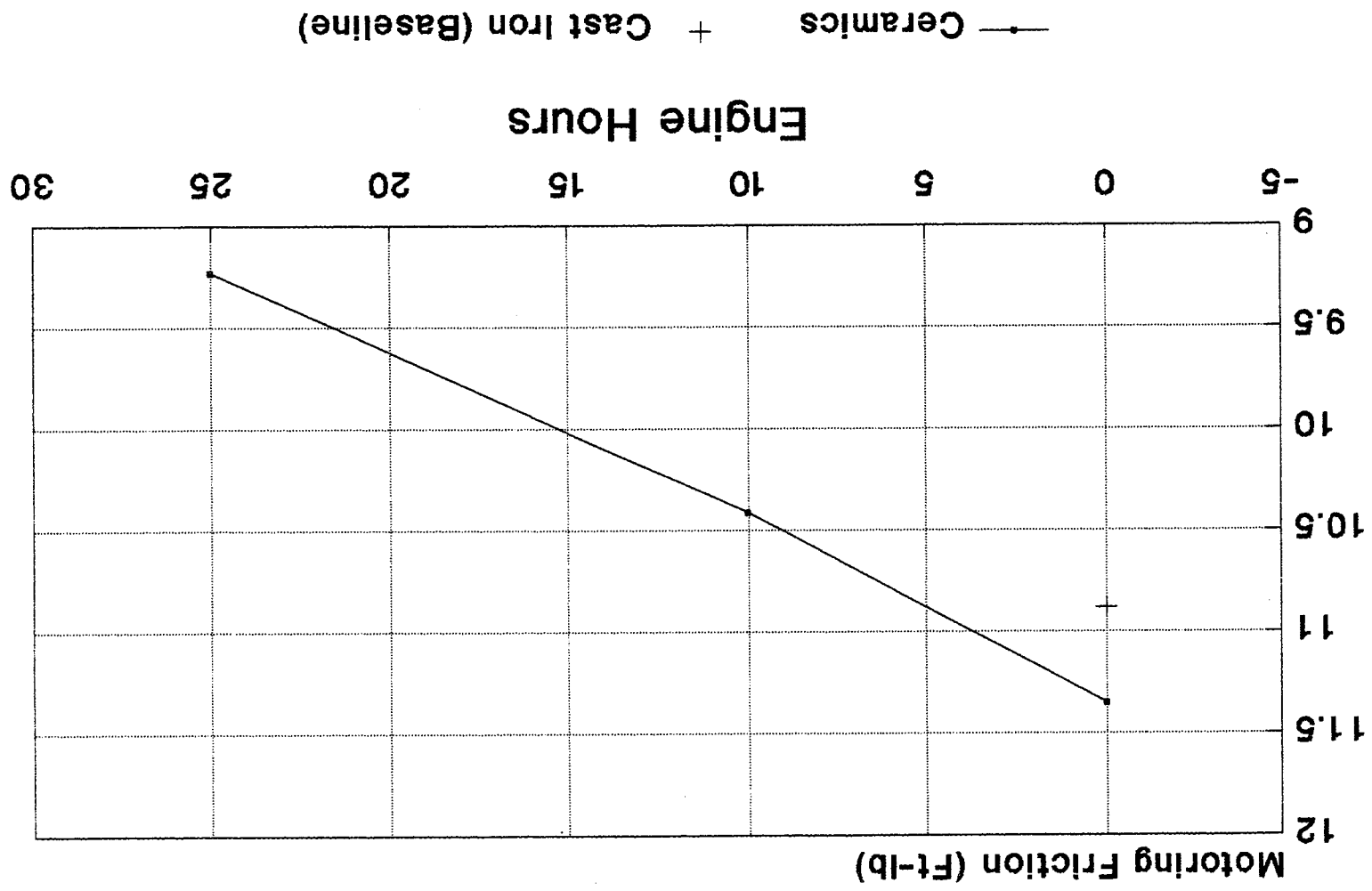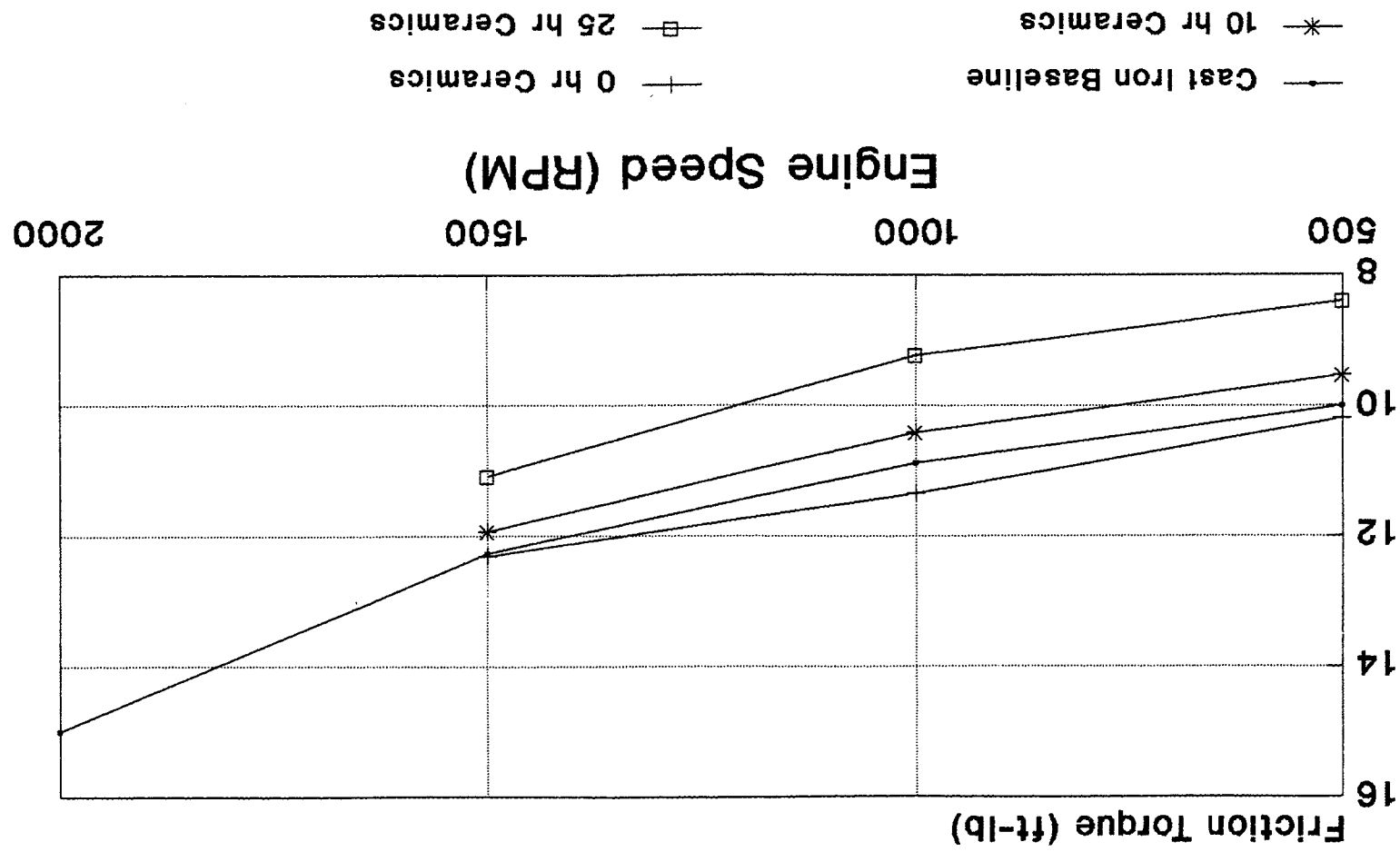
FIGURE 78. ENGINE PERFORMANCE TEST RESULTS, CAST IRON AND CERAMIC DATA

1000 RPM, 40 % Load
180 F Coolant Temp
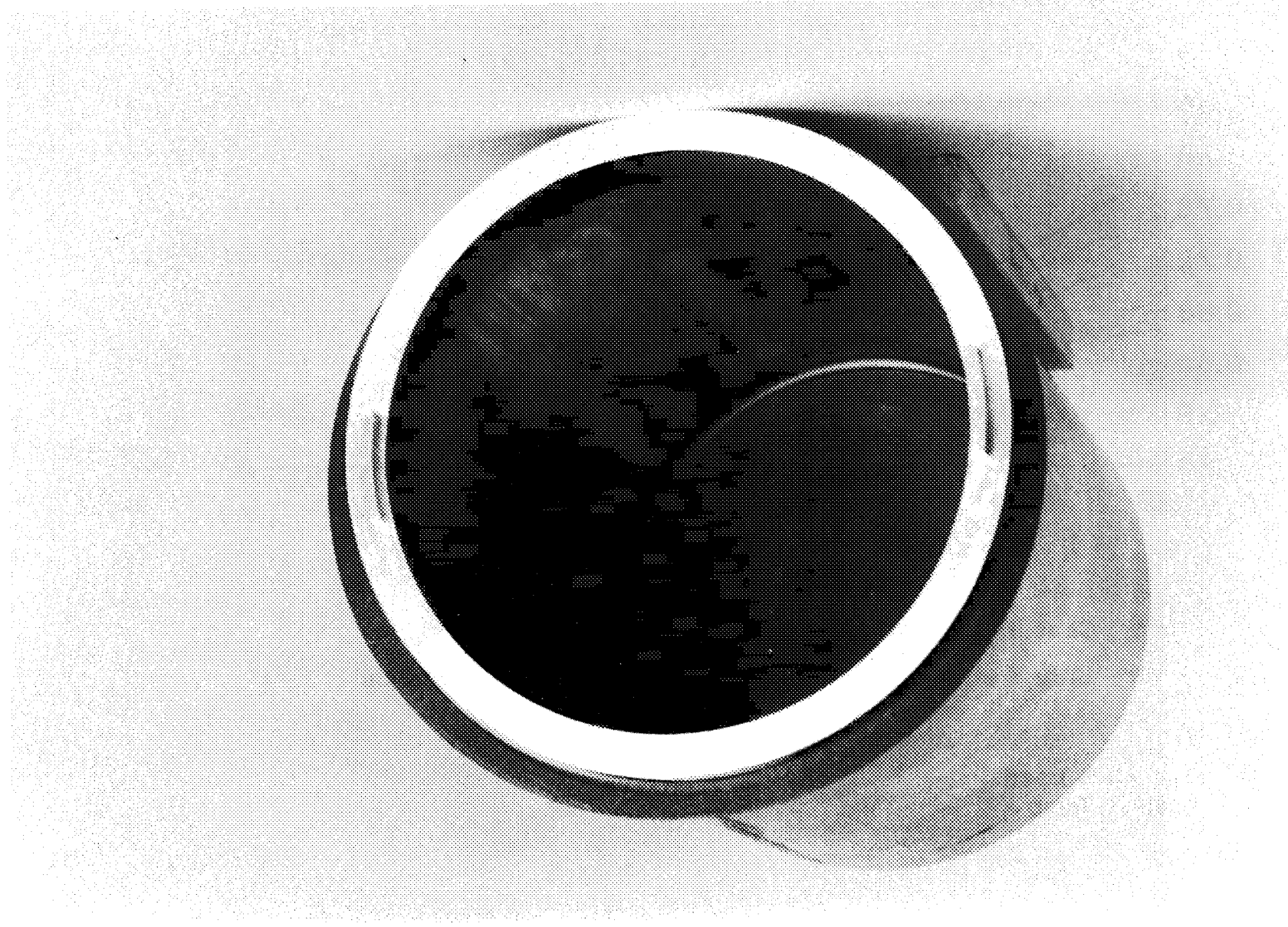
Power (Bhp)

BSFC (lb/Bhp-hr)

— Cast Iron Baseline   ✳ 10 hr Ceramics
+ 0 hr Ceramics   ▫ 25 hr Ceramics

ORIGINAL PAGE
BLACK AND WHITE PHOTOGRAPH

SCUFF MAT'L ANALYSIS

VFS = 8192   20.480

0.000

148

FIGURE 80. EDS SCUFF MATERIAL ANALYSIS

129

130

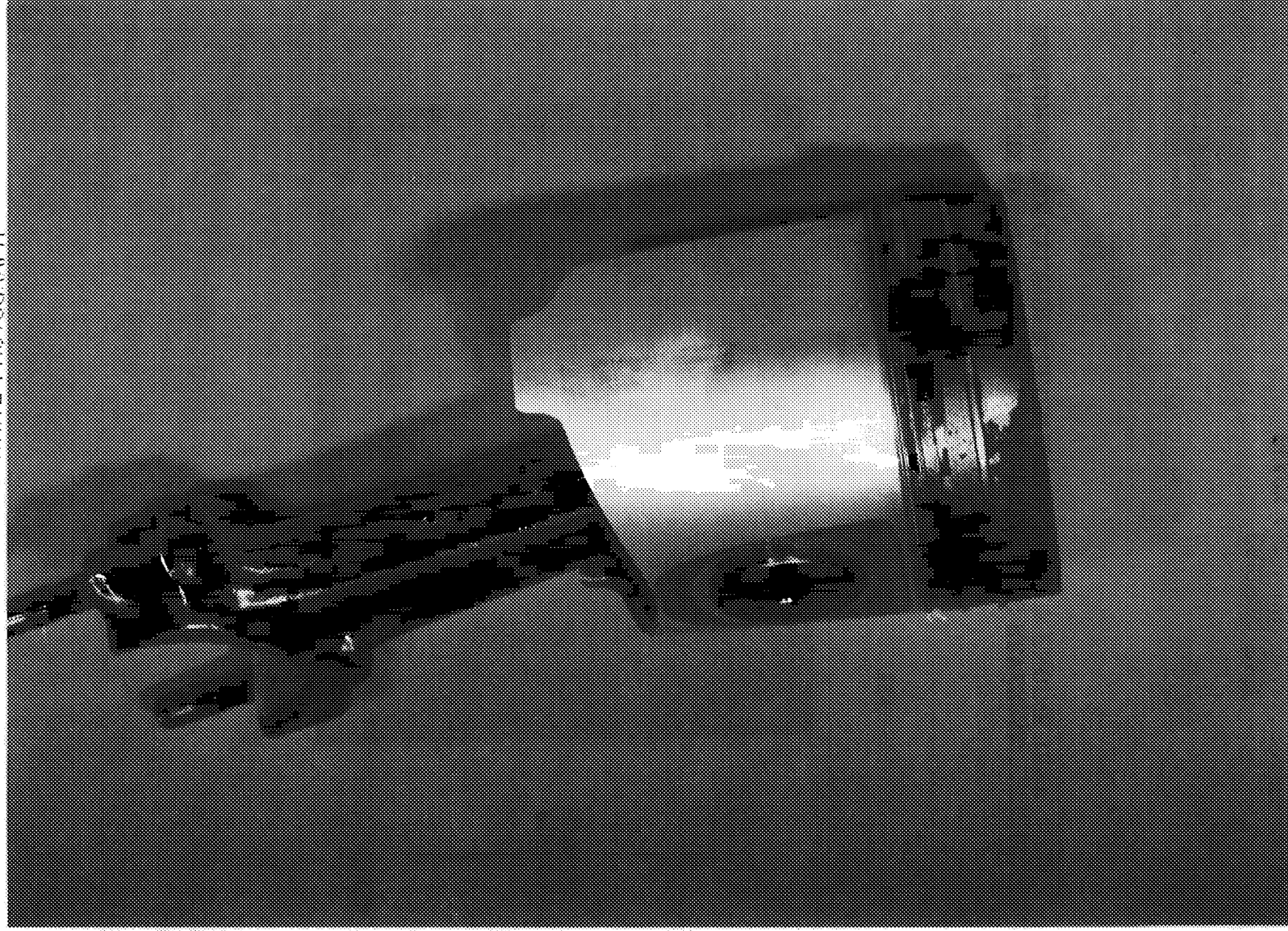FIGURE 82. PHOTOGRAPH OF PISTON AND Ni-Mo-TiC PISTON RINGS AFTER 30 HOUR ENGINE TEST

131

PISTON STROKE ←→

12x

FIGURE 83. SEM PHOTOGRAPH OF TOP RING REVERSAL REGION OF PSZ CYLINDER LINER AFTER 30 HOUR ENGINE TEST

132

FIGURE 84. COMPARISON OF EDS ANALYSIS FOR DARK AND
LIGHT REGIONS OF PSZ LINER AT TRR AFTER 30 HOURS

133

Series II Southwest Research Institute   THU 30-MAR-89 11:55
Cursor: 0.000keV = 0

0.000   2:TOP RING REVERSAL - 20KV, WD=32   VFS = 512   20.480
  175   1:UNWORN - BASE LINE - 20KV, WD=32   175
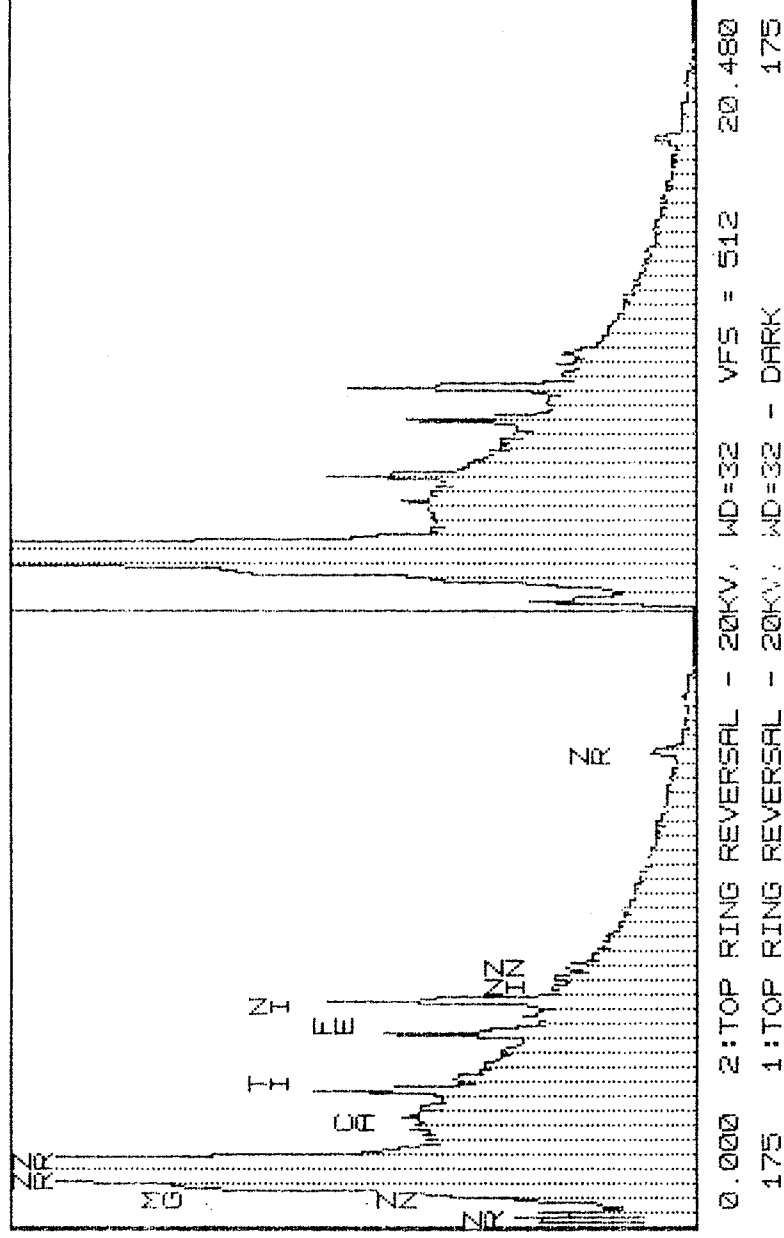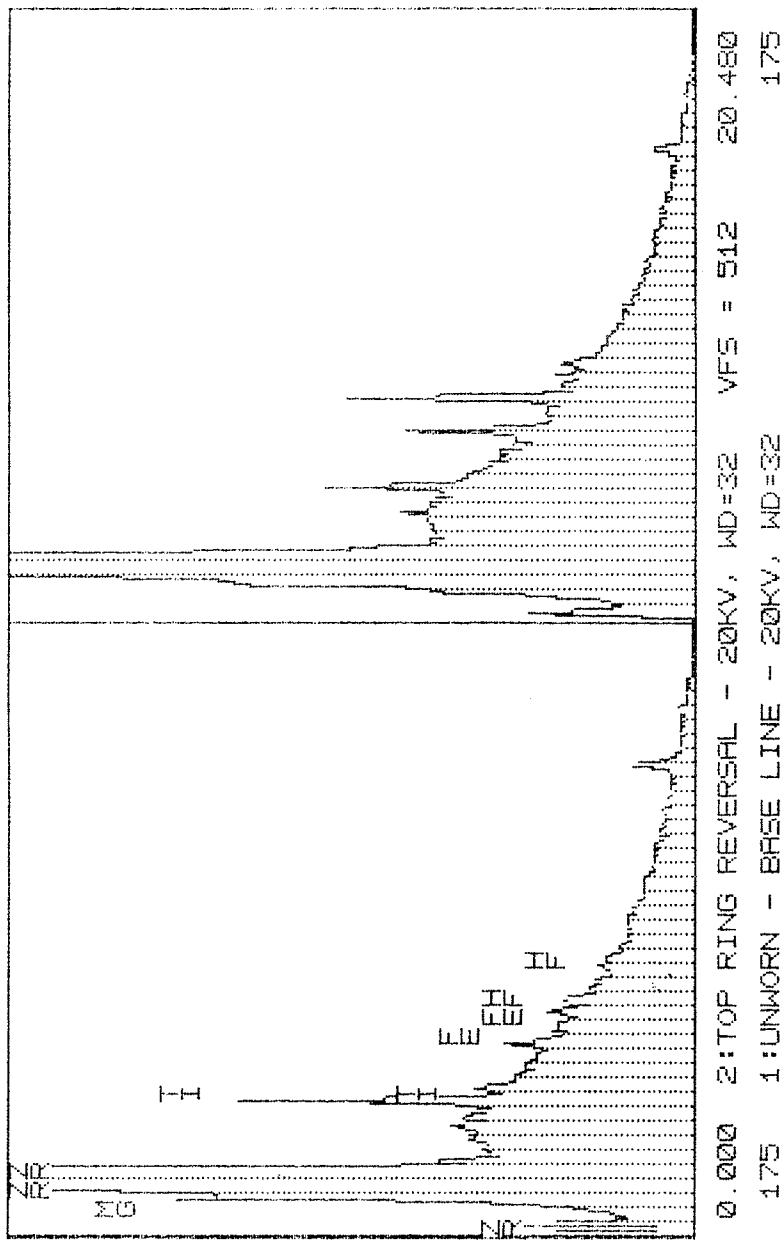
UNWORN REGION   TOP RING REVERSAL
   BASELINE

FIGURE 85. COMPARISON OF EDS ANALYSIS FOR TRR AND
           BASELINE REGIONS OF PSZ LINER AFTER 30 HOURS
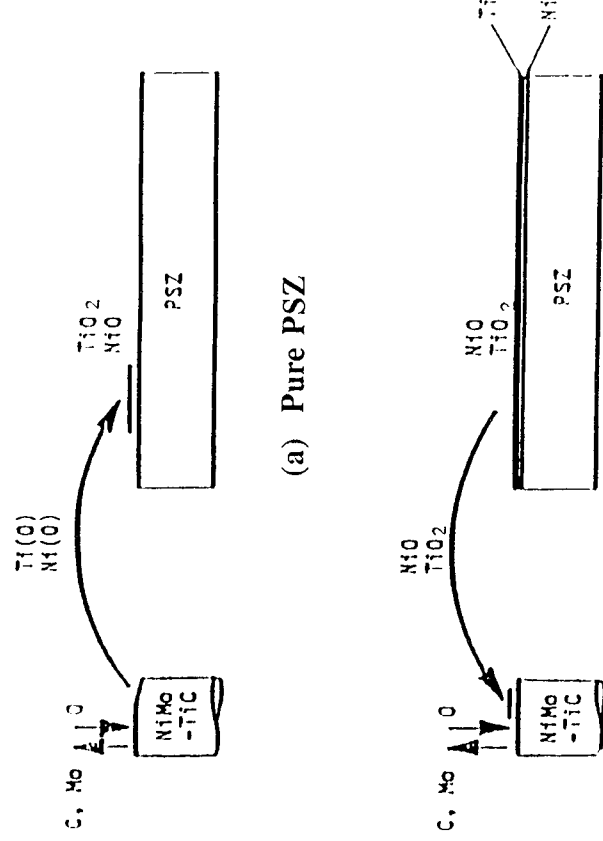
134

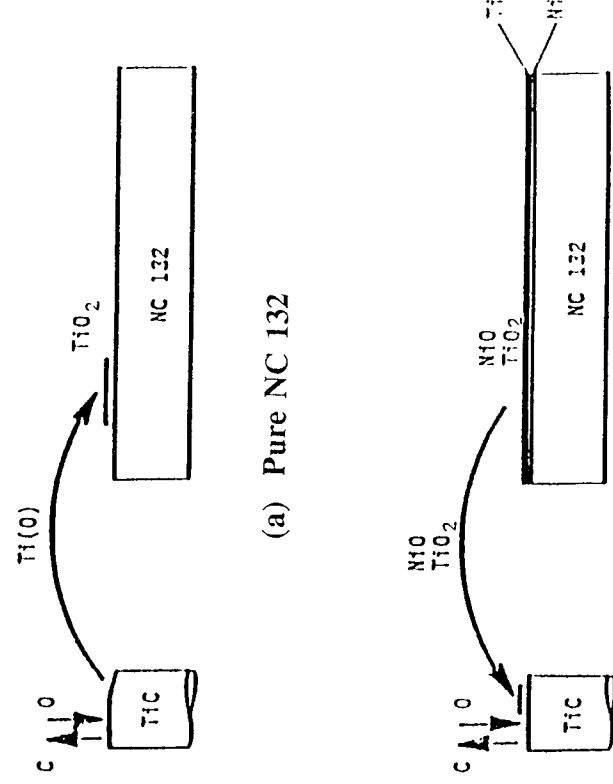**FIGURE 86. FILM-LUBRICANT TRANSFER IN THE Ni-Mo-TiC/PSZ SYSTEMS**

(a) Pure PSZ

(b) TiNi-Implanted PSZ

FIGURE 87. FILM-LUBRICANT TRANSFER IN THE TiC/NC 132 SYSTEMS

(a) Pure NC 132

(b) TiNi-Implanted NC 132

135

NASA
National Aeronautics and
Space Administration

Report Documentation Page

1. Report No. NASA CR-182262 DOE/NASA/0352-3	2. Government Accession No.	3. Recipient's Catalog No.
4. Title and Subtitle Sliding Seal Materials for Low Heat Rejection Engines		5. Report Date July 1989
		6. Performing Organization Code
7. Author(s) Kevin Beaty, James Lankford, and Shannon Vinyard		8. Performing Organization Report No. SwRI 06-7963
		10. Work Unit No.
9. Performing Organization Name and Address Southwest Research Institute 6220 Culebra Road, P.O. Box 28510 San Antonio, Tx 78284		11. Contract or Grant No. DEN3-352
		13. Type of Report and Period Covered Contractor Report Final
12. Sponsoring Agency Name and Address U.S. Department of Energy Office of Vehicle and Engine R&D Washington, D.C. 20545		14. Sponsoring Agency Code

15. Supplementary Notes

Prepared under Interagency Agreement DE-AI01-86CE50162. Project Manager, R.F. Barrows, Propulsion Systems Division, NASA Lewis Research Center, Cleveland, Ohio 44135.

16. Abstract

Sliding friction coefficients and wear rates of promising piston seal materials were measured under temperature, environmental, velocity, and loading conditions that are representative of the low heat rejection (LHR) diesel engine environment. These materials included carbides, oxides, and nitrides. In addition, silicon nitride and partially stabilized zirconia disks (cylinder liners) were ion-implanted with TiNi, Ni, Co, and Cr, and subsequently run against carbide pins (piston rings), with the objective of producing reduced friction via solid lubrication at elevated temperature. Friction and wear measurements were obtained using pin-on-disk laboratory experiments and a unique engine friction test rig. Unmodified ceramic sliding couples were characterized at all temperatures by friction coefficients of 0.24 and above during the pin-on-disk tests. The coefficient at 800 °C in an oxidizing environment was reduced to below 0.1, for certain material combination, by the ion-implantation of TiNi or Co. This beneficial effect was found to derive from the lubricious Ti, Ni, and Co oxides. Similar results were demonstrated on the engine friction test rig at lower temperatures. The structural integrity and feasibility of engine application with the most promising material combination were demonstrated during a 30-hour single-cylinder, direct-injection diesel engine test.

17. Key Words (Suggested by Author(s)) Ceramics; Friction; Wear; Temperature effects; Environmental effects; Ion implantation; Solid lubrication; Engines; Diesel; Insulated; Piston seals	18. Distribution Statement Unclassified – Unlimited Subject Category 27, 85 DOE Category UC-96	
19. Security Classif. (of this report) Unclassified	20. Security Classif. (of this page) Unclassified	21. No of pages 135	22. Price* A07

NASA FORM 1626 OCT 86   *For sale by the National Technical Information Service, Springfield, Virginia 22161